Dipl.-Ing. Martin Strobl, BSc.

Synthesis of NIR-emitting aza-BODIPY Dyes for Application in Optical Sensors

Dissertation

zur Erlangung des akademischen Grades

eines Doktors der technischen Wissenschaften

eingereicht an der

Technischen Universität Graz

Assoc.Prof. Dipl.-Chem. Dr.rer.nat. Torsten Mayr

Institut für Analytische Chemie und Lebensmittelchemie

Technische Universität Graz

Graz, März 2017

Eidesstattliche Erklärung

Ich erkläre an Eides statt, dass ich die vorliegende Arbeit selbstständig verfasst, andere als die angegebenen Quellen/Hilfsmittel nicht benutzt, und die den benutzten Quellen wörtlich und inhaltlich entnommenen stellen als solche kenntlich gemacht habe. Das in TUGRAZonline hochgeladene Textdokument ist mit der vorliegenden Dissertation identisch.

Statutory declaration

I declare that I have authored this thesis independently, that I have not used other than the declared sources/resources, and that I have explicitly indicated all material which has been quoted either literally or by content from the sources used. The text document uploaded to TUGRAZonline is identical to the present doctoral thesis.

_____ _____

Datum/Date Unterschrift/Signature

„Mehr Licht“

Johann Wolfgang von Goethe

Acknowledgement

This doctoral thesis is the final part of an exciting studying time and now it is time to say thank you. First of all I want to thank my supervisor Ass. Prof. Torsten Mayr for giving me the possibility to work on this project, for the patience during this time and for keeping me always motivated.

Special thanks go to Ass. Prof. Sergey Borisov for always helping and supporting me on the way and I also want to thank Univ.-Prof. Ingo Klimant for the fruitful discussions.

Thank you to the whole working group for creating probably the most amazing working atmosphere.

A big gratitude goes to all my friends and family who always supported me.

Kurzfassung

Der Fokus dieser Arbeit liegt auf der Synthese und Charakterisierung von fluoreszierenden pH-Indikatoren, welche speziell für die Anwendung in langzeitstabilen Sensoren geeignet sind. Bordifluorid tetraarylazadipyrromethen (aza-BODIPY) als Farbstoffklasse wurden aufgrund ihrer einzigartigen rot/nah-infrarot Absorptions- und Emissionseigenschaften und außergewöhnlichen Photostabilität ausgewählt. Die synthetisierten aza-BODIPY-Farbstoffe decken den pH-Bereich von 1,5 bis 13 ab. Aufgrund ihrer nahezu identischen photophysikalischen und spektralen Eigenschaften können pH-Sensoren mit erweitertem dynamischem Bereich hergestellt werden (Kapitel 1). aza-BODIPY-basierende Sensoren sind aber nicht nur zu Messung des pH-Werts geeignet, sondern auch für die Detektion von Ammoniak oder Kohlendioxid.

Kapitel 2 präsentiert faser-optische Ammoniaksensoren, welche auf aza-BODIPYs basieren und mittels Frequenz-Phasenfluorimetrie ausgelesen werden können. Der dynamische Bereich kann durch die Wahl des aza-BODIPYs und/oder des Polymers eingestellt werden und reicht von 10 mg/l gelöstem Ammoniak bis zu Spurenkonzentrationen unter 1 µg/l.

Kapitel 3 präsentiert sehr robuste pH-Sensoren, basierend auf nahinfrarot-absorbierende aza-BODIPYs und anorganischem Phosphor oder Upconversion-Materialien.

Im vierten Kapitel werden symmetrische diOH-aza-BODIPYs mit sehr hohen pK_a-Werten für die Anwendung in CO_2-Sensoren vorgestellt. Die Sensoren werden *via* absorptionsmoduliertem Inner-filter-Effekt ausgelesen und der dynamische Bereich kann durch unterschiedliche Substitution am aza-BODIPY-Farbstoff eingestellt werden.

Abstract

There is an enormous demand of stable and reliable pH monitoring devices, which are able of fulfilling the requirements of particular application fields. Herein, fluorescent pH sensors have become increasingly promising tools for precise pH determination and continuous monitoring compared to other conventional electrochemical methods. Although a wide variety of pH-sensitive fluorophores are available, only a few match the criteria for use in stable pH sensors.

This thesis presents the synthesis and characterization of novel fluorescent pH indicators for application in high-performance sensors for various ranges of pH. Borondifluoride azadipyrromethene (aza-BODIPY) dye class was selected due to its unique far red/near-infrared absorption and emission profiles, straightforward pK_a-tunability and remarkable photostability. The novel NIR-emitting aza-BODIPY dyes cover the pH range from 1.5 to 13 and have virtually identical spectral and photo-physical properties which provides the possibility of designing a pH sensor with an extended dynamic range (Chapter 1). Moreover, aza-BODIPY dyes are not only suitable for pH sensing applications, but also for detection of gases such as carbon dioxide and ammonia.

Chapter 2 presents a set of fiber-optic ammonia sensors, based on aza-BODIPYs. The dual-lifetime referenced sensors make use of phosphorescent Egyptian Blue as reference dye and are read-out *via* a phase-fluorometer. The dynamic range of the sensors can be tuned by the choice of aza-BODIPY and/or polymeric matrix, enabling detection of dissolved ammonia from 10 mg/l to even trace concentrations below 1 µg/l.

Chapter 3 demonstrates a new design concept for robust optical pH sensors based on the combination of a NIR-colorimetric aza-BODIPY dye and inorganic phosphors or upconversion particles (UCPs). In this concept the pH-dependent absorption changes are converted into luminescence response by utilizing inner-filter effect, resulting in highly stable pH sensing material.

Finally, chapter 4 presents a set of symmetrical di-OH-aza-BODIPY dyes with very high pK_a values for application in carbon dioxide sensors. The sensors are read out *via* absorption modulated inner-filter effect and the dynamic range can be easily tuned by variation of the substitution pattern of the aza-BODIPY dye.

Table of Contents

Introduction

pH as fundamental parameter plays a key role in a broad range of sciences and technology from environmental to biochemical to industrial. Its determination is of utmost importance because the vast majority of chemical reactions are dependent on it some way. Thus, there is an enormous demand for precise and robust measurement devices fulfilling the requirements which are given by particular application fields.

In the last three decades, there has been enormous progress in the development of optical pH sensors and nowadays they are offering tremendous advantages compared to other analytical tools such as (potentiometric) glass pH electrodes or ion-sensitive field-effect transistors (ISFET): They exhibit high sensitivity within their dynamic range, operate non-invasively and are suitable for continuous measurement while requiring low energy consumption. Additionally, the use of fibre-optic sensors enables remote sensing combined with high mechanical flexibility. Thus, optical sensors have found wide-spread application in many sciences and technology, particularly in biotechnology, medical diagnostics, biomedical research and environmental monitoring. Although a huge variety of pH indicators are nowadays available, only a few meet the requirements for use in optical pH sensors.

Aim of this work was the synthesis and characterization of novel fluorescent indicators for preparation of high-performance sensors for various ranges of pH. Borondifluoride azadipyrromethene (aza-BODIPY) dye class was selected due to its unique far red/near-infrared absorption and emission profiles, straightforward pK_a-tunability and remarkable photostability.

The relevant pH-range for optical sensors is predefined by its particular application area. For instance, acidic pH-values (pH 5.5-7) prevail in biotechnological process control while physiological applications (pH 7.3) or marine systems (pH 7.5-8.5) require a higher pH range. Here, a full set of eight aza-BODIPY dyes was synthesized, covering almost the entire pH scale. Moreover, pH-sensitive aza-BODIPY are also suitable for trace detection of ammonia and carbon dioxide. Aza-BODIPY dyes exhibiting extraordinary high pK_a values (pH 9-11) are suitable for application in CO_2-sensors, while ammonia detection requires pH dyes with low pK_a values (pH 3-5).

State-of-the-art optical pH sensors

An optical pH sensor usually consists of a pH sensitive indicator dye which is homogenously distributed in a hydrophilic immobilisation matrix (e.g. hydrogels).[1] Depending on pH, the spectral shape of absorption/emission, the fluorescence intensity (including quantum yield) or the luminescence decay time of the indicator dye is altered, which is then used as a source of analytical information.[2]

A wide variety of pH sensors based on colorimetric indicators have been reported in literature, exhibiting distinct pH-dependent absorption (reflectance) changes. However, absorption-based sensors can only be applied in a limited number of formats and the colorimetric signal is difficult to quantify, especially in scattering (biological) matter. Thus, fluorescent pH sensors have gained considerable attention due to their high sensitivity and well-established referencing read-out systems such as two-wavelength referencing (TWR) or dual-lifetime referencing (DLR).[3,4] They can be applied in various sensor formats such as planar optodes, nanoparticle formulation, fibre-optic or micro-sensors.[5,6] Desirable properties of a fluorescent pH indicator can be summarized as follows:

- High brightness (defined as product of molar absorption coefficient (ε) and luminescence quantum yield (φ)
- High photostability
- Tuneable pK_a value
- Easy accessibility to structural modifications
- Resistant towards aggregation
- Low cross-talk to ionic strength

The higher the brightness of the indicator, the higher is the obtained signal intensity and the better is the signal-to-noise ratio of the sensing material. A high signal intensity also enables a reduction of the sensing layer thickness, resulting in a lowered response time. High photostability is an important parameter regarding long-term measurements. It enables the recording of many measurements points while keeping the signal drift at a minimum. The indicator should be easily accessible to structural modifications for tuning its pK_a value or for substitution of functional groups (e.g. carboxy-, amino-groups or monomeric residues), which enables covalent immobilisation to the hydrophilic matrix.

The indicator should not be prone to aggregation, even at high concentrations. Dye aggregation leads to self-quenching, which severely compromises the fluorescence response. A disadvantage of optical pH sensors is their cross-sensitivity to ionic strength. In order to minimize this effect, the pH indicator should be low charged and embedded in an uncharged host polymer (e.g. hydrogel).[7]

Popular fluorescent indicators are xanthene derivatives (fluorescein, rhodamine), naphthalimides, hydroxyy-coumarines or hydroxy-1,3,6-trisulfonic acid (HPTS) but many of them exhibit limitations: Carboxy-fluorescein and especially its derivative 2'-7'-dihexylfluorescein show only moderate photostability and are prone to self-quenching. Threefold negatively charged HPTS is highly influenced by ionic strength and naphthalimides exhibit only low molar absorption coefficients. SNARF indicators are known for their low photostability. Moreover, all the fluorophores mentioned above have absorption/emission profiles in the UV/Vis range (400-600 nm).

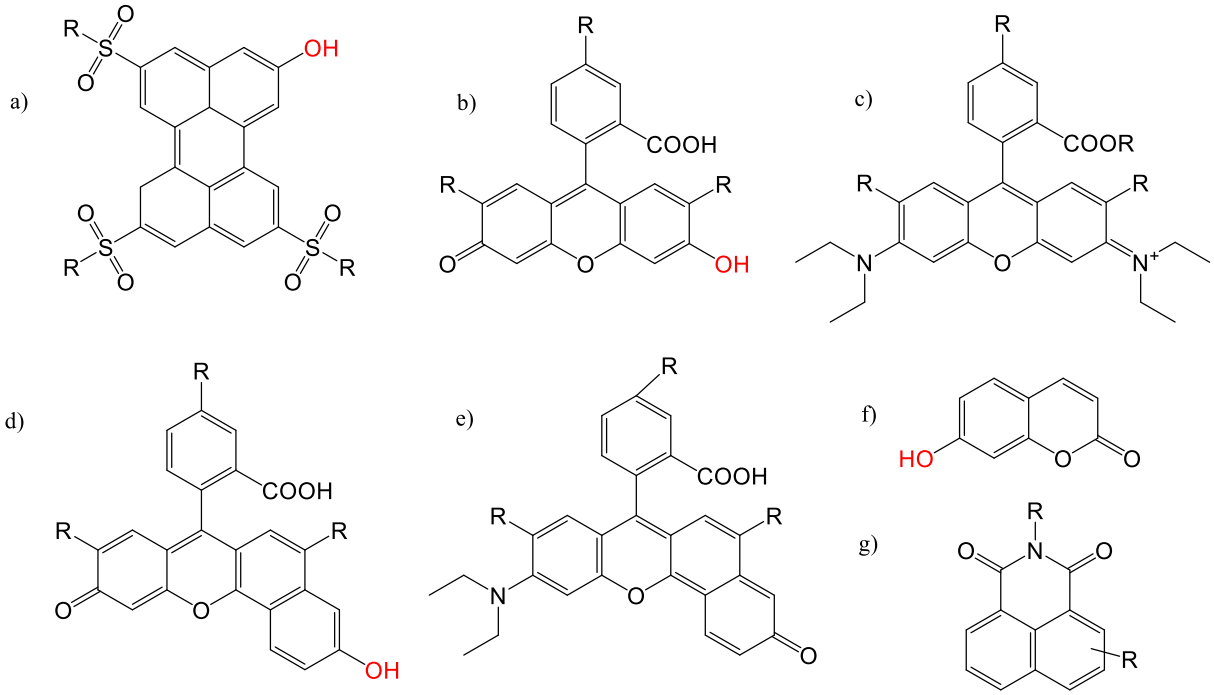

Figure 1) Chemical Structure of prominent fluorophores: a) HPTS b) Carboxy-fluorescein c) Rhodamine d) SNARF (Seminaphthorhodafluors) e) SNAFL (Seminaphtho-fluorescein) f) Hydroxy-coumarin g) Naphthalimide.

However, in many applications, e.g. for measuring in complex biological samples, it is preferable to use fluorophores with absorption/emission profiles in the long-wavelength

spectral region (650 – 750 nm). Such fluorophores provide significant advantages compared to conventional UV, blue and green light probes due to[8]

- Lower auto-fluorescence of biomolecules
- Less scattering of excitation or emission light
- Less photo-damage to cells and living organisms.
- Deep penetration of red and near-infrared light into (biological) probes

Especially for measurements *in vivo* the absorption and emission of the fluorophores should be located within the so-called "optical window" which is between 650 to 950 nm of the electromagnetic spectrum.[9] At shorter wavelengths, light is strongly absorbed by biomolecules (e.g. hemoglobin) and light-scattering by tissue is significantly enhanced while at longer wavelength the absorption by water becomes dominant.

It should be mentioned that long-wavelength emissive fluorophores naturally exhibit lower quantum yield due to their low energetic excited state, which favours non-radiative internal conversion. As a consequence, the quantum yield of NIR-emitting dyes usually does not exceed 30 % and chromophores with bathochromically shifted absorption bands above 900 nm show no detectable emission.[8] Photostability is another important property and varies extremely for different chromophore classes. In general, long-wavelength probes with conjugated aromatic system (porphyrins, aza-BODIPYs) are more photostable than fluorophores with conjugated polymethine groups (cyanine dyes).[8]

In summary, development of long-wavelength fluorophores is not an easy task and enormous research effort have been invested to find NIR-emissive dyes with desired optical properties and high photostability. The next chapter will give an overview of pH-sensitive NIR-emissive fluorophores.

Porphyrin-based probes

The pH-sensitivity of metal-free porphyrins derives from the nitrogen atoms at their pyrrole groups. Several attempts have been made to shift the original low pK_a value of the porphyrin, such as electrostatic stabilization by peripheral negative charges[10] (e.g. polyglutamic dendrimers) or substitution of dendrimers into the porphyrin's core[11] (figure **2a** and **b**). However, these modifications resulted in either extremely high cross-sensitivity to ionic strength or lowered NIR-fluorescence. Another interesting concept was the development of an electron-deficient Pt(II)porpholactone (figure **2c**).[12] Unexpectedly, an apparent pK_a value of 12.6 was determined, making this approach only suitable for specific applications. To sum up, although porphyrins represent interesting NIR-excitable fluorophores, they are not easily accessible to structural modifications in order to tune the pK_a value.

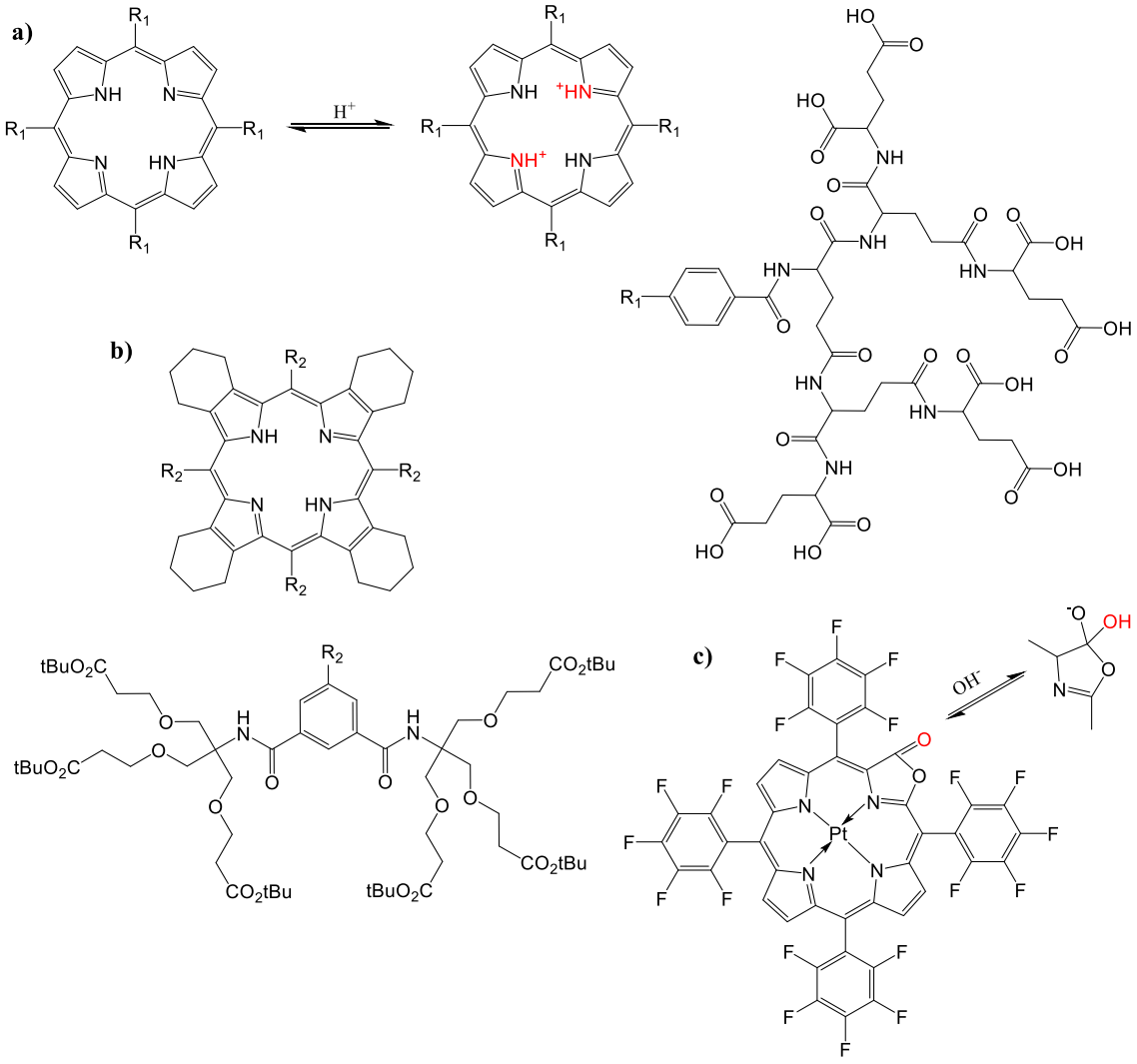

Figure 2) Chemical structure of long-wavelength emitting porphyrin and its analogous: **a)** metal-free porphyrin **b)** tetrabenzoporphyrin derivative **c)** Pt(II)porpholactone

Cyanine dyes

Cyanines exhibit dual pH-dependent NIR absorption and emission, making them highly interesting for two-wavelength ratiometric read-out and ratiometric imaging. Moreover, when substituted with benzothiazole group (Figure **3a**), the emission shifts about 70 nm upon deprotonation, allowing easy separation of the pH-dependent fluorescence signals in ratiometric read-out.[13] An interesting set of water-soluble pyrrolpyrrole cyanines were synthetized by Wiktorowski *et al.* (Figure **3b**).[11] These chromophores are excitable at 800 nm and have extremely high molar absorption coefficients ε (200 000 $M^{-1}cm^{-1}$). However, these cyanines can only be applied in very acidic environment (pK_a 2.4-3.4). Additionally, they show high dependency on the polarity of the environment and are prone to aggregation and accompanied self-quenching, even when substituted with PEG groups (MW 1000). He *et al.*[14] presented a cyanine-based dye (Figure **3c**), which is pH sensitive at two different pH ranges and showed their applicability for pH imaging in living cells and real-time monitoring in enzymatic reactions. However, cyanine dyes are known for their poor photostability and thus their use is limited, especially for long-term applications.

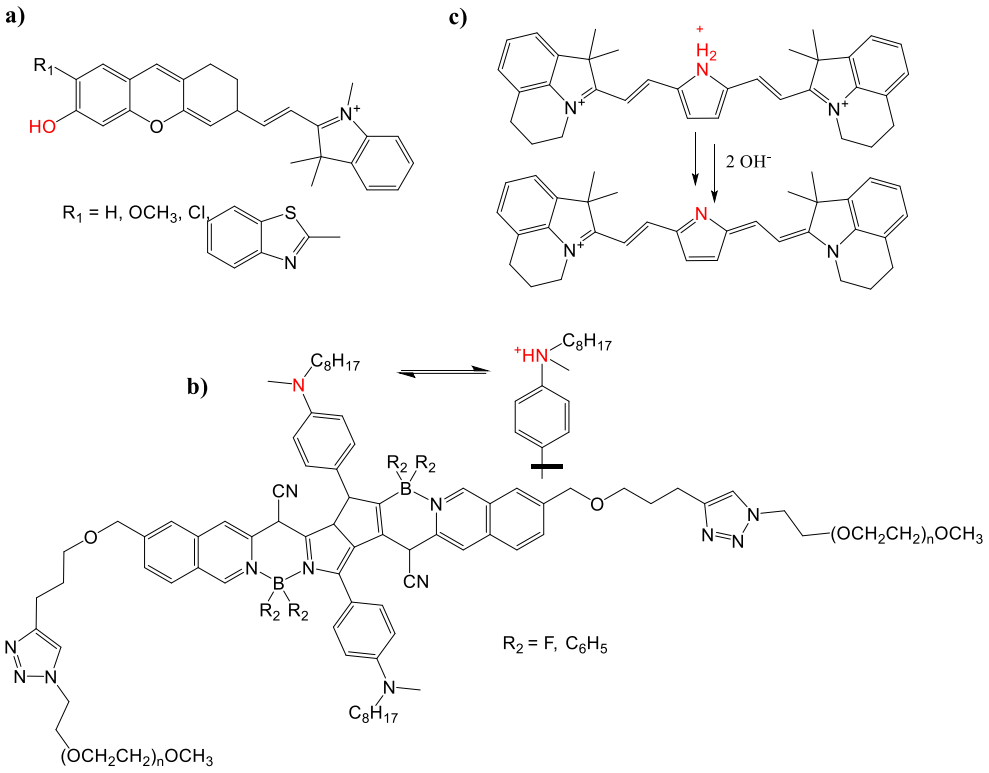

Figure 3) Chemical Structures of pH sensitive cyanine dyes: **a)** pH-sensitive hemicyanine **b)** water-soluble pyrrolpyrrole cyanines **c)** cyanine dye with pyrrole core.

Other NIR chromophores

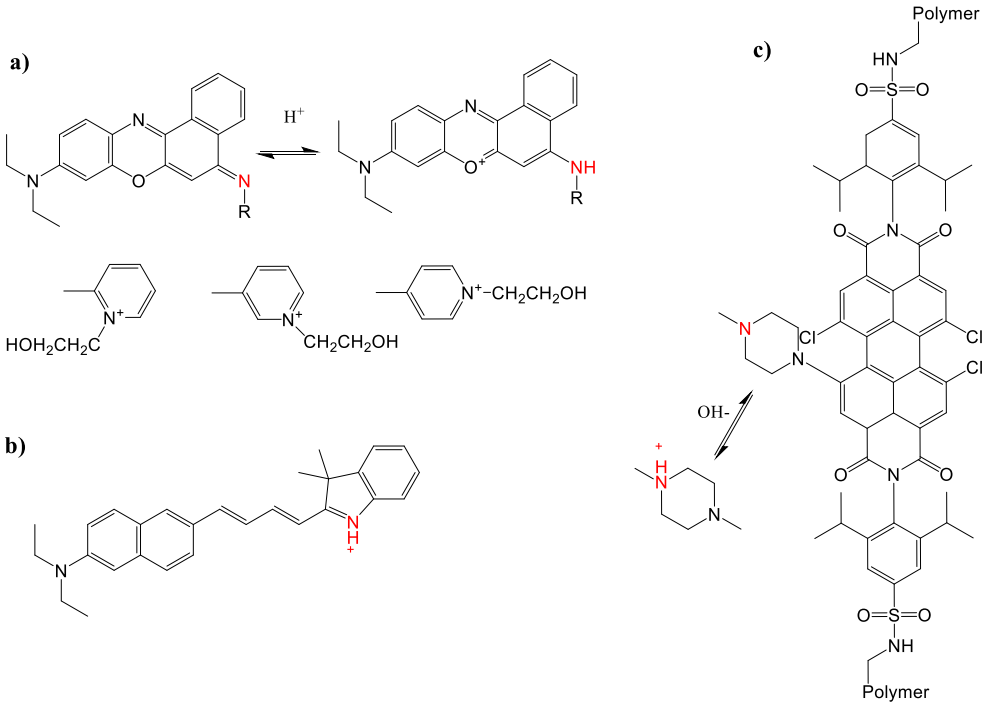

Figure 4) Chemical Structures of different chromophores with absorption/emission in the long-wavelength spectral region: **a)** benzo[a]phenoxazine **b)** coumarin derivative **c)** covalently coupled perylenes.

Liu *et al.*[15] presented interesting NIR-probes based on benzo[a]phenoxazine, where pK_a values can be easily tuned by varying the substitution pattern on the protonable imino group (Figure **4a**). π-extension at the coumarin core with an indole moiety (Figure **4b**) was realized by Ge *et al.*[16] and resulted in a long-wavelength emissive derivative with a relatively low pK_a value of 3.9. Notably, Aigner *et al.*[17] synthetized 1-aminoperylene bisimides, which were functionalized with a pH-sensitive piperazine group (pK_a 6.0, Figure **4.c**). Additionally, the indicator was covalently grafted onto cross-linked poly(acryloylmorpholine), resulting in complete elimination of dye aggregation or dye leaching out of the polymeric support.

BODIPY, aza-BODIPY and structural analogous

BODIPY (4,4-difluoro-4-bora-3a,4a-diaza-**s-indacene**, Figure 5**a** and **b**) dyes are strongly UV-absorbing molecules, which show high and relatively sharp emission around 520-600 nm and have found widespread application as molecular probes or laser dyes in the visible region.[18] Various modifications to the BODIPY core have been performed in order to bathochromically shift the absorption and emission in the red/NIR part of the electromagnetic spectrum (650-900 nm) and can be summarized into the following categories:

- Extension of the conjugated system by functionalization at the α-, β- or *meso*-position of the BODIPY
- Introduction of π-extended pyrroles
- N-substitution at the C^8-postion of the BODIPY core, so-called **aza-BODIP**Y.

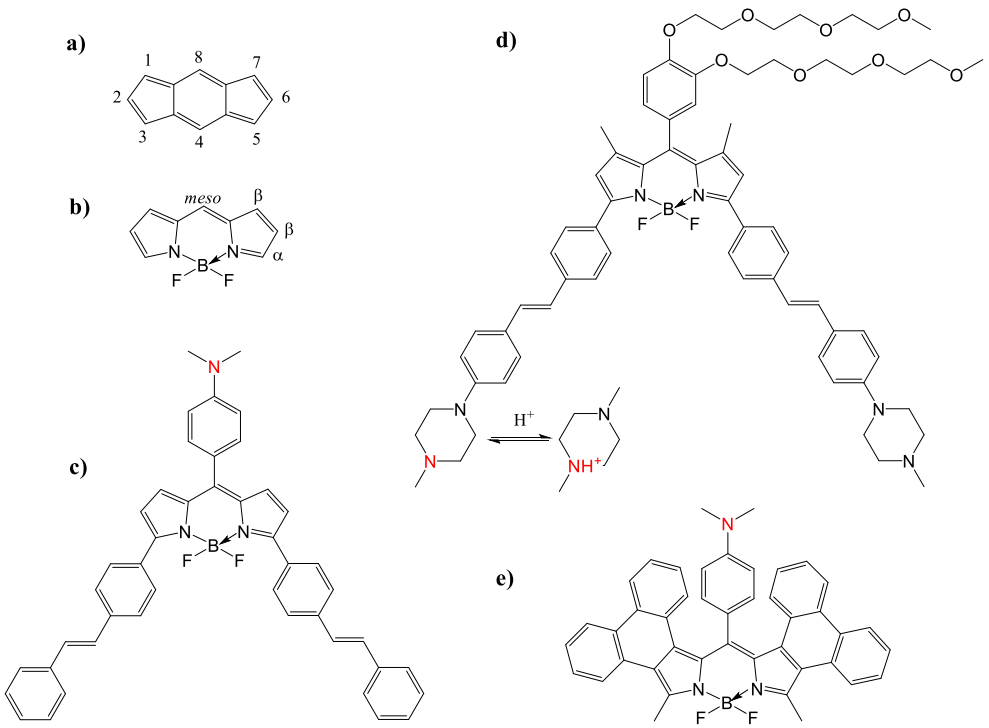

Figure 5) Chemical structures of *s*-indacene (**a**), BODIPY core (**b**) and styryl-substituted BODIPYs (**c, d**) and aryl-fused BODIPY (**e**) with pH-sensitive *N*-alkylated PET-moiety.

First attempts of designing NIR-emissive pH-sensitive BODIPY dyes were based on the introduction of an amino-moiety, acting as PET-functionality. Daub *et al.*[19] synthesized a styryl-substituted BODIPY which was further functionalized with a dimethylaminophenyl-recepter at the *meso*-positon of the BODIPY core (Figure **5c**). Similarly, Zhang *et al.*[20]

developed a set of π-extended BODIPYs, where the pH-sensitive piperazine group was introduced at the 3,5-position of the dye's core. Oligo ethylene chains were additionally added at the *meso*-position in order to avoid aggregation in aqueous solutions (Figure **5d**). Another interesting set of NIR-emissive BODIPYs was reported by Rurack *et al.*[21] where phenanthrene fusion to the β-pyrrole positons of the BODIPY resulted in bathochromically shifted absorption/emission profiles.

Especially, N-substitution at the C^8-postion of the BODIPY core, so-called **aza-BODIP**Y and related structural analogues have gained considerable attention and have been widely studied due to their unique properties[22]:

- Outstanding photostability
- High molar absorption coefficients (typically range from 80 000 to 110 000 $M^{-1}cm^{-1}$)
- Good quantum yield (~ 20%)
- Absorption/emission band in red/NIR-spectral region
- Accessibility to structural modifications.
- Resistance towards aggregation
- Excellent solubility in most organic solvents (excluding water)

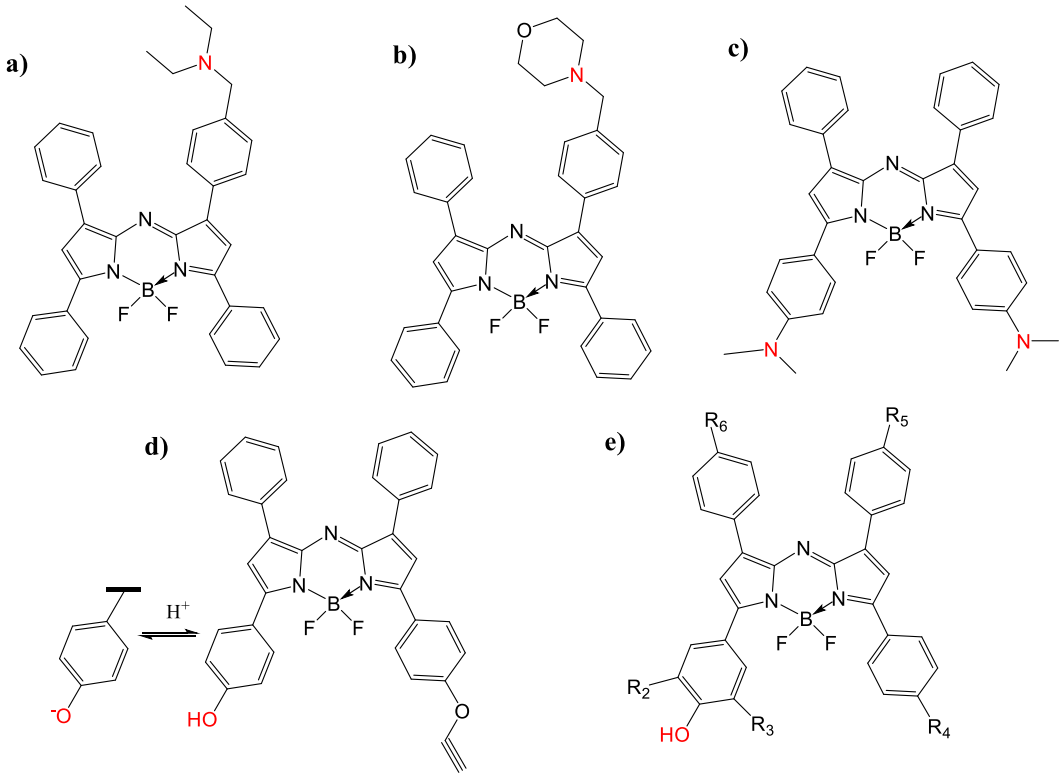

Figure 6) Chemical structures of pH probes, exhibiting *1,3,5,7*-tetraarylsubstituted aza-BODIPY as scaffold.

Aza-dipyrromethene was already discovered by Rogers *et al*. in the 1940s[18], but first borondifluoride azadipyrromethene was published by Boyer *et al.* in 1994.[23] O'Shea *et al.* finally adapted this class of chromophores for application as pH-sensitive probes (Figure **6a-d**) based on PET mechnism.[24–27] Introduction of dimethylamino- or morpholine-functionality (Figure **6a** and **b**) *via* a non-π- electron-conjugating methylene group results in an fluorescent "off-on response" to pH without altering absorption properties.[27] Notably, when pH-sensitive moiety is fully integrated into the chromophore (Figure **6c**), internal charge transfer (ICT) additionally becomes operative.[26] ICT originates from different electron intensities of protonated and deprotonated form of the fluorophore, resulting in pronounced shifts in absorption spectra. Murtagh *et al.*[25] presented an aza-BOPIPY bearing a phenolate receptor (Figure **6c**) instead of *N*-alkylated functionalities. Upon deprotonation of the phenol group (pK_a 6.9) the fluorescence emission is virtually "switched off" due to PET with simultaneously shifted absorption from 700 to 750 nm. Further work was done by Jokic *et al.*[28] (Figure **6e**). They demonstrated that the pK_a value of the aza-BODIPY dyes can be easily adjusted by substitution of electron-donating (alkoxy moieties) or electron-withdrawing (chlorine) groups at the pH-sensitive phenolate receptor. The authors show that all these indicators exhibit remarkable photostability and outperform most state-of-the-art NIR pH dyes (especially SNARF).

Referencing Techniques

Fluorescence intensity is a rather error-prone parameter, which is highly influenced by a number of factors, such as

- Intensity fluctuations of the excitation source
- Detector performance
- Artefacts originating from the optoelectronic system
- Coloration of the media
- Concentration of the indicator dye

The adverse effects from intensity-based measurements can be overcome by referencing methods such as TWR or DLR:

Two Wavelength Referencing (TWR)[29]

Here, referencing is based on the ratio of two different emission intensities, recorded at two different spectral windows with single excitation wavelength. Alternatively, read-out with dual excitation but fixed emission wavelength is also possible. However, only a few molecules exhibit two spectrally different emissions with overlapping excitation spectra.

PET-probes (e.g. aza-BODIPYs), for example, do not show a pH-dependent shift in fluorescent spectra and therefore require a second analyte-insensitive fluorophore or phosphor for referencing. This reference dye should fulfil the following criteria:

- Similar excitation spectrum but different emission spectra
- High photostability
- Good brightness
- (Photo)chemical inertness

It is worth mentioning that two-wavelength ratiometric read-out cannot compensate wavelength-dependent light-scattering.

Dual Lifetime Referencing (DLR)[3,30,31]

Alternatively, referencing of the fluorescence signal can also be performed *via* dual lifetime referencing (DLR) in the frequency domain and is especially used for fluorophores with short lifetimes. Similar to TWR, an analyte-insensitive reference dye with long decay time but overlapping excitation spectra is added along with the indicator dye. Both are simultaneously excited with a modulated light source. The modulated frequency of the excitation light is set according to the lifetime of the phosphor (approximately 100 µs). Consequently, the phosphorescent dye exhibits a phase-shift while the indicator has no phase delay. The overall phase angle shift (phi) is a function of the intensity ratios of the two fluorophores and changes with the amount of fluorescence emission from the indicator (figure **7**). However, it should be noted that DLR-method cannot compensate concentration changes of the indicator dye (e.g. photo-degradation or leaching from the host polymer).

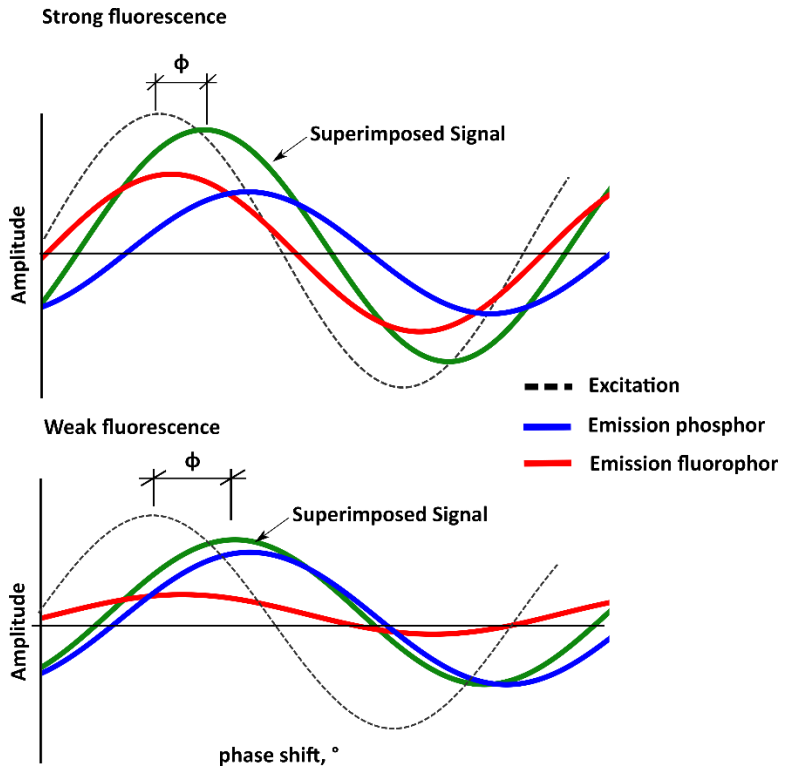

Figure 7) Principle of Dual-Lifetime Referencing (DLR) for read-out of fluorescent pH indicators.

Phosphorescent reference dyes for the application in a DLR-System should match the following criteria:

- Long-decay time (typically µs-ms range)
- Overlapping excitation spectrum with indicator dye (red/NIR spectral region)
- Insensitive towards the analyte
- Minor effect of temperature to luminescence lifetime
- No cross-sensitivity to molecular oxygen
- High photostability
- Good brightness

Egyptian blue pigment (EB) represents an excellent DLR-reference. EB is highly photostable and its luminescence decay time shows no cross-sensitivity to oxygen and only minimal temperature dependency (0.21%/K at 25 °C). Egyptian Blue[32] is a calcium copper silicate ($CaCuSi_4O_{10}$, ∅ 1-5 µm) with a lifetime around 126-160 µs (depending on grinding and sintering process). Its luminescence quantum yield (which is difficult to determine due to size-dependent scattering) is estimated to 10.5 %. EB exhibits a broad excitation/absorption band in the green-red part of the spectrum (λ_{max} = 600 nm) and its emission band is located at 900-1100 nm. Thus, EB is also an excellent candidate for ratiometric (two wavelength) read-out

since its excitation spectrum overlaps with a wide variety of fluorophores while its emission in the near-infrared spectral region (stokes shift > 200 nm) can be easily separated from the indicator's emission. This favours the elimination of potential interferences such as auto-fluorescence and Raman scattering.

Chromium(III) activated gadolinium aluminium borate($GdAl_3(BO_3)_4$) is another attractive DLR-reference.[33] Upon red light excitation, this phosphor shows strong NIR emission with a long luminescence decay time of approximately 100 µs. The luminescence decay time of Cr-GAB is minor effected by temperature and shows a decrease of 15 % when going from 1 to 50 °C. However, EB shows about threefold higher intensity signals compared to Cr-GAB when excited at the same wavelength (λ_{exc} 600 nm).

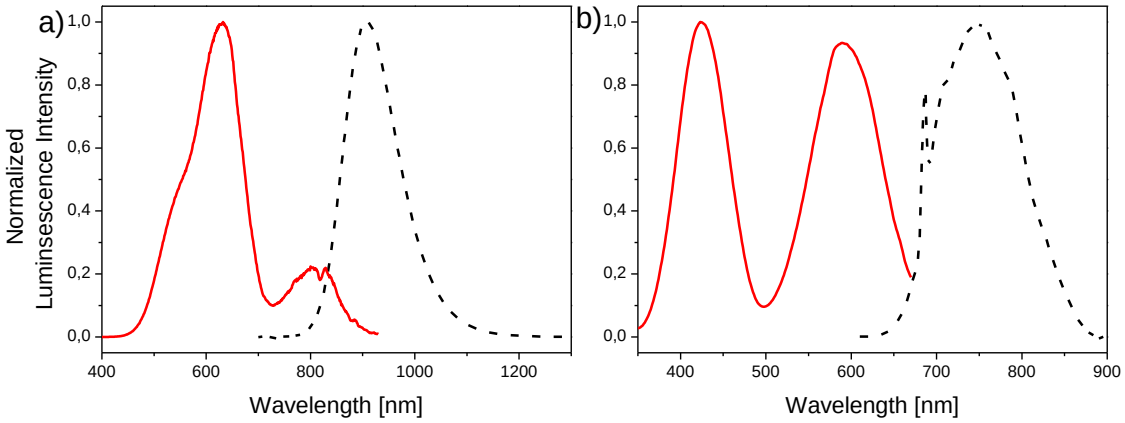

Figure 8a) Excitation (red line) and Emission spectrum (dotted lined) of Egyptian Blue and **b)** Cr-GAB powder.

Photon upconversion

Photon upconversion is a process in which an anti-Stokes photo-luminescence (visible) is generated upon excitation in the near-infrared (NIR) spectral region.[34,35] Due to excitation in the NIR, photon upconversion provides significant advantages[36]:

- Deep penetration of excitation light in biological samples
- Complete elimination of auto-fluorescence of (bio)molecules
- Absence of photodamage of biomolecules
- Less scattering

The upconversion process can be observed in transition metals and actinides but predominantly in lanthanide elements (or chemically similar elements such as yttrium and scandium). The Ln^{3+}-based upconversion process was first observed by Auzel *et al.*[34] in the 1960s. In this

pioneering work they demonstrated the upconversion of infrared to visible light by using pairs of lanthanide ions which act as sensitizer and emitter. Ytterbium (Yb^{3+}) is mainly used as sensitizer since it can be efficiently excited by NIR-light (980 continuous wave laser) and its $^2F_{7/2} \rightarrow {}^2F_{5/2}$ transitions are favorably resonant with many f-f transitions of other Ln^{3+}-ions (such as Er^{3+}, Ho^{3+}, Tm^{3+}, see Figure **9**). Lanthanide-doped materials show remarkable properties, such as extensive anti-Stokes shift, sharp emission lines and outstanding photostability. These advantages combined with NIR-excitation make these materials not only highly interesting for applications in bio-imaging,[37] bio-labelling or encoding applications[38] but also as upconverting emitters in optical sensing materials, including pH sensors.[35]

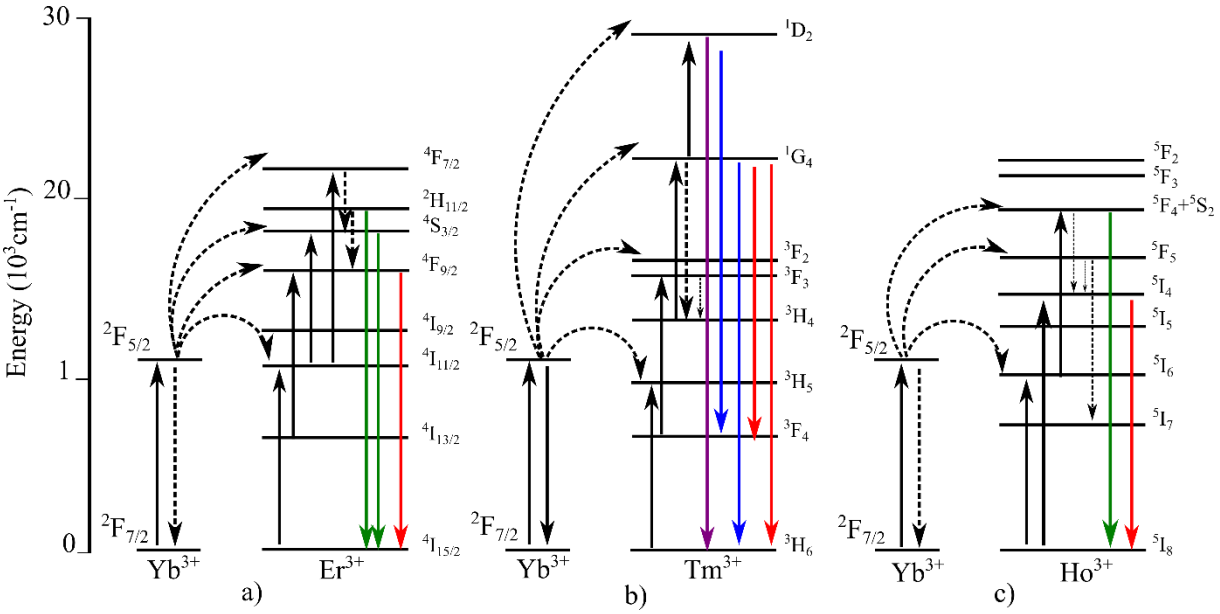

Figure **9**: Upconversion mechanism of Upconversion Particles co-doped with **a**)Yb^{3+} and Er^{3+} **b**) Yb^{3+} and Tm^{3+} **c**)Yb^{3+} and Ho^{3+}.[39]

Chapter 1

NIR-emitting aza-BODIPY Dyes – New Building Blocks for Broad-range Optical pH Sensors

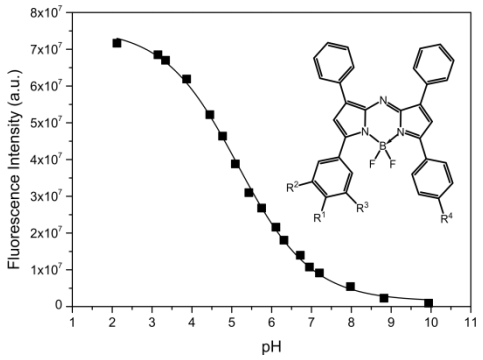

NIR-emitting aza-BODIPY Dyes – New Building Blocks for Broad-range Optical pH Sensors

This chapter was published in **Analyst**, 2015, 140, 7150-7153; doi: 10.1039/c5an01389e

Authors: **Martin Strobl**, Tanja Rappitsch, Sergey M. Borisov, Torsten Mayr and Ingo Klimant

New aza-BODIPY indicators which cover the pH scale from 1.5 to 13 are presented. The new indicators feature absorption/emission bands in the red/near-infrared (NIR) spectral region, exhibit high molar absorption coefficients (~ 80 000 $M^{-1}cm^{-1}$) and show good quantum yields (~ 20 %). All dyes exhibit virtually identical spectral and photophysical properties and, thus, represent promising building blocks for the development of a broad-range sensor for various pH-ranges. *Combination of four of these pH indicators yields a pH sensor with an extended dynamic range from pH 2 to 9.*

Introduction

Determination of pH is probably the most frequently performed analytical measurement in a wide range of sciences and technology, including chemistry, biochemistry, biotechnology[40,41], medical diagnostics, biomedical research[42,43] and many industrial applications. Traditionally, electrochemical methods have been used for pH analysis providing accurate results within a relatively short time. In the last decade, optical pH sensors (pH optodes) were established. They offer important advantages compared to (potentiometric) glass pH electrodes and ion-sensitive field-effect transistors (ISFET). They offer higher sensitivity within their dynamic range, enable contactless measurement, and are not prone to electromagnetic interferences. Additionally, the use of fiber-optic sensors allows a high degree of mechanical flexibility combined with ease of miniaturization, low production cost and the possibility of mass production[1,44,45]. A pH optode is composed of a pH sensitive indicator dye which is entrapped into a hydrophilic host polymer. The indicator dye possesses distinct optical properties associated with its protonated (acidic) and deprotonated (basic) form[46]. Depending on the concentration of hydrogen ions (pH), the absorption (color) or fluorescence emission of the indicator dye is altered, which is used as a source of analytical information.

Especially fluorescent pH sensors have gained considerable attention over absorption-based techniques due to high sensitivity and straightforward read-out in fiber-optic sensors[47–

[50]. However, the operating range of a pH indicator dye, which is controlled by its pK_a value, is fixed to a certain pH range and is limited to 3 pH units. Some attempts have been made to extend the dynamic range of optodes, for example by using a mixture of two or more pH indicators with different pK_a values or by using a single indicator with multiple dissociation constants. Several classes of fluorescent pH indicators, including coumarin-based dyes, naphthalimide derivatives or perylene bisimide probes were employed for designing a pH sensor covering a broad-range[51–55]. However, most broad-range pH sensors presented in literature suffer from several drawbacks such as complex calibration models, poor photostability and low brightness of pH dyes or excitation with UV or blue light [53], which limits their use for many applications.

Table **1**: Chemical structures of new aza-BODIPYs

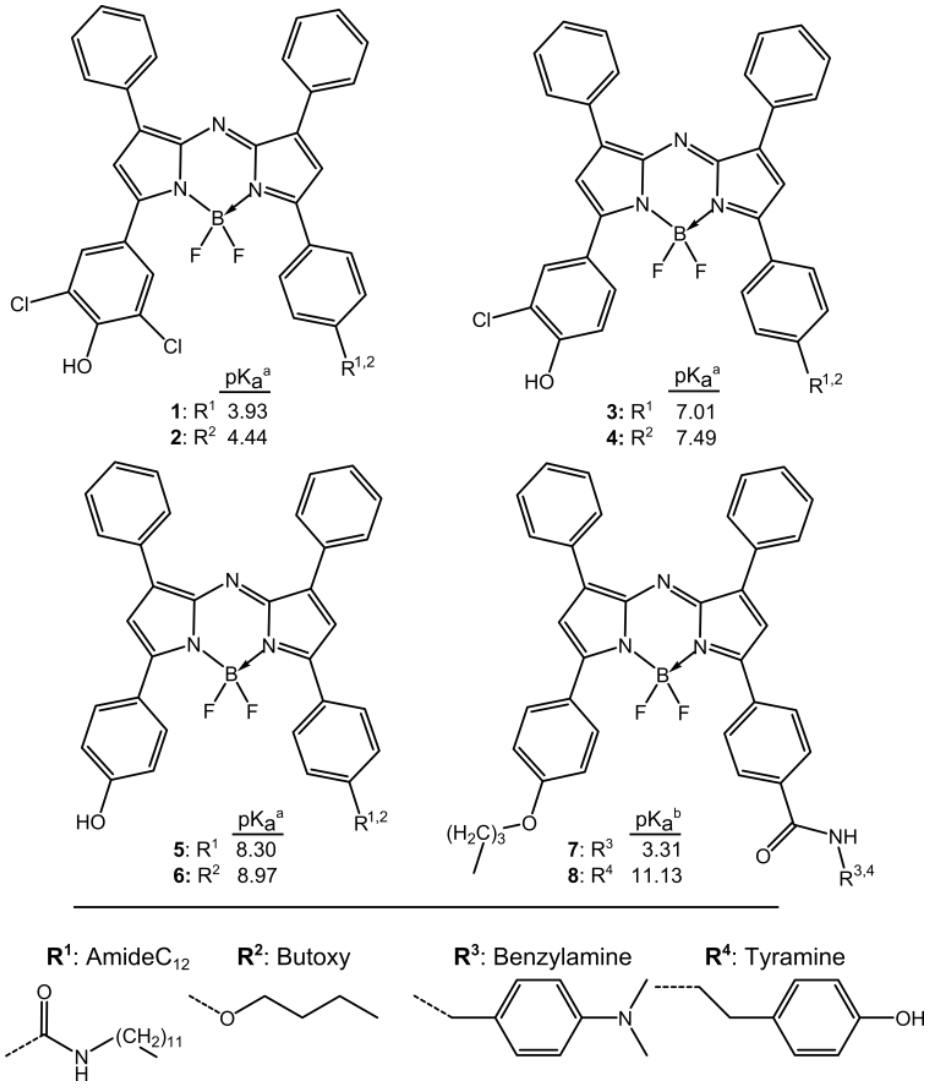

[a] pK_a value from absorption and [b] apparent pK_a' value determined from emission spectra in EtOH/buffer mixture [1:1 (v/v)], ionic strength 150 mM. For reaction conditions, see Supporting Information.

The choice of the fluorophore class plays a key role in the design of fluorescent sensors with an extended dynamic range and require to fulfill the following criteria: (i) easy accessibility of the dye structure to modification including the introduction of electron-donating or -withdrawing groups for tuning the pK_a value. (ii) virtually identical spectral properties of the used indicator dyes. This means that the functionalities determining the pK_a value should have only minimal influence on absorption or emission spectra in order to allow excitation at the same wavelength and should not significantly affect the quantum yield or the absorption coefficient. (iii) outstanding photostability of all fluorescent probes or at least equal photo-degradation rates to ensure a consistent calibration function over time. (iv) suitability for immobilization of the indicator dye by covalent linkage or by adding a lipophilic moiety to structure. This prevents the dye from leaching out of the sensor material which ensures signal stability and keeps signal drift at a minimum. In many applications, e.g. for measuring in complex biological samples, it is preferable to use fluorophores with absorption/emission profiles in the long-wavelength spectral region (650 – 750 nm) which provides many advantages: lower auto-fluorescence of biomolecules, less scattering background and deep light penetration into (biological) probes.

Among all those fluorophores presented in literature, BF_2-chelated tetraarylazadipyrromethene dyes (aza-BODIPYs) proved to be excellent candidates capable of fulfilling the requirements mentioned above. These indicator dyes are

exceptionally photo-stable, show sharp absorption/emission bands in the near-infrared region (NIR) and are highly accessible to structural modifications.[56] The pH sensitivity is obtained by a photoinduced electron transfer (PET) from an amino group or a phenolate to the aza-BODIPY's backbone causing effective fluorescence quenching in the deprotonated form. Several pH sensitive aza-BODIPY dyes functionalized with amino- or hydroxyl substituents were reported by O'Shea and co-workers[57–59]. Further work was done by Jokic *et al.*[28]. They showed that pK_a values can be tuned easily from 6 to 8, but spectral properties remain virtually identical. However, these probes cover only the near-neutral and basic range whereas aza-BODIPY dyes exhibiting pK_a values in the acidic and also very basic regions of the pH scale are not available, yet.

Aim of this work was to develop a full set of aza-BODIPY indicators to enable pH-sensing over the entire pH range. We synthesized 8 new aza-BODIPY dyes with pK_a values evenly covering the pH scale from 2.06 to 11.90. The pK_a values are lowered by substitution of one or two chlorine atoms at the pH sensitive phenol group of the indicators (probe **1 - 4**). Additional

fine tuning of the pK_a is achieved by introduction of either an electron-withdrawing carboxamide group (probe **1, 3** and **5**) or an electron-donating butoxy moiety (probe **2, 4** and **6**) as remote substituents. In order to cover extremely acidic or basic regions of the pH scale a new design concept for probe **7** and **8** was investigated. The pH sensitive PET-group is covalently linked to the aza-BODIPY via a non-π- electron-conjugating spacer group [amide moiety with methylene group(s)].

Results and Discussion

Table **2** provides an overview of the spectral and photophysical properties of the new aza-BODIPY compounds. The molar absorption coefficients ε are ranging from 80 000- 95 000 $M^{-1}cm^{-1}$ and fluorescence quantum yield are found to be within 17 -23 % in THF. The absorption of the protonated form of all dyes is similar (670-690 nm) and the emission maxima are located between 697-715 nm. pK_a values of the new probes were determined in mixtures of ethanol and aqueous buffer [1:1 (v/v)] and were derived from both absorption and emission spectra. Since in probe **1-6** the pH-sensitive phenol group is fully integrated into the dye's molecule, the absorption shifts bathochromically upon deprotonation whereas the absorption of probe **7** and **8** is pH independent. The fluorescence emission of the aza-BODIPY probes is quenched upon deprotonation which is characteristic for efficient photoinduced electron transfer from the protonated to deprotonated from.

Table **2**: Photophysical properties of the aza-BODIPY dyes: absorbance maxima for the acidic ($\lambda_{abs\text{-}acid}$) and the basic forms ($\lambda_{abs\text{-}base}$), emission maxima for the acidic form ($\lambda_{em\text{-}acid}$), molar absorption coefficients (ε) and luminescence quantum yield (ϕ_F), n.m. not measureable.

dye	$\lambda_{abs\text{-}acid}/\lambda_{abs\text{-}base}$[a] (nm)	$\lambda_{em\text{-}acid}$[a] (nm)	ε (THF)[b] ($M^{-1}cm^{-1}$)	ϕ_F (THF) % acidic/basic	pK_{abs} (D4)	pK'_{em} (D4)	pK_{abs}[a]	pK'_{em}[a]
1	670/744	697	80500	17 / n.m.	4.66	4.25	3.93	3.87
2	683/755	715	88200	19 / n.m.	5.61	5.03	4.44	4.72
3	677/738	703	91600	20 / n.m.	6.66	6.32	7.01	6.47
4	687/750	724	93500	20 / n.m.	7.57	6.54	7.49	6.54
5	678/730	708	86300	22 / n.m.	8.21	7.59	8.30	8.02
6	690/743	729	95500	23 / n.m.	9.05	8.47	8.97	8.78
7[c]	675/675	704	85300	22 / n.m.	-	2.6	-	3.31
8[c]	675/675	703	84600	19 / n.m.	-	11.9	-	11.13

[a] (EtOH/H_2O-1:1), [b] for the protonated form, [c] No pH dependence in absorption.

The pH sensors were prepared via non-covalent entrapment of the indicator dye into commercially available polyurethane-based uncharged hydrogel (Hydromed D4). It exhibits high proton-permeability with a water uptake capacity of about 50 %. The pK_a values of the aza-BODIPY derivatives can be tuned over a wide range by introducing electron-withdrawing/donating substituents in adjacent or remote positions. When probe **5** (with pK_a of 8.21) is modified at the *m*-position with a chlorine atom, the pK_a drops to 6.66 (**3**). If two chlorine atoms are substituted in the *m*-positions the pK_a further decreases to 4.66 (**1**). On the other hand, when the amide-functionality in the *p*-position of the Ar^2 ring of dye **(1, 3, 5)** is replaced by the electron-donating butoxy group (**2**, **4**, **6**), the pK_a value increases to approximately 0.9 pH units respectively. The apparent pK_a values in D4 derived from fluorescence emission are 0.4 - 0.6 pH units lower than those determined from absorption data. This may be explained by the fact that the dye's concentration is much higher in D4 than in the solution. Consequently, the indicator molecules are close enough to enable intermolecular radiationless energy transfer (FRET), which results in a lowered apparent pK_a' value [28].

These novel pH sensing materials exhibit dynamic ranges which cover the pH scale from pH 2 to pH 13. Moreover, the new aza-BODIPY dyes show virtually identical spectral

properties and thus provide the possibility of designing a pH sensor with an extended dynamic range. Probes **1**, **2**, **3** and **5** (ratio 1:1:1:1) were mixed together in the same host polymer (D4) for this purpose. Indeed, the new sensor provides a dynamic range from 2 to 9, thus an extended working range by ~ 4 pH units compared to sensors based on a single indicator.

Simple Boltzmann-fitting yields a smooth sigmoidal calibration curve (R^2 0.998) which is not distorted due to evenly distributed pK_a values.

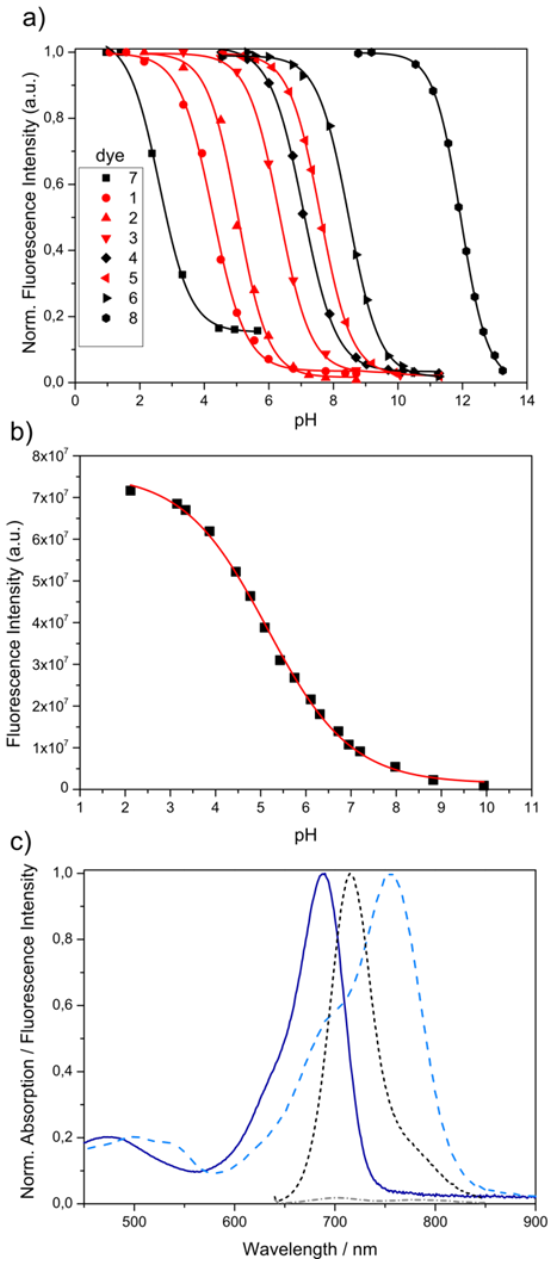

Figure 10. **a)** Calibration curves of probe **1-8**, determined in D4 from emission spectra. Combination of probe (**1, 2, 3** and **5**) (red) in D4 yields a broad-range sensor (**b**) with an extended dynamic range from pH 2 to 9. **c)** Absorption of protonated (line) and deprotonated (dashed) form and fluorescence (dashed) of the broad-range sensor.

It should be emphasized that the aza-BODIPY dyes show outstanding photostability, even under extreme illumination with a 642-nm high-power 10 W LED array for 3 hours (6300 µmol $s^{-1}m^{-2}$, see supporting information [SI]) and outperform established prominent NIR-chromophores such as cyanine dyes or lipophilic SNARF derivatives[31,60].

Additionally, the photostability of the aza-BODIPY dyes is not affected by substitution of electron-donating or -withdrawing groups. This is in contrast to other classes of pH indicators (e.g. fluorescein) where pK_a determining functionalities have a significant impact on the photostability and therefore the development of a pH sensor with broadened operating range is compromised (see SI)[61]. Moreover, cross-sensitivity to ionic strength is minimized due to the facts that aza-BODIPY dyes carry only one charge in their deprotonated form and that they are embedded into a neutral polymeric matrix [7] All dyes were modified with an alkyl chain. Consequently, due to pronounced hydrophobicity the indicator dyes do not leach out from hydrogel D4 into the aqueous solution (see SI).

Notably, probes **1, 3** and **5** exhibit a carboxy moiety before they are functionalized with an alkyl chain. Ongoing work will focus on the covalent immobilization of the aza-BODIPY dyes to a polymeric matrix via amide bond formation.

Conclusion

We presented a set of novel NIR-emitting aza-BODIPY indicators which cover the pH scale from 1.5 to 13. All dyes exhibit virtually identical spectral and photophysical properties and, thus, represent building blocks for the development of a broad-range sensor for various pH-ranges. We have shown that combination of four of these remarkably photo-stable pH dyes yields a pH sensor with an extended dynamic range from pH 2 to 9. Especially for biotechnological applications there is a surprising scarcity of pH dyes which exhibit pK_a values at acidic pH and additionally have absorption and emission bands in the red/near-infrared region. Here, aza-BODIPY dyes fulfill these requirements which make them ideal fluorophores for pH determination in most fermentation processes and also complex biological samples (e.g. growth media).

Acknowledgments

Financial support by the European Union FP7 Project BIOINTENSE – Mastering Bioprocess integration and intensification across scales (Grant Agreement Number 312148) is gratefully acknowledged.

Supporting material

Absorption and Fluorescence:

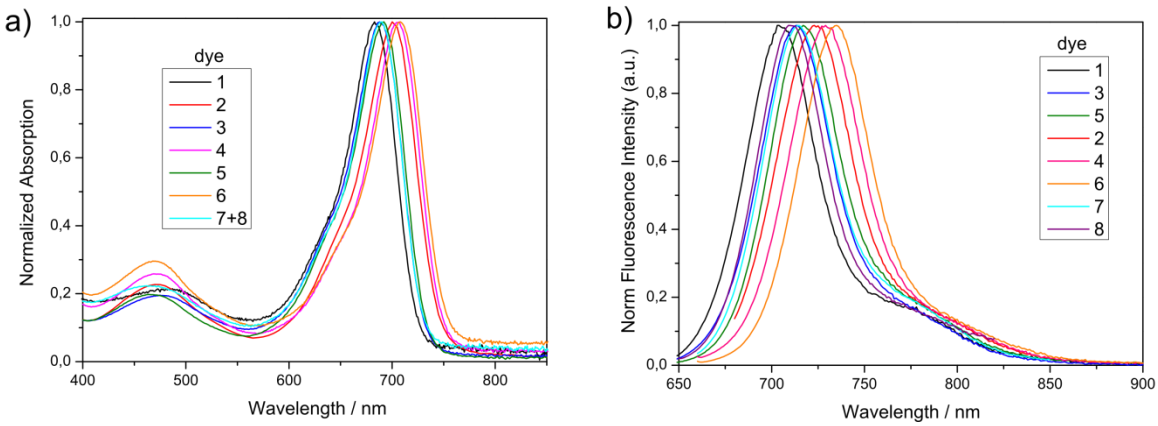

Figure S11. Normalized absorption (a) and fluorescence (b) of dyes (**1-8**)

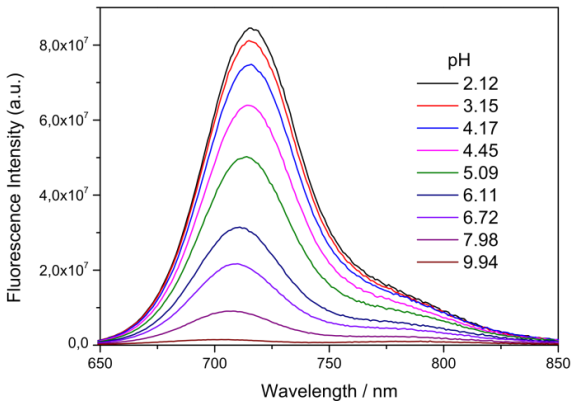

Figure S2. pH dependence of fluorescence emission of the novel broad-range pH sensor based on the mixture of dyes 1, 2, 3 and 5.

Table S1. Boltzmann equation

Model	Boltzmann
Equation	y = A2 + (A1-A2)/(1 + exp((x-x0)/dx))

Table S2. Parameters of the non-linear curve fit (Boltzmann) of broad-range sensor

A1	A2	x0	dx	R^2
7,57E+07	1,44E+06	5,14789	0,92544	0,99851

Leaching test

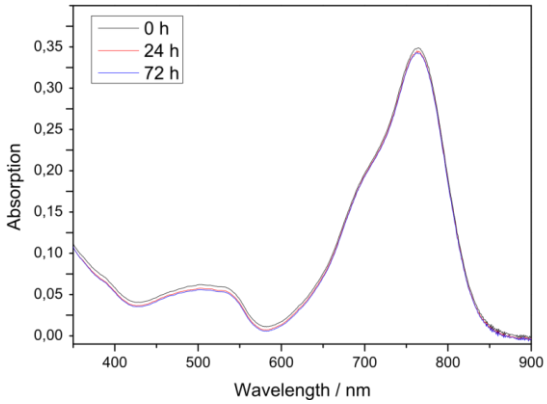

Figure S3. Absorption spectra of the broad-range sensor (dye 1, 2, 3 and 5) under continuous flushing with aqueous buffer (pH 9.2, IS 150mM). No leaching is observed.

Photostability

Photobleaching experiments of the broad-range pH sensor were performed by irradiating the samples with the light of a 642-nm high-power 10W LED array (~ 6300 µmol $s^{-1}m^{-2}$). In fact, continuous illumination for over 3 hours caused no changes in the absorption.

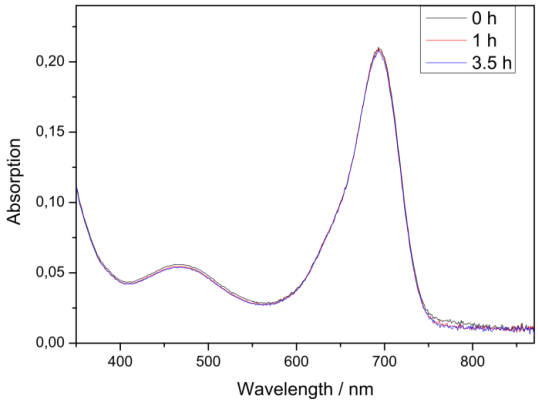

Figure S4. Absorption spectra of the broad-range sensor under continuous irradiation with a high-power LED.

Comparison with Fluorescein derivatives:

Figure **S5** shows a broad-range pH sensor based on three lipophilic fluorescein derivatives. However, the pK_a determining functionalities have significant effect on the photostability of the indicator dyes respectively. Consequently, after irradiating the pH sensor with the light of high power 10 W LED array (λ_{max} 458nm, ~ 3900 µmol $s^{-1}m^{-2}$) for 30 minutes, the calibration curve is considerably altered due to photo-bleaching of the less photo-stable 2,7-dihexyl- fluorescein-octadodecylamide. This exemplifies that other classes of pH indicator dyes (here fluorescein) are not suitable for the development of a broad-range sensor due to different photo-degradation rates.

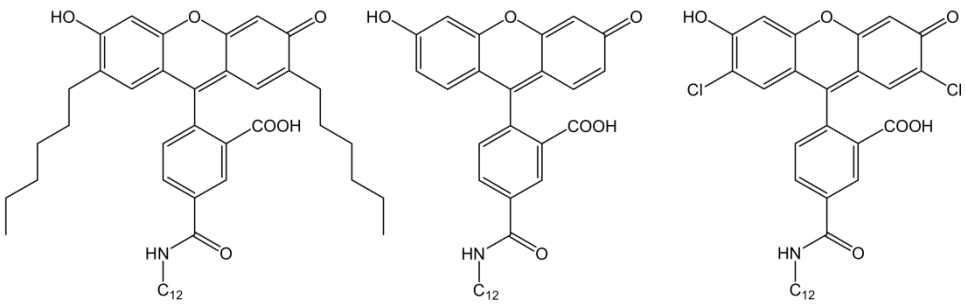

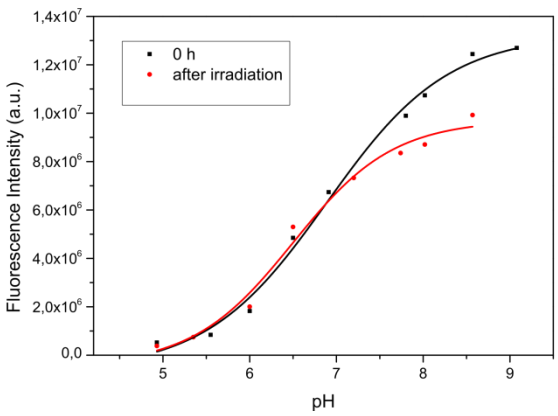

Figure S5 up: Chemical Structures of the used fluorescein derivatives. Below: calibration curve of the sensor before and after irradiation with blue LED.

Aggregation test

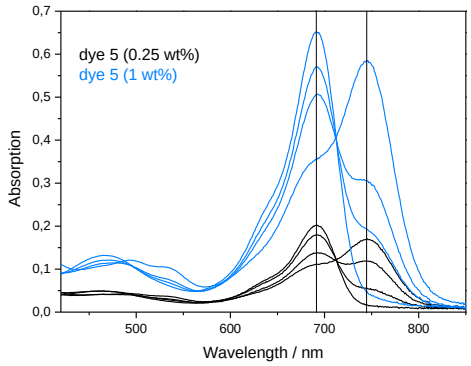

Figure S6 Aggregation

The new aza-BODIPY dyes exhibit pronounced hydrophobicity, which may favor aggregation when physically entrapped in hydrophilic host polymer. Thus, pH sensors with different dye concentrations (probe **5**, 0.25 wt% and 1wt%, respectively) were prepared and their potential aggregation was investigated via absorption measurements. No aggregation could be observed, even at high dye concentrations. The absorption peaks are not broadened and the absorption maxima of the (de)protonated form (690 nm and 745 nm, respectively) are not batho- or hypsochromically shifted and also the isobestic point remains at 711 nm when increasing the dye concentration from 0.25 to 1wt% in D4.

Materials

4'-butoxyactophenone, 4'-acetylbenzoic acid, 1-(3-dimethylaminopropyl)-3-ethylcarbodiimide hydrochloride, diisopropylethylamine, benzaldehyde and boron trifluoride diethyl etherate were purchased from TCI Europe (http://www.tcichemicals.com/en/eu/). 3',5' Dichloro-4'-hydroxyacetophenone was obtained from AApin Chemicals. (http://www.apinchemicals.com/) and 4'-hydroxychalcone was bought from ABCR (http://www.abcr.de/startseite/). 3'-Chloro-4'-hydroxyacetophenone, nitromethane, ammonium acetate, dodecylamine, 1-hydroxybenzotriazole hydrate, MOPS buffer and anhydrous sodium sulfate were purchased from Sigma Aldrich (http://www.sigmaaldrich.com/austria.html). Deuterated chloroform ($CDCl_3$) and dimethyl sulfoxide (DMSO-d_6) were obtained from Euriso-top (www.eurisotop.com). All other solvents (synthesis grade) as well as sodium chloride and the buffer salts (MES, HEPES, and CHES) were purchased from Carl Roth (www.roth.de). Silica-gel (0.04-0.063 mm) was bought from

Acros (www.fishersci.com). Polyurethane hydrogel (Hydromed D4) was purchased from AdvanSource biomaterials (www.advbiomaterials.com). Poly-(ethylene glycol terephthalate) support (Mylar) was from Pütz (http://www.puetz-folien.com/wb/pages/englisch/home.php).

Methods

Absorption measurements were performed on a Cary 50 UV-VIS spectrophotometer from Varian, Palo Alto, United States (www.varianinc.com) at medium scan rate using baseline correction and an adequate blank sample.

Fluorescence spectra of dye solutions were recorded on a Hitachi-F-7000 spectrofluorometer (www.hitachi.com), equipped with a R980 photomultiplier and corrected for detector response. Fluorescence measurements for the pH sensors were performed on a Fluorolog3 spectrofluorimeter (Horiba J. Y., www.horiba.com) equipped with a NIR-sensitive photomultiplier R2658 from Hamamatsu (300-1050 nm). Relative fluorescence quantum yields were determined by using tetra-*tert*-butyl-29*H*,31*H*-phthalocyanine as a standard (ϕ = 0.44, Fluka, www.sigmaaldrich.com) according to Demas and Crosby.

The pH of the buffer solution (acetate, MES, HEPES, CHES) was adjusted with a pH meter using a glass electrode (InoLab pH/ion, WTW GmbH & Co. KG, www.wtw.com). The pH meter was calibrated at 25°C with standard buffers of pH 7.01 and pH 4.01 (WTW GmbH & Co. KG, www.wtw.com). Ionic strength (IS = 150mM) of the buffers was adjusted by using sodium chloride as the background electrolyte.

The NMR spectroscopic experiments were performed on a 300 MHz instrument (Bruker) in DMSO-d_6 or $CDCL_3$ with TMS (tetramethylsilane) as a standard. Chemical shifts (δ) are given in parts per million (ppm) relative to TMS and coupling constants *J* are stated in Hz.

Preparation of optical sensor

A "cocktail" containing an indicator (0.25 mg), hydrogel D4 (100 mg) in 700 µl EtOH/H_2O (9:1 v/v), and tetrahydrofuran (300 µl) was knife-coated on a dust-free PET support to obtain a ~2.5 µm thick sensing layer after solvent evaporation.

The "cocktail" for the broad-range pH sensor was prepared similarly from a mixture of indicator **1**, **2**, **3**, **4** (0.05 mg respectively, total Σ 0.20 % w/w), hydrogel D4 (100mg) and dissolved in 700 µl EtOH/H_2O (9:1 v/v) and tetrahydrofuran (300 µl). Subsequently it was knife-coated in the same way as mentioned above.

Experimental Section

1-(3-chloro-4-hydroxyphenyl)-4-nitro-3-phenylbutan-1-one and 1–(4-hydroxyphenyl)-4-nitro-3-phenylbutan-1-one were synthesized according to Jokic et al.[28] 1-(4-butoxyphenyl)-4-nitro-3-phenylbutan-1-one was prepared according to literature procedure[62] The synthesis of the new aza-BODIPYs were performed in a routine step, starting from diaryl α,β-unsaturated ketones (chalcones) which were prepared by Claisen-Schmidt condensation from the corresponding acetophenone and benzaldehyde. Michael-addition of nitromethane to these chalcones provide 1,3-diaryl-4-nitrobutan-1-ones. Condensation with ammonium acetate at elevated temperature gave a mixture of azadipyrromethene dyes which were separated via chromatography. Carboxy-functionalized compounds (1, 3, 5) were modified with dodecylamine by using EDC (1-Ethyl-3-(3-dimethylaminopropyl)carbodiimide) as carboxyl activating agent in order to yield an amide bond. Attachment of dodecylamine was performed prior to complexation reaction which avoids solubility problems. Finally, complexation reaction with boron trifluoride gave the new aza-BODIPYs in moderate yield.

.

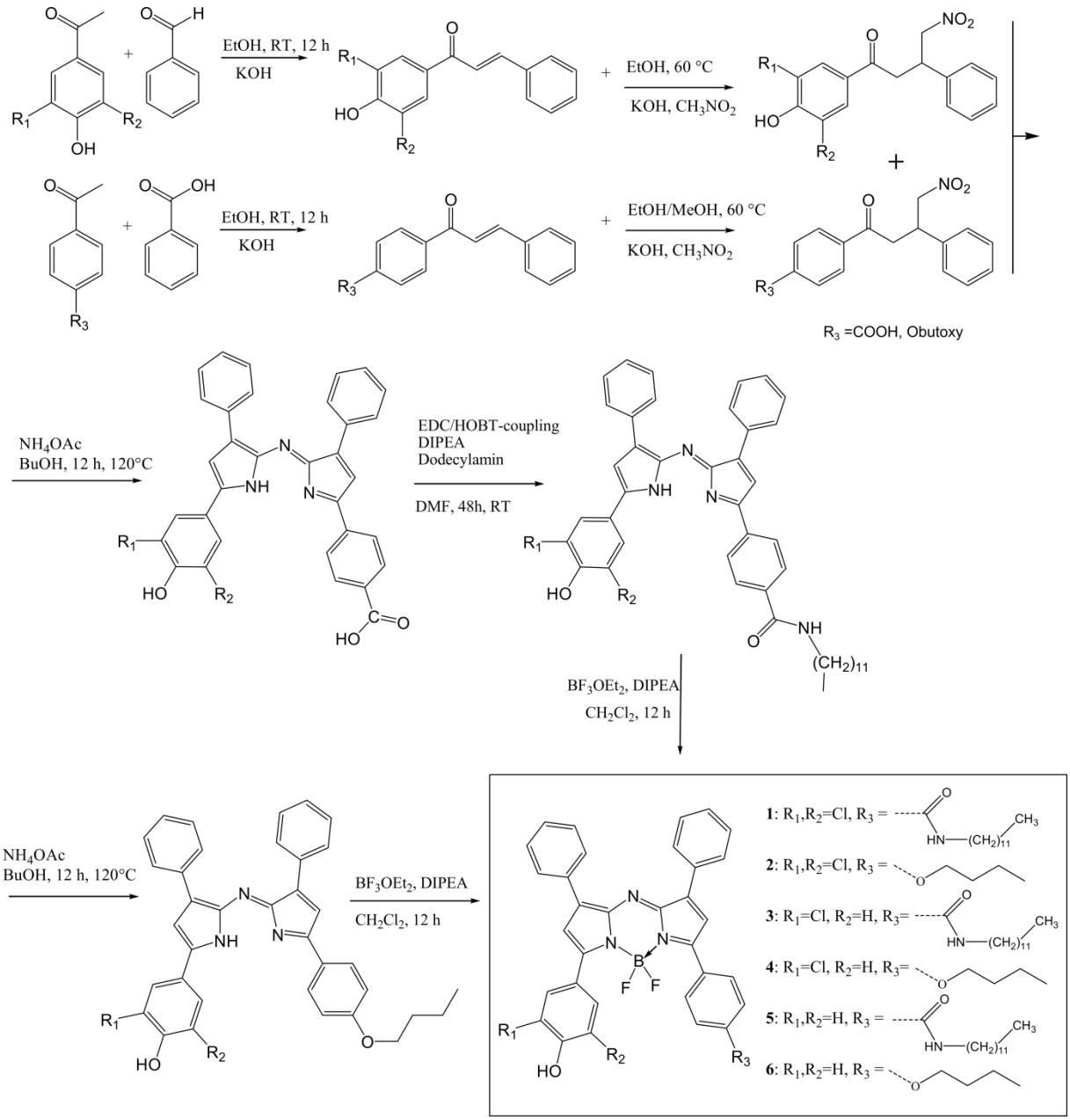

Figure **S7** Synthetic pathway of dye 1-6

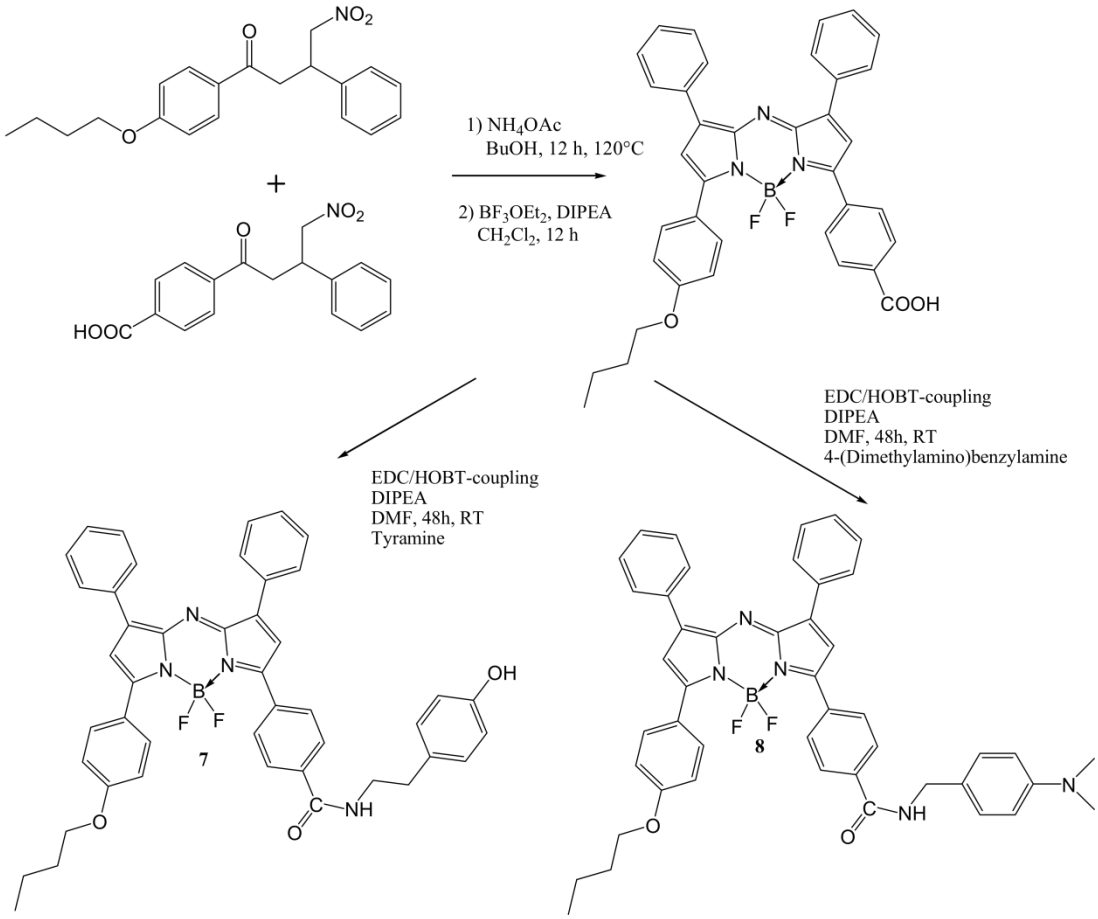

Figure S8 Synthetic pathway of dye 7 and 8

Synthesis of compound 1

4-(7-(3,5-dichloro-4-hydroxyphenyl)-5,5-difluoro-1,9-diphenyl-5H-5λ^4,6λ^4-dipyrrolo[1,2-c:2',1'-f][1,3,5,2]triazaborinin-3-yl)-N-dodecylbenzamide (1)

1-(3,5-dichloro-4-hydroxyphenyl)-3-phenylprop-2-en-1-one

3, 5 Dichloro-4-hydroxyacetophenone (1 eq, 2.01 g, 9.8 mmol), benzaldehyde (1 eq, 997 µl, 9.8 mmol) and potassium hydroxide (3 eq, 1.65 g, 29.4 mmol in 8 ml H_2O) were dissolved in ethanol (20ml) and stirred at room temperature for 12 hours. During the course of the reaction the product partly precipitates from the reaction mixture. Then, the reaction solution was acidified with hydrochloric acid (1M) and the resulting light yellow precipitate was isolated by filtration and washed with water. The precipitate was dried under reduced pressure and was used for the next step without further purification (2.85 g).

1-(3,5-dichloro-4-hydroxyphenyl)-4-nitro-3-phenylbutan-1-one (**1a**)

After 1-(3-chloro-4-hydroxyphenyl)-3-phenylpropenone (1 eq, 3.10 g, 120 mmol) was dissolved in ethanol/methanol (5:1 v/v, 60 ml), nitromethane (20 eq, 1.96 ml, 239 mmol) and potassium hydroxide (1.3 eq, 0.87 g, 15.6 mmol) were added and the reaction was heated at 65 °C for three hours. After cooling, the solvent was removed in vacuum and the resulting oily residue was acidified with hydrochloric acid (0.1 M) and was partitioned between ethyl acetate and water in a separating funnel. The organic layer was separated, dried over sodium sulfate and the solvent evaporated under reduced pressure. The obtained product was used for the next step without purification (3.37g, 88.0 %)

4-((E)-3-phenylacryloyl) benzoic acid

A solution of 4-acetylbenzoic acid (1 eq, 2.50 g, 15 mmol) and benzaldehyde (1 eq, 1.55 ml, 15 mmol) and potassium hydroxide (3 eq, 2.56 g, 47 mmol in 8 ml H_2O) in ethanol (100ml) was stirred at room temperature for 12 hours. During the course of the reaction the product partly precipitated from the reaction mixture. Then, the reaction solution was acidified with hydrochloric acid (1M) and the solid was collected on a filter and washed with distilled water to afford the title compound in quantitative yields (3.8 g).

4-(4-nitro-3-phenylbutanoyl) benzoic acid (**1b**)

4-((E)-3-phenylacryloyl) benzoic acid (1 eq, 3.80 g, 15.1 mmol) was dissolved in methanol (175 ml) nitromethane (20 eq, 16 ml, 301 mmol) and potassium hydroxide (1.3 eq, 1.10 g, 19.6

mmol) were added and the reaction was heated under reflux for 6 hours. After cooling to room temperature, the solvent was removed in vacuum. The resulting oily residue was acidified with 0.1 N HCl and was partitioned between ethyl acetate and distilled water in a separating funnel. The organic layer was separated, dried over sodium sulfate and evaporated under reduced pressure. (3.27 g, 67.6 %)

(Z)-4-(5-((5-(3,5-dichloro-4-hydroxyphenyl)-3-phenyl-2H-pyrrol-2-ylidene)amino)-4-phenyl-1H-pyrrol-2-yl)benzoic acid (**1c**)

Compound **1a** (1 eq, 1.55 g, 4.4 mmol) and compound **1b** (1 eq, 1.37 g, 4.4 mmol) and ammonium acetate (35 eq, 17.10 g, 222 mmol) were dissolved in butanol (35 ml) and heated under reflux for 12 hours while stirring. After cooling, the solvent was removed under reduced pressure. The obtained solid was washed with water three times and the crude product was purified by column chromatography on silica-gel eluting with a MeOH/CH_2Cl_2 mixture. After eluting the symmetrical by-product with 2% MeOH/CH_2CL_2 the final product was obtained by gradually increasing the polarity to 12-18% MeOH/CH_2Cl_2 and the solvent evaporated under vacuum. The final product was recrystallized from hexane/tetrahydrofuran mixture (1:1) and dried in an oven at 60 °C. (231 mg, 8 %) For the calculation, the theoretical yield of the asymmetrical product is set as 100%.

(Z)-4-(5-((5-(3,5-dichloro-4-hydroxyphenyl)-3-phenyl-2H-pyrrol-2-ylidene)amino)-4-phenyl-1H-pyrrol-2-yl)-N-dodecylbenzamide (**1d**)

A solution of **1c** (1 eq, 231 mg, 0.4 mmol), 1-hydroxybenzotriazole hydrate (1.2 eq, 64.8 mg 0.48 mmol), 1-(3-dimethylaminopropyl)3-ethylcarbodiimide hydrochloride (EDC, 1,2 eq, 91,8 mg, 0.48 mmol) dodecylamine (1 eq, 74.0 mg, 0.4 mmol) and diisopropylethylamine (DIPEA, 5 eq, 333 µl, 2 mmol) in DMF was stirred at room temperature for 48 hours. Then the product was precipitated by adding saturated NaCl solution and collected by centrifugation. The crude solid was purified by column chromatography on silica gel, eluting with 2.5 % EtOH/CH_2Cl_2. The fractions were united and the solvent was removed under reduced pressure and the resulting blue solid was recrystallized from hexane/tetrahydrofuran. (32 mg, **19.8** %)

4-(7-(3,5-dichloro-4-hydroxyphenyl)-5,5-difluoro-1,9-diphenyl-5H-5λ^4,6λ^4-dipyrrolo[1,2-c:2',1'-f][1,3,5,2]triazaborinin-3-yl)-N-dodecylbenzamide (**1**)

1d (1 eq, 25 mg, 0.035 mmol) was dissolved in dry CH_2Cl_2 (20 ml) N,N-diisopropylethylamine (DIPEA, 10 eq, 0.35 mmol 61 µl) and boron trifluoride diethyl etherate (15 eq, 0.53 mmol, 65

µl) were added under inert atmosphere (N_2) and the solution was stirred at room temperature for 12 hours. The green-blue solution was shaken with water and dichloromethane three times and dried over sodium sulfate. The product was purified by column chromatography on silica gel using 2-4 % EtOH/ CH_2Cl_2 as eluent. The fractions containing the product were united and the solvent was removed under reduced pressure. Further purification was achieved by crystallization from hexane/tetrahydrofuran to give the final product as a blue powder. (15 mg, 55.6 %)

^{1}H- NMR (300 MHz, $CDCl_3$) δ: 8.12-8.04 (m, 8H); 7.94-7.85 (m, 2H); 7.47-7.34 (m, 6H); 7.07 (s, 1H); 6.98 (s, 1H); 6.2 (t, *J* =5.3 Hz, 1H) 3.47 (1, *J* = 6.8 Hz, 2H); 1.67-1.58 (m, 3H); 1.36-1.27 (m, 18H); 0.88 (t, *J* = 5.8 Hz, 3H)

MALDI-TOF *m/z* found 792.2934 calculated 792.2988.

Synthesis of compound 2

(Z)-4-(2-((5-(4-butoxyphenyl)-3-phenyl-1H-pyrrol-2-yl)imino)-3-phenyl-2H-pyrrol-5-yl)-2,6-dichlorophenol (2a)

Compound **1a** (1 eq, 1.16 g, 3.3 mmol) and 1-(4-butoxyphenyl)-4-nitro-3-phenylbutan-1-one (1 eq, 1.12 g, 3.3 mmol) were dissolved in butanol (30 ml). Ammonium acetate (35 eq, 17.10 g, 115 mmol) was added and the reaction solution was heated at 120 °C under reflux for 12 hours. After cooling to room temperature, the solvent was removed under reduced pressure. Afterwards the solid was redissolved in CH_2Cl_2 and washed with water three times. Then, the solid was purified by column chromatography on silica gel. After eluting the first symmetrical by-product with cyclohexane/dichloromethane (1:1 v/v), the product was eluted with dichloromethane and the solvent was removed under reduced pressure. Further purification was achieved by crystallization from hexane/tetrahydrofuran to give the dye as blue powder. For the calculation, the theoretical yield of the asymmetrical product is set as 100 %. (526 mg, 26.6 %)

4-(7-(4-butoxyphenyl)-5,5-difluoro-1,9-diphenyl-5H-4λ^4,5λ^4-dipyrrolo[1,2-c:2',1'-f][1,3,5,2]triazaborinin-3-yl)-2,6-dichlorophenol ***(2)***

Compound **2a** (1 eq, 526 mg, 0.87 mmol) was dissolved in CH_2Cl_2 (25 ml). *N*,*N*-diisopropylethylamine (DIPEA, 10 eq, 8.7 mmol, 1.51 ml) and boron trifluoride diethyl etherate (15 eq, 13.0 mmol, 1.59 ml) were added under N_2-atmosphere and the reaction solution was

stirred at room temperature overnight. Then, the green solution was washed with water three times. The product was purified by column chromatography (silica gel in cyclohexane). The product was obtained by gradually increasing the polarity of cyclohexane/CH_2Cl_2 (1:1.5 -1:3 v/v). Further purification was achieved by crystallization from hexane/tetrahydrofuran to give the final product as a red-metallic solid. (162 mg, 30.8 %)

^{1}H NMR (300 MHz, $CDCl_3$) δ: 8.15 (d *J* = 9.0 Hz, 2H); 8.06 (m, *J* = 8.6 Hz; 4H); 8.03 (s, 2H); 7.46 (t, *J* = 7.4 Hz, 6H); 7.16 (s, 1H); 7.03 (d, 2H); 6.90 (s, 1H); 4.12 (t, *J* = 7.86 Hz, 2H); 1.75 (q, 2H); 1.47 (q, 2H); 0.96 (t, *J* = 7.3 Hz, 3H)

MALDI-TOF *m/z* found 653.1664 calculated 653.1626

Synthesis of compound 3

(Z)-4-(5-((5-(3-chloro-4-hydroxyphenyl)-3-phenyl-2H-pyrrol-2-ylidene)amino)-4-phenyl-1H-pyrrol-2-yl)benzoic acid (3a)

1-(3-chloro-4-hydroxyphenyl)-4-nitro-3-phenylbutan-1-one (1 eq, 2.03 g, 6.3mmol) was dissolved in butanol (100 ml). Compound **1b** (1 eq, 1.99 g, 6.3 mmol) and ammonium acetate (35 eq, 17.10 g, 222 mmol) were added and the reaction solution was heated at 120 °C for 12 hours. After cooling to room temperature the solvent was removed under reduced pressure. Afterwards the solid was washed with water three times. The crude solid was purified by column chromatography on silica gel using CH_2Cl_2. After eluting impurities and symmetrical by-product with 5% MeOH/CH_2Cl_2, the final product was obtained by increasing the polarity of the eluent (10-12% MeOH/CH_2Cl_2). Afterwards the blue-black solid was recrystallized from hexane/tetrahydrofuran mixture. For the calculation, the theoretical yield of the asymmetrical product is set as 100 %. (359 mg, **10.4 %**)

*(Z)-4-(5-((5-(3-chloro-4-hydroxyphenyl)-3-phenyl-2H-pyrrol-2-ylidene)amino)-4-phenyl-1H-pyrrol-2-yl)-N-dodecylbenzamide **(3b)***

3a (1 eq, 122 mg, 0.224 mmol) was dissolved in DMF (20 ml). N-hydroxysuccinimide (1.01 eq, 26.1 mg 0.227 mmol), dodecylamine (1.01 eq, 42.0 mg, 0.227 mmol) and 1-(3-dimethylaminopropyl)3-ethylcarbodiimide hydrochloride EDC (1.01 eq, 43.5 mg, 0.227 mmol) were added and the reaction solution was stirred at room temperature for 48 hours. Then, the dye was precipitated by adding saturated NaCl-solution and separated by centrifugation. The crude product was purified by column chromatography on silica gel, eluting with 2.5 %

EtOH/CH_2Cl_2. Further purification was achieved by crystallization from hexane-THF mixture. (32 mg, **19.8 %)**

*4-(7-(3-chloro-4-hydroxyphenyl)-5,5-difluoro-1,9-diphenyl-5H-5λ^4,6λ^4-dipyrrolo[1,2-c:2',1'-f][1,3,5,2]triazaborinin-3-yl)-N-dodecylbenzamide **(3)***

3b (1 eq, 25 mg, 0.035 mmol) was dissolved in dry CH_2Cl_2 (20 ml) *N*,*N*-diisopropylethylamine (DIPEA, 10 eq, 0.35 mmol 61 µL) was added and the solvent wat stirred at room temperature. Boron trifluoride diethyl etherate (15 eq, 0.53 mmol, 65 µL) was added under N_2-atmosphere and the reaction solution was stirred overnight. The green-blue solution was partitioned with water and dichloromethane three times and dried over sodium sulphate. The crude solid was purified by column chromatography on silica gel in CH_2Cl_2. The product was obtained by gradually increasing the polarity to 2-4 % EtOH/ CH_2Cl_2. The fractions containing the product were united and the solvent was removed under reduced pressure. Further purification was achieved by crystallization from hexane/tetrahydrofuran to give the final product as a blue powder. (15 mg, **55.6 %)**

^{1}H- NMR (300 MHz, $CDCl_3$) δ: 8.10-7.94 (m, 7H); 7.86-7.83 (d, *J* = 8.4 Hz, 2H); 7.45-7.43 (m, 6H); 7.14-7.11 (s, 1H); 7.03 (d, *J* = 7.4 Hz, 2H); 6.24 (t, *J* =5.5 Hz, 1H) 3.46 (m, 2H); 1.64-1.60 (m, 4H); 1.34-1.26 (m, 18H); 0.88 (t, *J* = 6.4 Hz, 3H)

MALDI-TOF: *m/z* found 758.3310, calculated 758.3378.

Synthesis compound 4

(Z)-4-(2-((5-(4-butoxyphenyl)-3-phenyl-1H-pyrrol-2-yl)imino)-3-phenyl-2H-pyrrol-5-yl)-2-chlorophenol (4a)

1-(3-chloro-4-hydroxyphenyl)-4-nitro-3-phenylbutan-1-one (1 eq, 2.93 g, 9.16 mmol) and 4-butoxyphenyl)-4-nitro-3-phenylbutan-1-one (1 eq, 2.55 g, 7.46 mmol) were dissolved in 100 ml 2-propanol and ammonium acetate (35 eq, 20.12 g, 261 mmol) was added. Then the solution was heated at 110 °C and stirred overnight. The next day, the solvent was removed under reduced pressure and the residue was redissolved in CH_2Cl_2 and washed with water three times. The crude solid was purified by column chromatography on silica gel, eluting with CH_2Cl_2/n-hexane (1:1 v/v). Further purification was achieved by crystallization from hexane/tetrahydrofuran to give the final product as a red-metallic solid. (1.49 g, **35 %**).

^{1}H-NMR (300 MHz, DMSO-*d6*) : 8.07 (d, *J* = 6.7 Hz, 5H); 7.98 (d, *J* = 8.6 Hz, 2H); 7.89 - 7.82 (m, 1 H); 7.58 (s, 1 H); 7.53 (s, 1H); 7.42 (dt, *J* = 15.3 Hz,7.0 Hz, 6H); 7.18 (d, *J* = 8.5 Hz, 1H); 7.14 - 7.06 (m, 2H); 4.09 (t, *J* = 6.4 Hz, 2H); 1.75 (p, *J* = 6.5 Hz, 2H); 1.48 (h, *J* = 7.2 Hz, 2H); 0.97 (t, *J* = 7.3 Hz, 3H)

*4-(7-(4-butoxyphenyl)-5,5-difluoro-1,9-diphenyl-5H-4λ^4,5λ^4-dipyrrolo[1,2-c:2',1'-f][1,3,5,2]triazaborinin-3-yl)-2-chlorophenol (**4**)*

Compound **4a** (1.41 g, 2.47 mmol) was dissolved in anhydrous CH_2Cl_2 under inert atmosphere (N_2). Afterwards *N'N*-diisopropylethylamine (DIPEA, 10 eq, 4.2 ml, 24.7 mmol) and BF_3 diethyl etherate (15 eq, 4.57 ml, 37.0 mmol) were added and the solution was stirred over night at room temperature. Then, the green solution was washed with water three times. The product was purified by column chromatography (silica gel in cyclohexane). The product was obtained by eluting with cyclohexane/CH_2Cl_2 (1:1 v/v). Further purification was achieved by crystallization from hexane/tetrahydrofuran to give the final product as a red-metallic solid. 370 mg (**25 %**).

^{1}H NMR (300 MHz, DMSO-*d6*) δ: 8.23-8.15 (m, 7H); 8.04-8.01 (m, 1H); 7.64-7.45 (m, 9H); 7.16-7.1 (m, 3H); 4.12 (t, *J*= 6.4 Hz, 2H); 1.83-1.66 (m, 2H); 1.57-1.38 (m, 2H); 0.96 (t, *J*= 7.4 Hz, 3H)

MALDI-TOF *m/z* found 619.157 calculated 619.201

Synthesis of compound 5

(Z)-4-(5-((5-(4-hydroxyphenyl)-3-phenyl-2H-pyrrol-2-ylidene)amino)-4-phenyl-1H-pyrrol-2-yl)benzoic acid (5a)

1–(4-hydroxyphenyl)-4-nitro-3-phenylbutan-1-one (1 eq, 2 g, 7 mmol), compound **1b** (1 eq, 2.19 g, 7 mmol) and ammonium acetate (35 eq, 15.22 g, 245 mmol) were dissolved in butanol (100 ml) and the solution was heated under reflux at a temperature of 120 °C for 12 h while stirring. After the reaction was cooled down to room temperature the solvent was removed in vacuum. The obtained solid was washed with water three times. Then the raw product was purified by column chromatography by gradually increasing the polarity to 10-18% THF/CH_2Cl_2. The final product was recrystalized from hexane/tetrahydrofuran mixture and dried in the oven at 60 °C. For the calculation, the theoretical yield of the asymmetrical product is set as 100%. (300 mg, **12 %**)

^{1}H NMR (300 MHz, DMSO-*d6*) δ: 8.19-8.06 (m, 8H); 7.99-7.96 (d, J = 8.3 Hz, 2H); 7.87 (s 1H), 7.51-7.33 (m, 7H); 7.08-7.05 (d, J= 8.6 Hz, 2H)

Electron impact direct insertion time-of-flight (EI-DI-TOF) *m/z* [MH^+] found 510.184, calc. 510.1818.

*(Z)-N-dodecyl-4-(5-((5-(4-hydroxyphenyl)-3-phenyl-2H-pyrrol-2-ylidene)amino)-4-phenyl-1H-pyrrol-2-yl)benzamide (**5b**)*

5a (1 eq, 150 mg, 0.295 mmol) was dissolved in DMF (20 ml). N-hydroxysuccinimide (1.01 eq, 34 mg 0.297 mmol), dodecylamine (1.01 eq, 55 mg, 0.297 mmol) and EDC (1.01 eq, 57 mg, 0.297 mmol) were added and the reaction solution was stirred at room temperature for 48 hours. Then, the dye was precipitated by adding saturated NaCl solution and separated by centrifugation. The crude product was purified by column chromatography on silica gel, eluting with 2.5 % EtOH/CH_2Cl_2. Further purification was achieved by crystallization from hexane-THF mixture. (50 mg, **25 %**)

^{1}H NMR (300 MHz, DMSO-*d6*) δ: 8.57 (t, J= 6.0 Hz, 1H); 8.18-7.96 (m, 12H); 7.85 (s, 1H); 7.53-7.33 (m, 7H); 7.05 (d, J= 8.6 Hz, 3H); 1.56 (m, 2H); 1.36-1.22 (m, 20 H); 0.84 (m, 3H)

*4-(5,5-difluoro-7-(4-hydroxyphenyl)-1,9-diphenyl-5H-5λ^4,6λ^4-dipyrrolo[1,2-c:2',1'-f][1,3,5,2]triazaborinin-3-yl)-N-dodecylbenzamide **(5)***

5b (1 eq, 50 mg, 0.074 mmol) was dissolved in dry CH_2Cl_2 (20 ml) *N,N*-diisopropylethylamine (DIPEA, 10 eq, 0.74 mmol 122 µl) was added and stirred at room temperature. Afterwards boron trifluoride diethyl etherate (15 eq, 1.11 mmol, 139 µl) was added under N_2-atmosphere and the reaction solution was stirred overnight. The green-blue solution was partitioned with water and dichloromethane three times and dried over sodium sulphate. The crude solid was purified by column chromatography on silica gel in CH_2Cl_2. The product was obtained by gradually increasing the polarity from 2-4 % EtOH/ CH_2Cl_2. The fractions containing the product were united and the solvent was removed under reduced pressure. Further purification was achieved by crystallization from hexane/tetrahydrofuran to give the final product as a blue powder. (29.7 mg, **55.6 %**)

^{1}H NMR (300 MHz, DMSO-*d6*) δ: 8.6-6.5 (m, 20H); 1.6-0.8 (m, 25H)

MALDI-TOF *m/z* found 724.368 calculated 724.376

Synthesis of compound 6

(Z)-4-(2-((5-(4-butoxyphenyl)-3-phenyl-1H-pyrrol-2-yl)imino)-3-phenyl-2H-pyrrol-5-yl)phenol (6a)

1–(4-hydroxyphenyl)-4-nitro-3-phenylbutan-1-one (1 eq, 1.75 g, 6.15 mmol), 1-(4-butoxyphenyl)-4-nitro-3-phenylbutan-1-one (1 eq, 2.10 g, 6.15 mmol) and ammonium acetate (35 eq, 16.6 g, 215 mmol) were dissolved in butanol (100 ml) and heated under reflux at a temperature of 120 °C for 12 h while stirring. After the reaction was cooled down to room temperature the solvent was removed in vacuum. The obtained solid was washed with water three times. Then the raw product was purified by column chromatography, eluting with CH_2Cl_2/n-hexane (1:1 v/v). The final product was recrystallized from hexane/tetrahydrofuran mixture and dried in the oven at 60 °C. For the calculation, the theoretical yield of the asymmetrical product is set as 100%. (352 mg, **32 %**)

^{1}H NMR (300 MHz, DMSO-*d6*) δ: 8.09 (d, J= 7.3 Hz, 4H); 7.98 (d, *J* = 8.7 Hz, 4H); 7.59-7.35 (m, 8H); 7.18 (d, *J*=8.8 Hz, 2H); 7.02 (d, J= 8.6 Hz, 2H); 4.11 (t, *J*= 6.4 Hz,2H); 1.8-1.71 (m, 2H); 1.54 -1.4 (m, 2H); 0.97 (t, *J*= 7.3 Hz, 3H)

*4-(7-(4-butoxyphenyl)-5,5-difluoro-1,9-diphenyl-5H-4λ^4,5λ^4-dipyrrolo[1,2-c:2',1'-f][1,3,5,2]triazaborinin-3-yl)phenol (**6**)*

Compound 6c (1eq, 200 mg, 0.37 mmol) was dissolved in dry CH_2Cl_2 (20 ml) N,N-diisopropylethylamine (DIPEA, 10 eq, 3.7 mmol 618 µl) was added and stirred at room temperature. Afterwards boron trifluoride diethyl etherate (15 eq, 5.6 mmol, 702 µl) was added under N_2-atmosphere and the reaction solution was stirred overnight. The green-blue solution was partitioned with water and dichloromethane in a separating funnel three times and dried over sodium sulphate. The crude solid was purified by column chromatography on silica gel in CH_2Cl_2. The product was obtained by gradually increasing the polarity to 2-4 % EtOH/ CH_2Cl_2. Further purification was achieved by crystallization from hexane/tetrahydrofuran to give the final product as a blue powder. (121 mg, **55.6 %**)

^{1}H NMR (300 MHz, DMSO-*d6*) δ: 8.17-8.12 (m, 8H); 7.63 (s, 1H); 7.57-7.43 (m, 7H); 7.13 (d, *J*= 8.8 Hz, 2H); 6.95 (d, 8.7Hz, 2H); 4.11 (t, J= 6.4 Hz, 2H); 1.74 (m, 2H), 1.47 (m, 2H; 0.96 (t, *J*= 7.4 Hz, 3H)

MALDI-TOF *m/z* found 585.180 calculated 585.240

Synthesis of compound 7

(Z)-4-(5-((5-(4-butoxyphenyl)-3-phenyl-2H-pyrrol-2-ylidene)amino)-4-phenyl-1H-pyrrol-2-yl)benzoic acid (7a)

Compound **1b** (4.59 g, 14.67 mmol, 1eq) and 1-(4-butoxyphenyl)-4-nitro-3-phenylbutan-1-one (5.03 g, 14.67 mmol, 1 eq.) and ammonium acetate (41.6, 539 mmol, 35 eq.) were dissolved in butanol (100 ml) and stirred at 120 °C for 18 hours. The solvent of the blue mixture was removed by rotary evaporation and the residue was extracted with dichloromethane and H2O and the combined organic layers were concentrated under reduced pressure. The crude product was purified by column chromatography on silica-gel by eluting with 5 % THF/CH_2Cl_2. Finally the product was re-crystallized from hexane /tetrahydrofuran to obtain green-red shimmered crystals (1.083 g, **13 %**)

*3-(4-butoxyphenyl)-7-(4-carboxyphenyl)-5,5-difluoro-1,9-diphenyl-5H-dipyrrolo[1,2-c:2',1'-f][1,3,5,2]triazaborinin-4-ium-5-uide **(7b)***

Compound 7a (1.083 g, 1.914 mmol, 1eq.) was dissolved in dry dichloromethane (350 ml) under inert atmosphere by using nitrogen. Then, boron trifluoride diethyletherate (3.6 ml, 29.18 mmol, 15 eq.) and DIPEA (3.188 ml, 19.16 mmol, 10 eq.) were added with a syringe and the reaction was stirred for 21 hours at room temperature. Then, the green solution was partitioned between dichloromethane and H_2O in a separating funnel and the organic layer dried over sodium sulphate. The crude product was purified by column chromatography on silica-gel by eluting again with 5 % THF/CH_2Cl_2. Hexane and tetrahydrofuran was used for crystallisation. (0.907 g, **77.2 %**)

^{1}H NMR (300 MHz, DMSO-d_6) δ:8.17-7.18 (m, 20H), 4.13 (t, *J* = 6.2 Hz, 2H), 1.79-1.69 (m, J = 6.6 Hz, 2H), 1.52-1.39 (m, *J*= 7.4 Hz, 2H), 0.95 (t, *J* = 7.4 Hz, 3H).

*3-(4-butoxyphenyl)-7-(4-((4-(dimethylamino)benzyl)carbamoyl)phenyl)-5,5-difluoro-1,9-diphenyl-5H-dipyrrolo[1,2-c:2',1'-f][1,3,5,2]triazaborinin-4-ium-5-uide **(7)***

Compound **7 b** (102.6 mg, 0.167 mmol, 1 eq.), EDC (40 mg, 0.208 mmol, 1.2 eq), 1-hydroxybenzotriazole hydrate (30.5 mg, 0.225 mmol 1.2 eq.) and 4-(dimethylamino)benzylamine (29.3 mg, 0.225 mmol, 1 eq.) were dissolved in DMF. Then *N*,*N*-diisopropylethylamine (140 µL, 0.841 mmol, 5 eq.) was added, the mixture was stirred at room temperature for 22 hours and the solvent was removed by rotary evaporation. The solvent was extracted with dichloromethane (100 ml) and H_2O (100 ml), dried over sodium sulphate and

purified via column chromatography on silica gel by eluting with 2 % THF/ CH_2Cl_2. Hexane and tetrahydrofuran was used for crystallization. (0.097 g, **64.0 %**)

^{1}H NMR (300 MHz, Chloroform-d_6) δ: 8.14-8.03 (m, *J* = 14.3 Hz, 8H), 7.87-7.84 (d, *J* = 8.4 Hz, 2H), 7.48-7.40 (m, *J* = 7.3 Hz, 6H), 7.24 (s, 2H), 7.01-6.98 (d, *J* = 8.7 Hz, 3H), 6.75-6.72 (d, *J* = 8.7 Hz, 2H), 6.31 (t, *J* = 4.5 Hz, 1H), 4.57-4.55 (d, *J* = 5.2 Hz, 2H), 4.05 (t, *J* = 6.4 Hz, 2H), 2.95 (s, 6H), 1.84-1.75 (m, *J* = 6.6 Hz, 2H), 1.54-1.47 (m, 2H), 0.99 (t, *J* = 7.4 Hz, 3H).

Synthesis of compound 8

3-(4-butoxyphenyl)-5,5-difluoro-7-(4-((4-hydroxybenzyl)carbamoyl)phenyl)-1,9-diphenyl-5H-dipyrrolo[1,2-c:2',1'-f][1,3,5,2]triazaborinin-4-ium-5-uide (8)

Compound **7 b** (50 mg, 0.08 mmol, 1 eq.), EDC (18.7 mg, 0.09 mmol, 1.2 eq), 1-hydroxybenzotriazole hydrate (13.2 mg, 0.09 mmol 1.2 eq.) and 4-hydroxyphenethylamine (11.2 mg, 0.08 mmol, 1 eq.) were dissolved in DMF. Then *N*, *N*-diisopropylethylamine (70 µL, 0.4 mmol, 5 eq.) was added, the mixture was stirred at room temperature overnight. The solvent was extracted with dichloromethane (50 ml) and H_2O (50 ml), dried over sodium sulphate and purified via column chromatography on silica gel by eluting with 4 % THF/ CH_2Cl_2. Hexane and tetrahydrofuran was used for crystallization. (32.2 g, **54.0 %**)

^{1}H NMR (300 MHz, Chloroform-d_6) δ: 8.14-8.03 (m, 8H), 7.78-7.75 (m,2H), 7.51-7.37 (m, 6H), 7.14-7.09 (m, 3H), 7.01-6.97 (m, 4H), 4.07-4.03 (t, 2H), 3.73-3.66 (m, 2H), 2.87 (t, 2H), 1.81-1.76 (m, 2H), 1.55-1.47 (m, 2H), 1.02-0.97 (t, *J* = 7.4 Hz, 3H)

H-NMR Spectra and MALDI-TOF Spectra

Compound 1

4-(7-(3,5-dichloro-4-hydroxyphenyl)-5,5-difluoro-1,9-diphenyl-5H-5λ^4,6λ^4-dipyrrolo[1,2-c:2',1'-f][1,3,5,2]triazaborinin-3-yl)-N-dodecylbenzamide

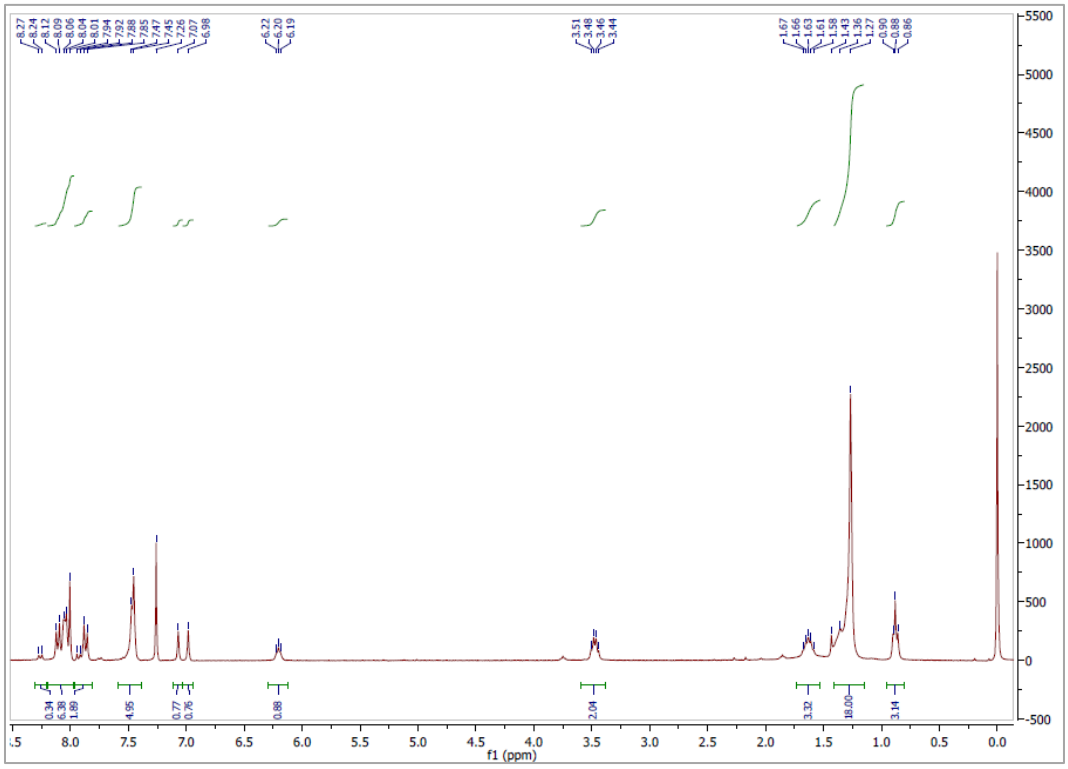

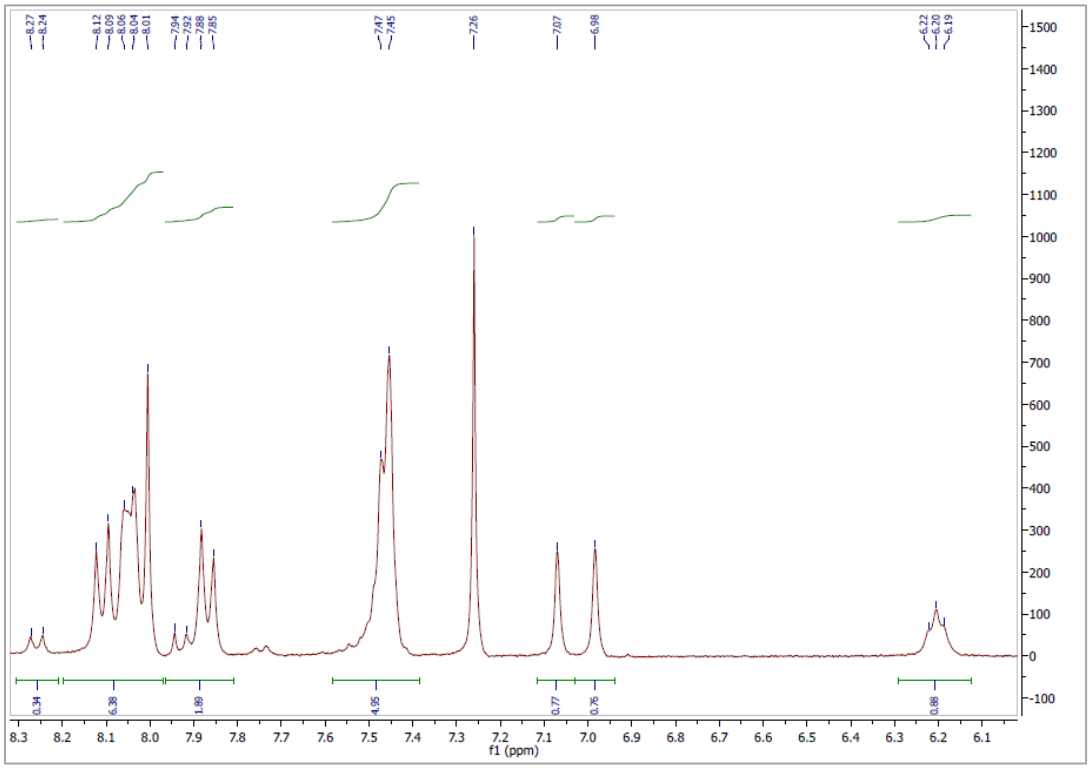

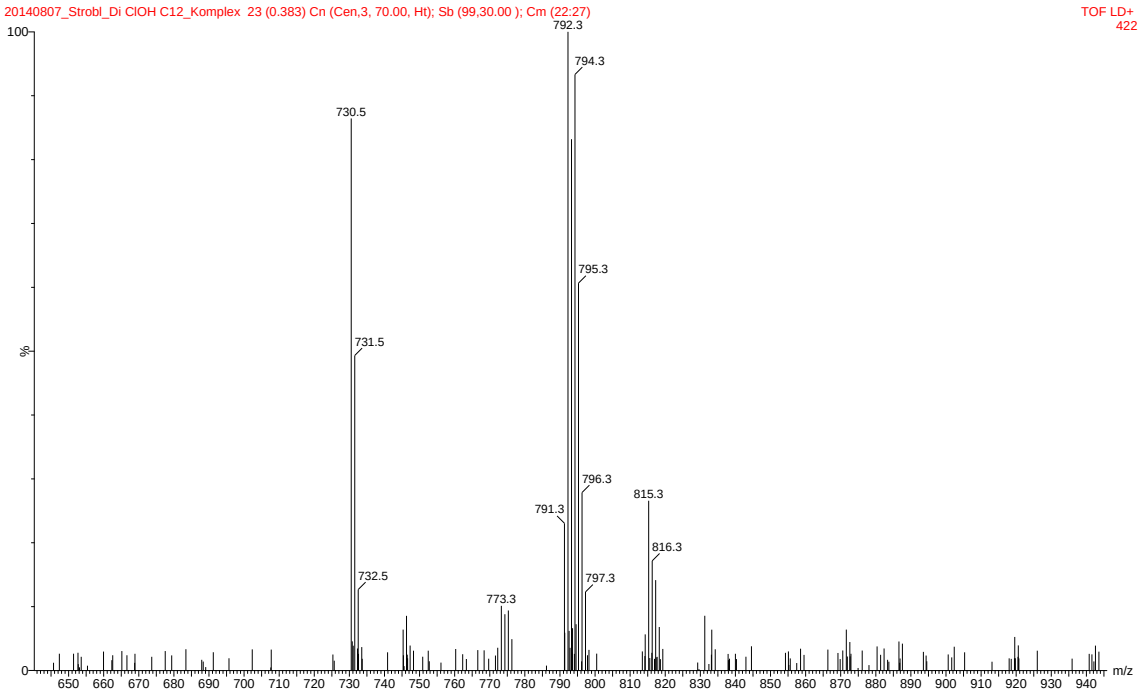
20140807_Strobl_Di ClOH C12_Komplex 23 (0.383) Cn (Cen,3, 70.00, Ht); Sb (99,30.00); Cm (22:27)
TOF LD+
422
100
%
0
792.3
794.3
730.5
795.3
731.5
796.3
815.3
791.3
816.3
732.5
797.3
773.3
650 660 670 680 690 700 710 720 730 740 750 760 770 780 790 800 810 820 830 840 850 860 870 880 890 900 910 920 930 940
m/z

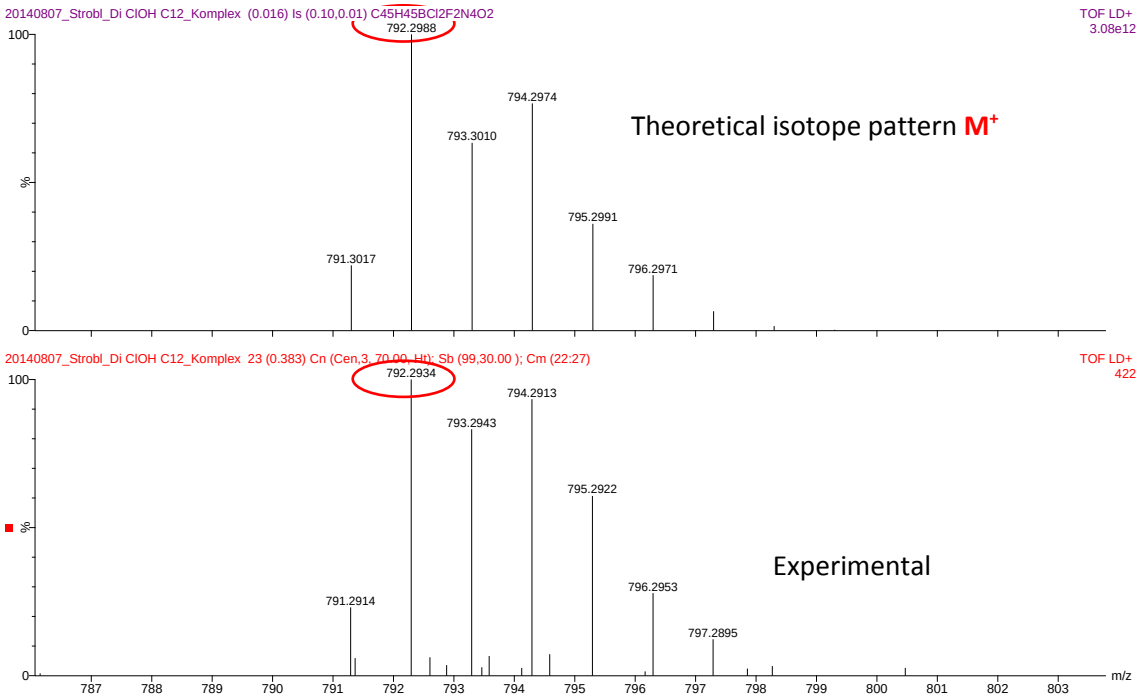
20140807_Strobl_Di ClOH C12_Komplex (0.016) Is (0.10,0.01) C45H45BCl2F2N4O2
TOF LD+
3.08e12
100
%
0
792.2988
794.2974
793.3010
795.2991
791.3017
796.2971
Theoretical isotope pattern M+
20140807_Strobl_Di ClOH C12_Komplex 23 (0.383) Cn (Cen,3, 70.00, Ht); Sb (99,30.00); Cm (22:27)
TOF LD+
422
100
%
0
792.2934
794.2913
793.2943
795.2922
791.2914
796.2953
797.2895
Experimental
787 788 789 790 791 792 793 794 795 796 797 798 799 800 801 802 803
m/z

Compound 2

4-(7-(4-butoxyphenyl)-5,5-difluoro-1,9-diphenyl-5H-4λ^4,5λ^4-dipyrrolo[1,2-c:2',1'-f][1,3,5,2]triazaborinin-3-yl)-2,6-dichlorophenol ***(2)***

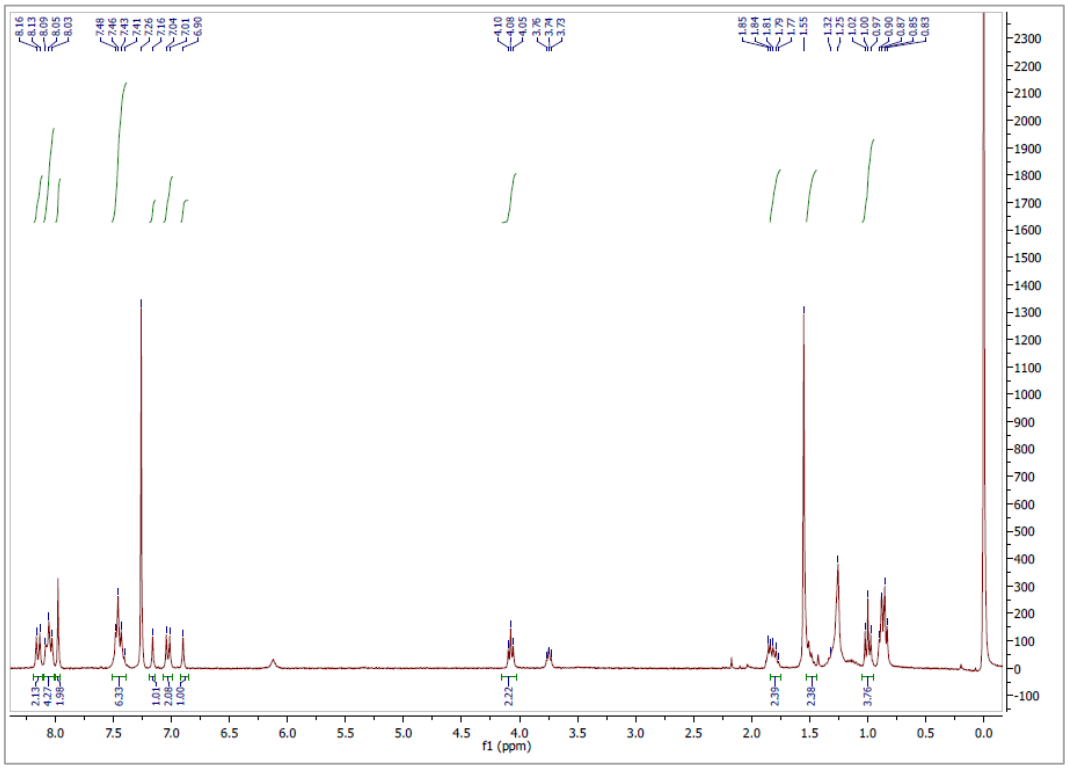

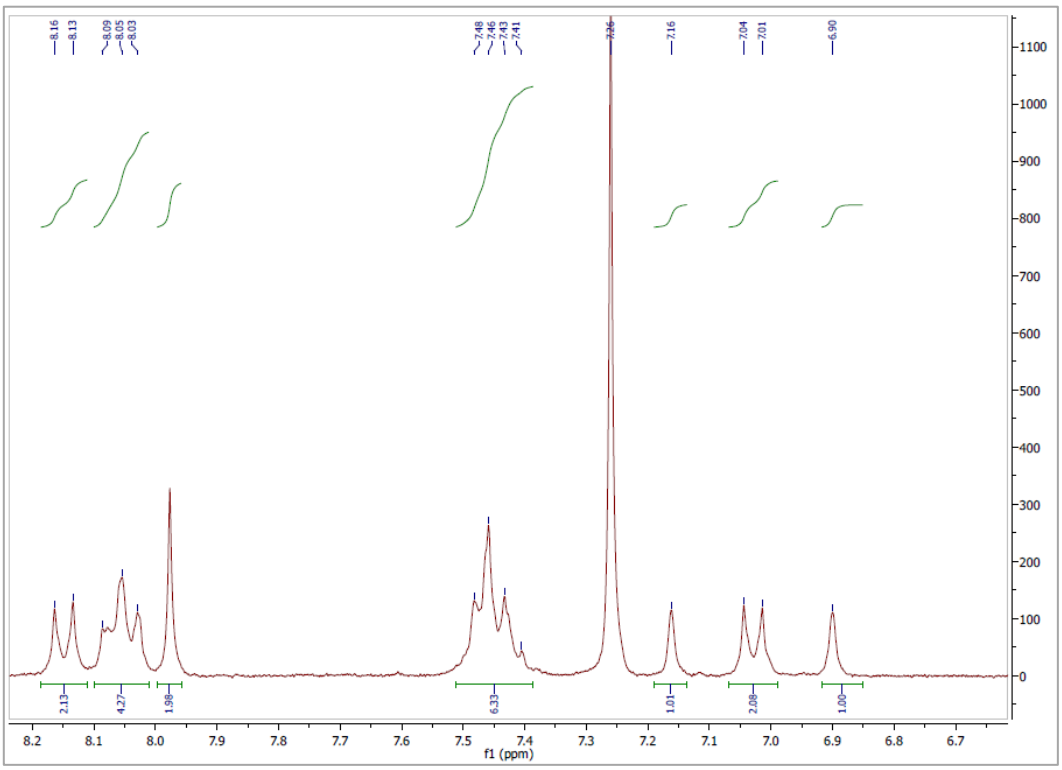

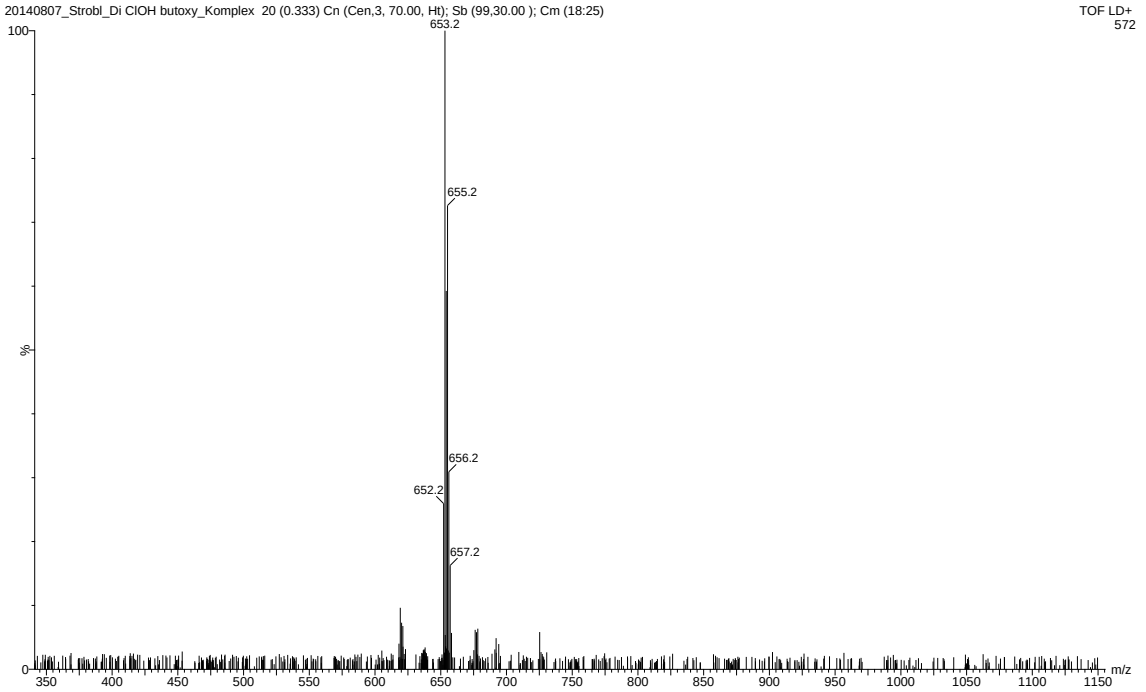

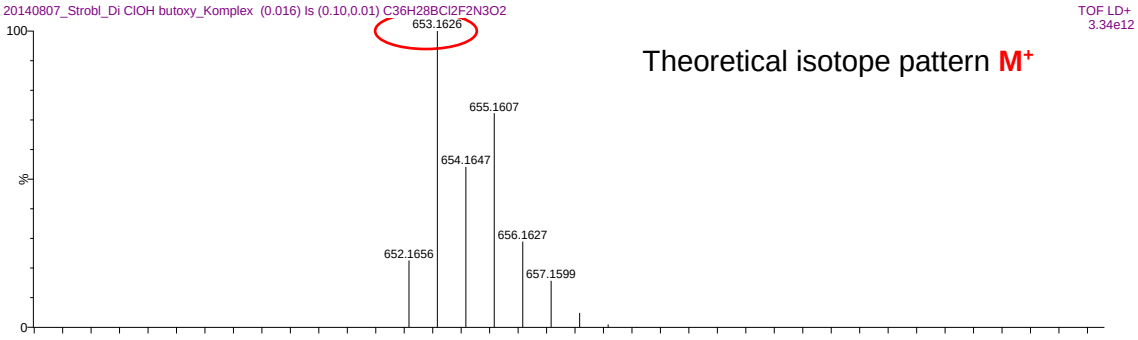

Theoretical isotope pattern **M⁺**

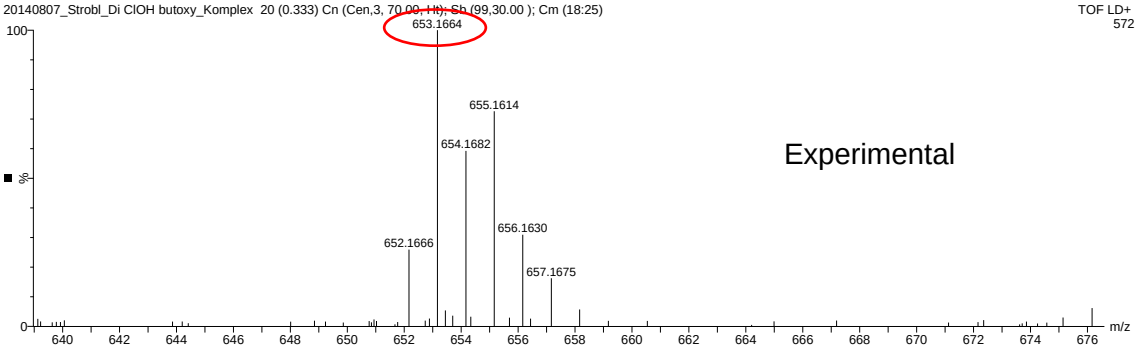

Experimental

Compound 3

4-(7-(3-chloro-4-hydroxyphenyl)-5,5-difluoro-1,9-diphenyl-5H-5λ^4,6λ^4-dipyrrolo[1,2-c:2',1'-f][1,3,5,2]triazaborinin-3-yl)-N-dodecylbenzamide ***(3)***

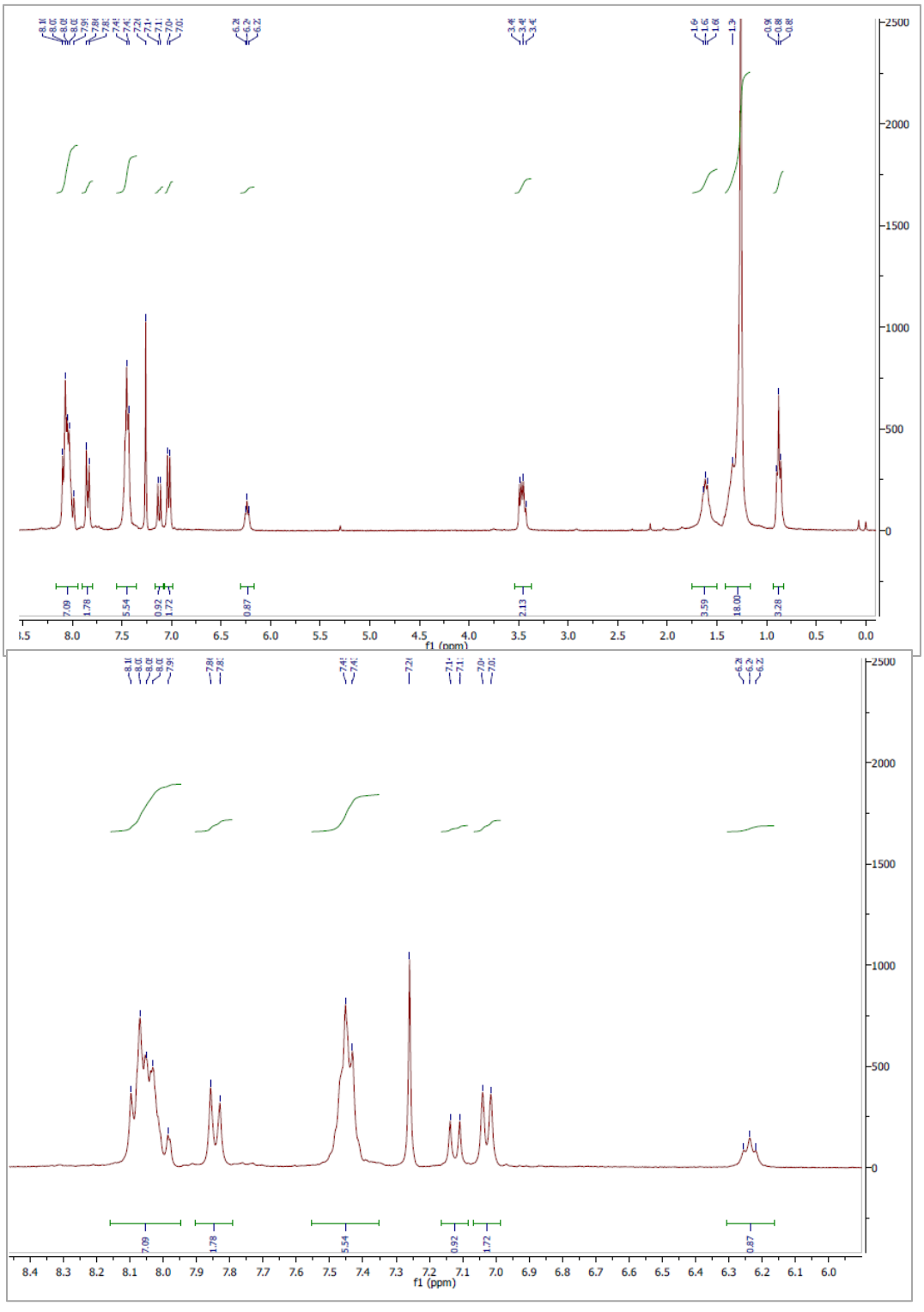

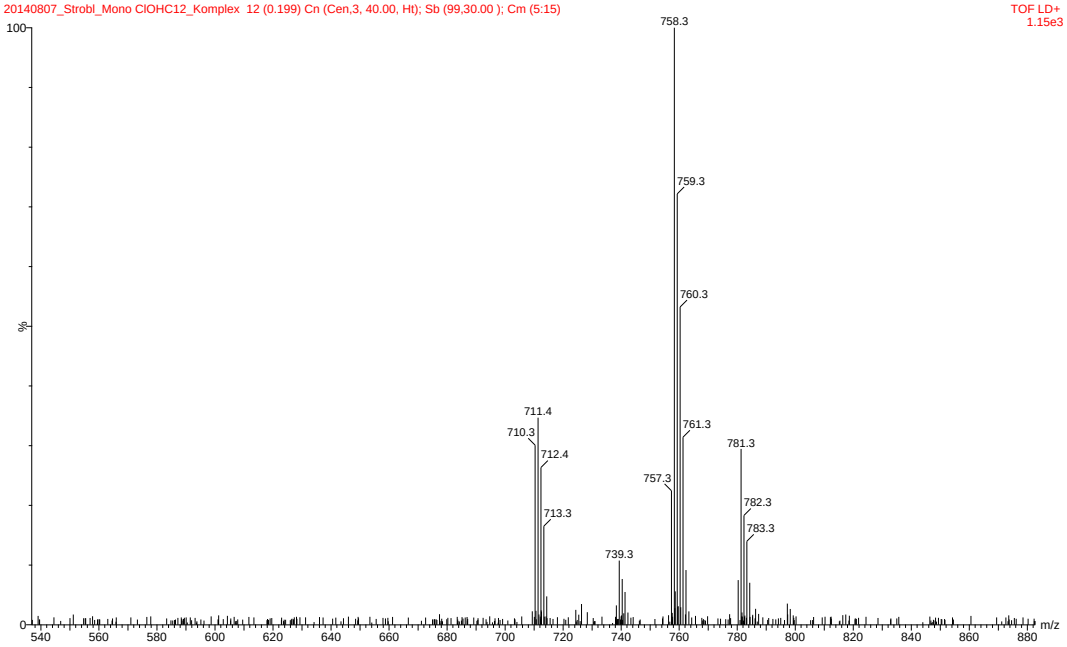
20140807_Strobl_Mono ClOHC12_Komplex 12 (0.199) Cn (Cen,3, 40.00, Ht); Sb (99,30.00); Cm (5:15)
TOF LD+
1.15e3
758.3
759.3
760.3
761.3
711.4
710.3
712.4
713.3
757.3
781.3
782.3
783.3
739.3
m/z

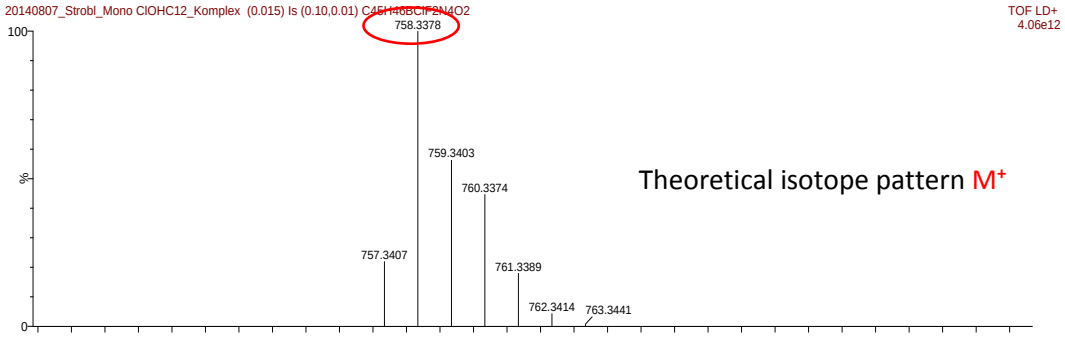
20140807_Strobl_Mono ClOHC12_Komplex (0.015) Is (0.10,0.01) C45H46BClF2N4O2
TOF LD+
4.06e12
758.3378
759.3403
760.3374
757.3407
761.3389
762.3414
763.3441
Theoretical isotope pattern M+

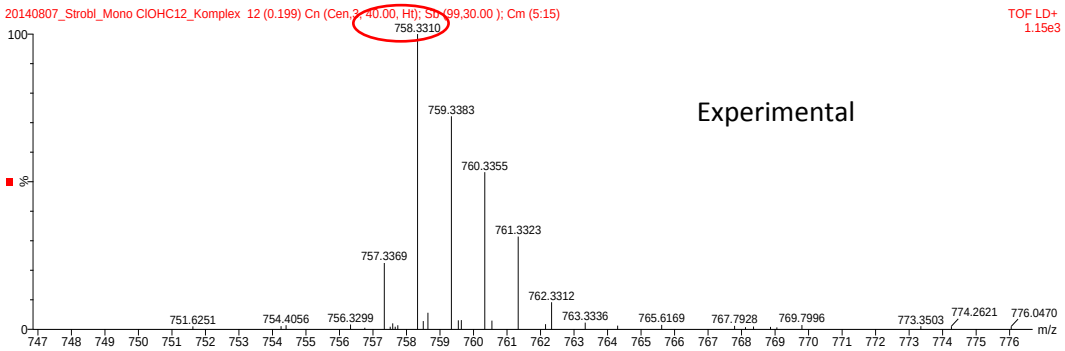
20140807_Strobl_Mono ClOHC12_Komplex 12 (0.199) Cn (Cen,3, 40.00, Ht); Sb (99,30.00); Cm (5:15)
TOF LD+
1.15e3
758.3310
759.3383
760.3355
761.3323
757.3369
762.3312
751.6251
754.4056
756.3299
763.3336
765.6169
767.7928
769.7996
773.3503
774.2621
776.0470
Experimental
m/z

Compound 4

*4-(7-(4-butoxyphenyl)-5,5-difluoro-1,9-diphenyl-5H-4λ^4,5λ^4-dipyrrolo[1,2-c:2',1'-f][1,3,5,2]triazaborinin-3-yl)-2-chlorophenol (**4**)*

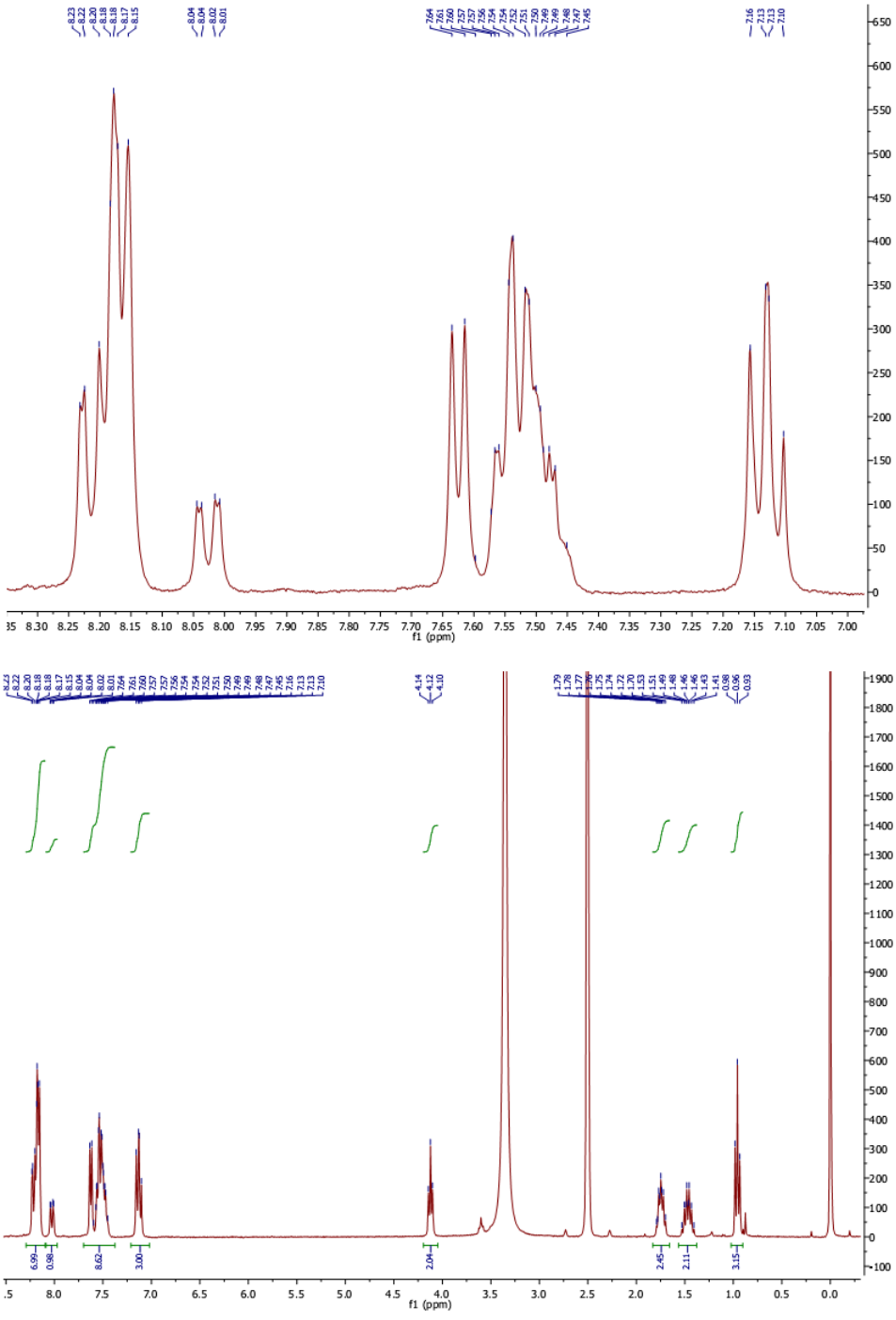

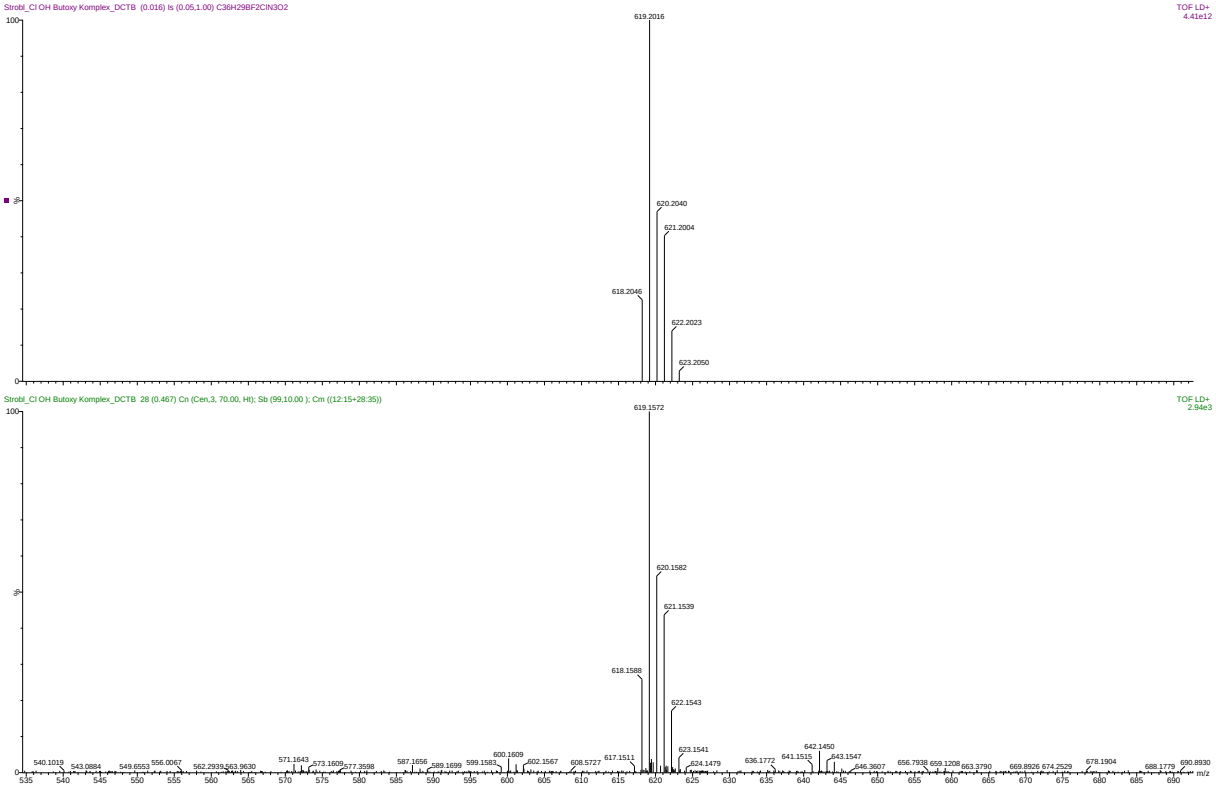
Strobl_Cl OH Butoxy Komplex_DCTB (0.016) Is (0.05,1.00) C36H29BF2ClN3O2
TOF LD+
4.41e12
619.2016
620.2040
621.2004
618.2046
622.2023
623.2050
Strobl_Cl OH Butoxy Komplex_DCTB 28 (0.467) Cn (Cen,3, 70.00, Ht); Sb (99,10.00); Cm ((12:15+28:35))
TOF LD+
2.94e3
619.1572
620.1582
621.1539
618.1588
622.1543
623.1541
642.1450
600.1609
m/z

Compound 5

4-(5,5-difluoro-7-(4-hydroxyphenyl)-1,9-diphenyl-5H-5λ^4,6λ^4-dipyrrolo[1,2-c:2',1'-f][1,3,5,2]triazaborinin-3-yl)-N-dodecylbenzamide ***(5)***

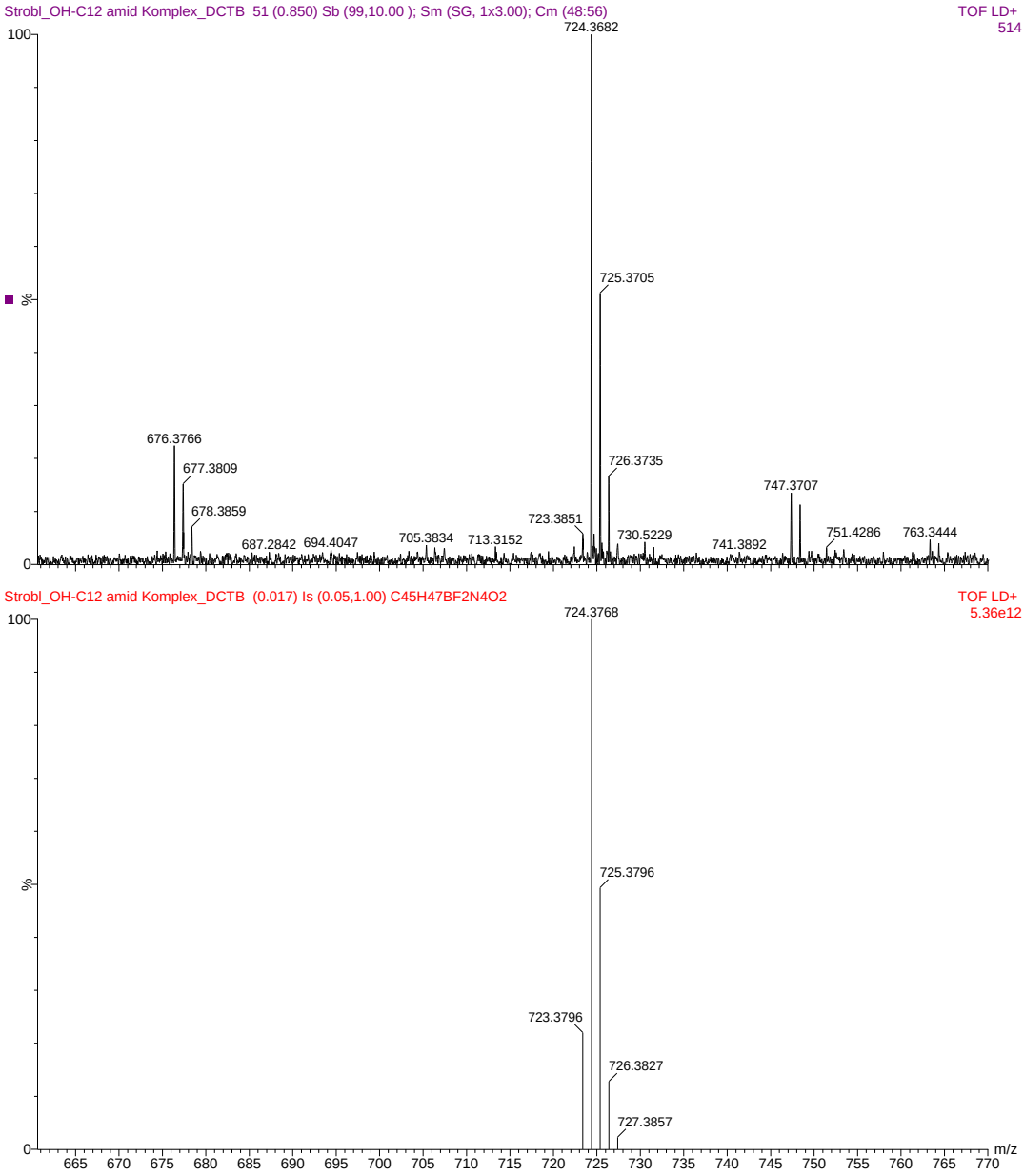

Compound 6

*4-(7-(4-butoxyphenyl)-5,5-difluoro-1,9-diphenyl-5H-4λ^4,5λ^4-dipyrrolo[1,2-c:2',1'-f][1,3,5,2]triazaborinin-3-yl)phenol (**6**)*

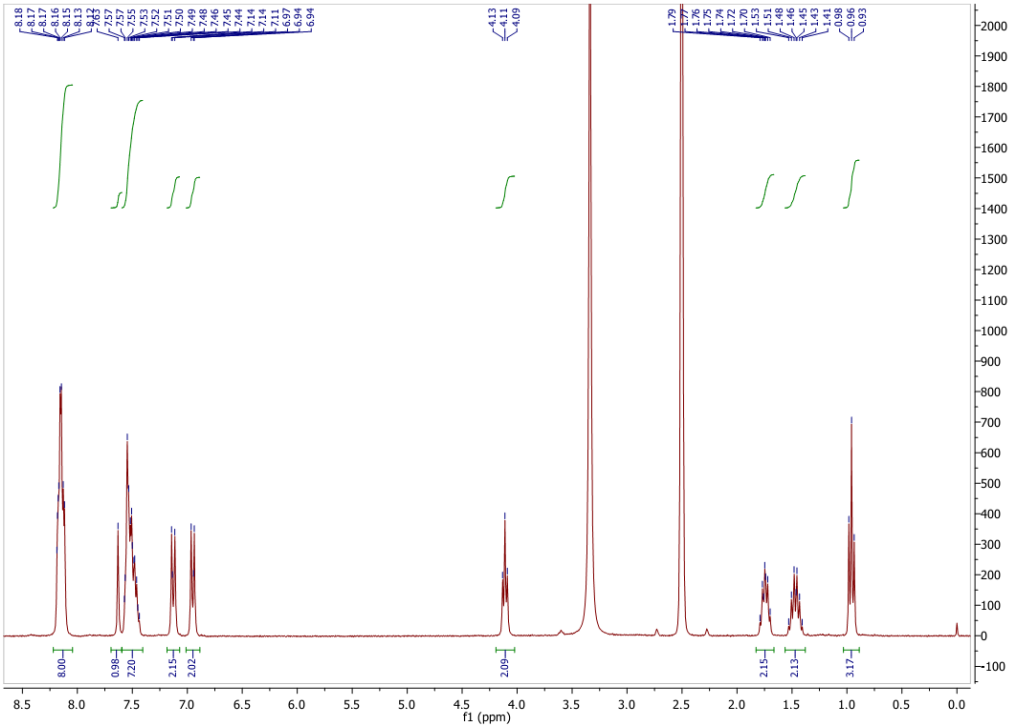

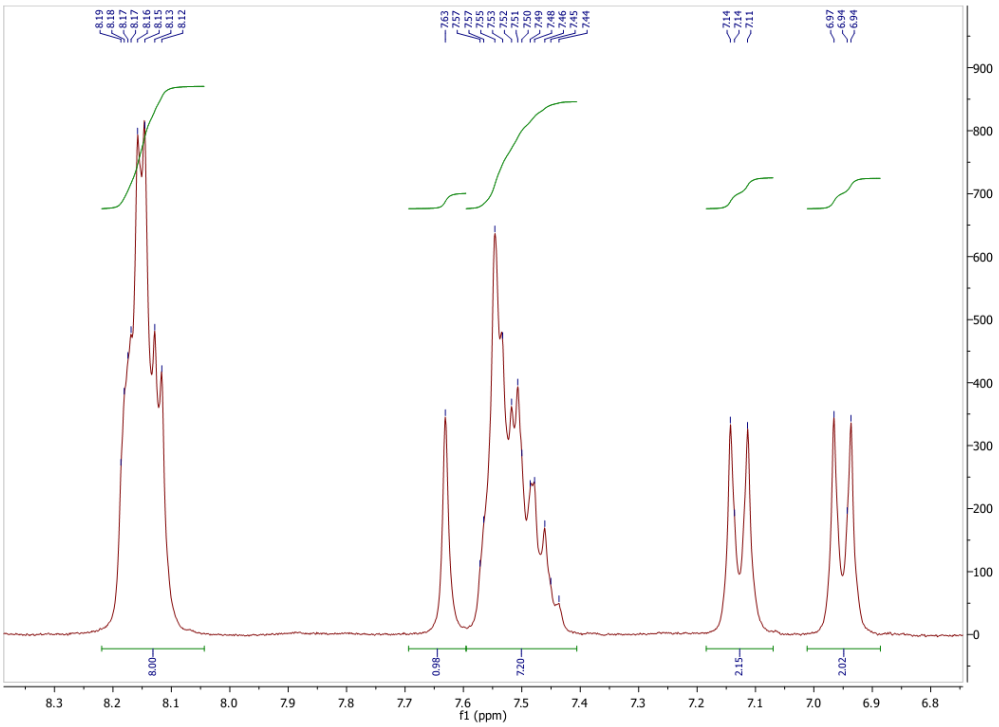

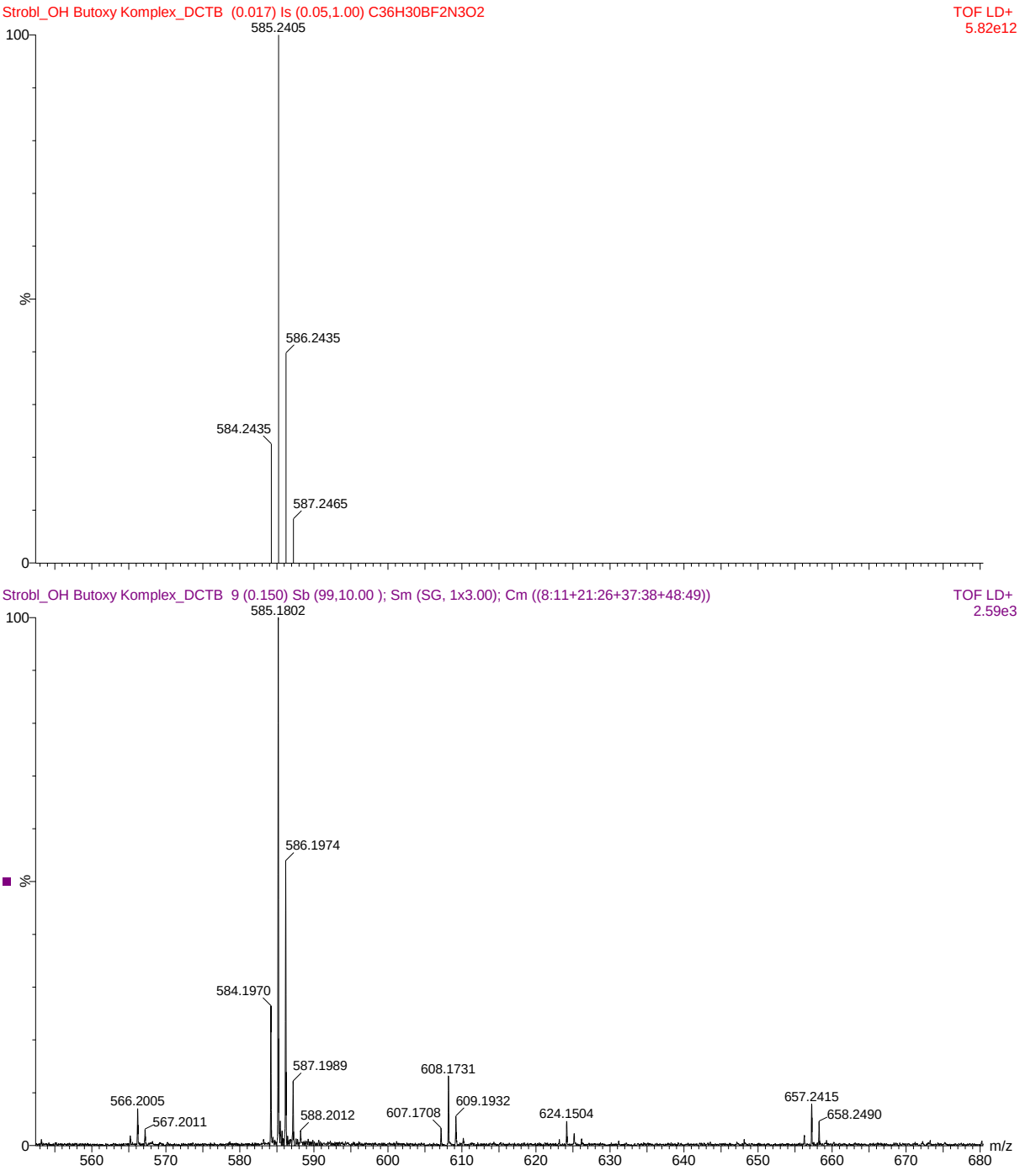
Strobl_OH Butoxy Komplex_DCTB (0.017) Is (0.05,1.00) C36H30BF2N3O2
TOF LD+
5.82e12
100
%
0
585.2405
586.2435
584.2435
587.2465
Strobl_OH Butoxy Komplex_DCTB 9 (0.150) Sb (99,10.00); Sm (SG, 1x3.00); Cm ((8:11+21:26+37:38+48:49))
TOF LD+
2.59e3
100
%
0
585.1802
586.1974
584.1970
587.1989
608.1731
566.2005
567.2011
588.2012
607.1708
609.1932
624.1504
657.2415
658.2490
560
570
580
590
600
610
620
630
640
650
660
670
680
m/z

Compound 7

3-(4-butoxyphenyl)-7-(4-((4-(dimethylamino)benzyl)carbamoyl)phenyl)-5,5-difluoro-1,9-diphenyl-5H-dipyrrolo[1,2-c:2',1'-f][1,3,5,2]triazaborinin-4-ium-5-uide ***(7)***

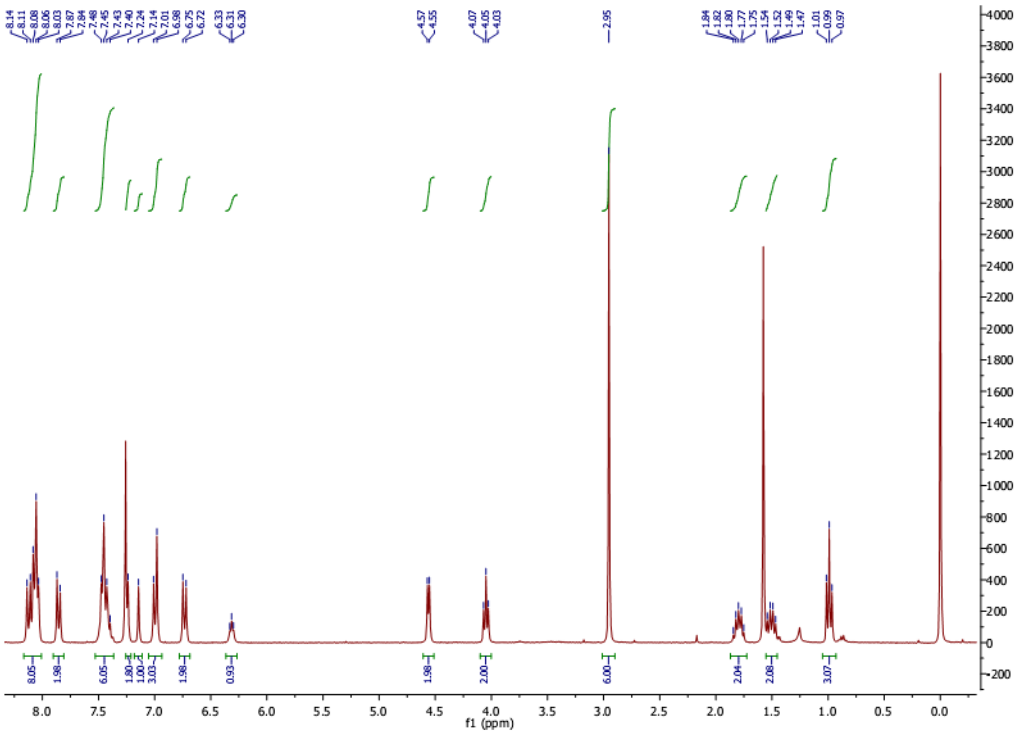

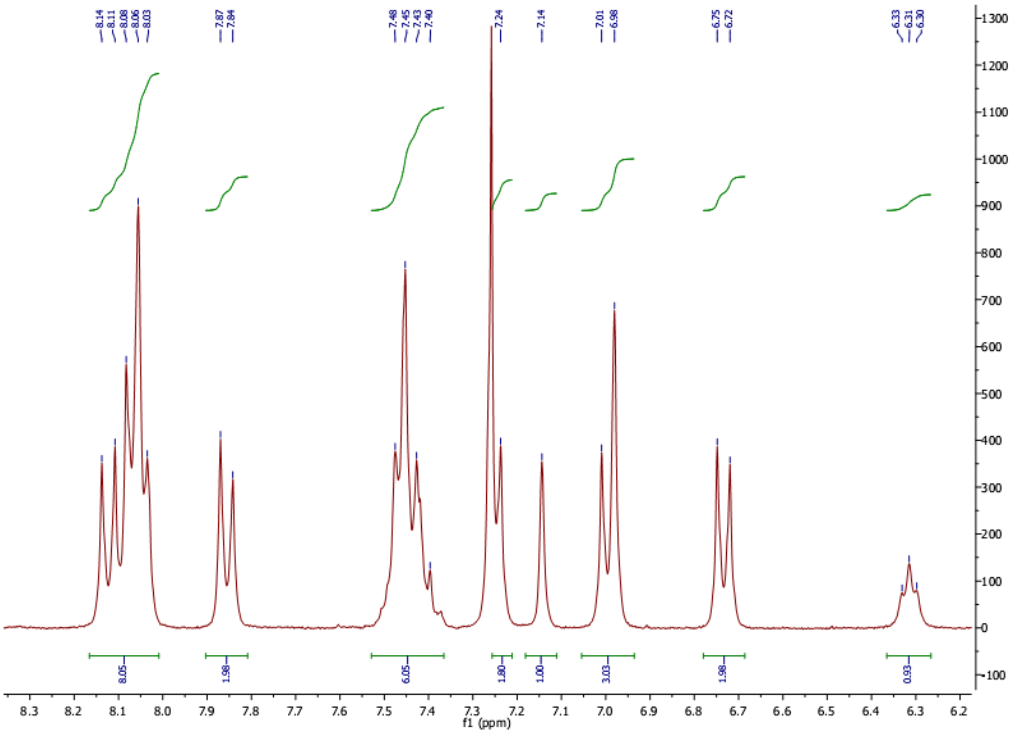

Chapter 2

Trace ammonia sensors based on fluorescent NIR-emitting aza-BODIPY dyes

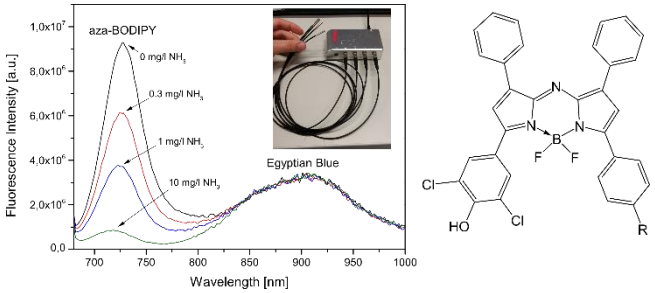

Trace ammonia sensors based on fluorescent NIR-emitting aza-BODIPY dyes

This chapter was submitted in **Analytical Chemistry**,

Martin Strobl, Anna Walcher, Torsten Mayr, Ingo Klimant and Sergey M. Borisov

Highly sensitive ammonia sensors for environmental monitoring are presented. The sensing materials are based on fluorescent aza-BODIPY dyes physically entrapped in polyurethane hydrogels and dispersed in silicone rubber. This layer is covered by a hydrophobic porous Teflon membrane used as an additional proton barrier and light scattering layer. The dual-lifetime referenced (DLR) sensors make use of NIR emitting Egyptian blue as a reference material and in combination with optical fibres are read-out via a compact phase-fluorometer. The detectable concentration range can be tuned by the choice of aza-BODIPY dye or/and the hydrogel matrix. The most sensitive sensor has an LOD of 0.11 µg/l and the upper detectable concentration of 300 µg/l. No cross sensitivity towards pH is observed. The sensors show remarkable operational stability with no noticeable drift over a period of two weeks.

Key words: optical sensor, fluorescence, ammonia, Dual-Lifetime Referencing, near infrared, aza-BODIPY

Introduction

Ammonia is toxic to humans and any kind of animals. Especially for aquatic organisms dissolved ammonia is already hazardous at concentrations above 25 µg/l.[1] Thus, ammonia detection in environmental monitoring is a crucial application, particularly in fish farming[2], where it can easily accumulate and harm the aquatic life. Many different methods have been developed for analytical detection of dissolved ammonia and have been mainly based on electrochemical or optical transduction. Electrochemical methods including potentiometric,[3] amperometric[4] or conductometric[5] techniques have high selectivity, detection limits in the ppm range and fast response time, but drawbacks still exist regarding cross-sensitivity to salinity[6,7], signal drift and miniaturization of the reference electrode.[8] NH_3 detection employing colorimetric approaches, mostly based on Nessler's reaction[9] or Berthelot's indophenol method[10,11] are established in routine analysis. However, slow kinetics, chemical consumption of the reagents and the irreversibility of the reaction itself makes them poorly suitable for continuous monitoring.[12,13]

Thus, ammonia sensors based on pH indicators have gained considerable attention due to advantages provided by optical measurement.[14] They operate reversibly, do not consume the analyte, have good selectivity and sensitivity. Several classes of colorimetric and fluorescent pH indicators, including triphenylmethane dyes[15,16], xanthene dye[17–21], coumarin derivatives[22–24] and oxazine perchlorate[25] were employed for designing an ammonia sensor. However, only a few exhibit good photostability and show sufficient sensitivity for determining precisely dissolved ammonia at trace level. For instance, highly sensitive ammonia sensors based on triphenylmethane dye in hydrogel have been reported[12] but they showed poor long-term stability and were operational only for several days.

BF_2-chelated tetraarylazadipyrromethene dyes (aza-BODIPYs)[26–36] represent a promising alternative capable of fulfilling the requirements mentioned above. These dyes show absorption and emission bands in the long-wavelength spectral region (650 – 750 nm)[37] which is beneficial due to low auto-fluorescence of biomolecules, less scattering background and the applicability of low cost excitation sources (bright red LEDs) and photodetectors (silicon photodiodes). Notably, aza-BODIPYs are exceptionally photostable[29] which makes them ideal fluorophores for long-term measurements. In this study we present dually-lifetime referenced ammonia sensors based on aza-BODIPY indicator dyes bearing o,o-dichlorophenol receptor. Different host polymers and sensor assemblies have been investigated with the aim of designing a robust sensor with high sensitivity.

We show that the dynamic range can be tuned over a wide range, depending on the host polymer and choice of aza-BODIPY dye. The NIR-emitting dyes are excitable with red LED (620 nm) making them compatible with a commercially available miniaturized phase fluorometer in combination with optical fibers. This enables a wide variety of potential applications. As an example, a real-world application in wastewater treatment is demonstrated for this fibre-optic ammonia sensor.

Experimental Section

Materials

The aza-BODIPY dyes (DiClBut, 4-(7-(4-butoxyphenyl)-5,5-difluoro-1,9-diphenyl-5H-4l4,5l4-dipyrrolo[1,2-c:2',1'-f][1,3,5,2]triazaborinin-3-yl)-2,6-dichlorophenol) and (DiClC12, 4-(7-(3,5-dichloro-4-hydroxyphenyl)-5,5-difluoro-1,9-diphenyl-5H-5l4,6l4-dipyrrolo[1,2c:2',1'f][1,3,5,2] triazaborinin-3-yl)-N-(2l5,12l3-dodecan-2-yl)benzamine) were synthetized in our lab as described previously.[30] Microcristalline powder of silanized Egyptian Blue was prepared as described elsewhere.[38] Sodium dihydrogen phosphate and disodium hydrogen phosphate were bought from Carl Roth GmbH (Karlsruhe, Germany). Hydromed D7 was purchased from AdvanSource biomaterials and Hydrothane 15 was from CT Biomaterials Cardiothech International (Wilmington, MA, United Stated). Hydromed D7 was washed with water prior to use. 1,1,2-Trichloro-1,2,2-trifluoro-ethane (Freon) and 4-dodecylbenzene sulfonic acid (DBSA) was purchased from Sigma Aldrich. FluoroporeTM membrane PTFE (0.45 µm pore) was from Merck Millipore Ltd. (Cork, Ireland). Poly(ethylene naphthalate) (PEN) foil Teonex was from Pütz (Tanusstein, Germany). Cellulose acetate propionate (CAP) and cellulose acetate butyrate (CAB) were bought from Acros organics. Ethyl cellulose (ethoxyl content 49 %) was purchased from Scientific Polymers Products and polysulfone from Polysciences (Warrington, PA, United States). Silicone Elastosil E43 was obtained from Wacker (Munich, Germany).

Sensor foil preparation

Silanized Egyptian Blue (35 mg) was homogenously dispersed in a polysulfone solution (3 g, 10 %w/w in $CHCl_3$) and knife-coated on a roughened, dust-free PEN support by using a bar film applicator (1 mil, wet film thickness 25.4 µm). 0.125 mg of DiClC12 (43 µl of 2.9 mg/ml stock solution in THF) were added to 200 mg of hydrogel D7 solution in $CHCl_3$ (10% w/w, 20 mg of hydrogel) to obtain a "cocktail" for sensor **A**. Alternatively, the same dye amount was added to 200 mg of Hydrothane 15 solution in $CHCl_3$ (10% w/w, 20 mg of hydrothane) to obtain a "cocktail" for sensor **B**. Then, 4-dodecylbenzene sulfonic acid (DBSA, 0.53 mg, 63 µl of 8.4 mg/ml stock solution in THF) and silicone elastosil E43 (300 mg) were added to the "cocktails". The mixture was emulsified for 10 minutes and knife-coated (25 µm wet layer) on the back side of the PEN foil which was previously coated with Egyptian Blue suspension. Immediately after the knife-coating step, a Fluoropore^{TM} membrane PTFE was carefully laid

onto the still wet film. After 24 hours the silicone rubber is polymerized and the ammonia sensing material is ready to use. Sensors **C** and **D** were prepared similarly to sensors **A** and **B** but using 0.25 mg of **DiClBut** (125 µl of 2 mg/ml stock solution in THF, 1.25 % w/w with respect to polymer) instead. For Sensor **E**-**H**, a "cocktail" of **DiClBut** (0.25mg, 86 µl of 2.9 mg/ml stock solution in THF), Hydrothane solution (HT 15, 1 g, 10 %w/w in $CHCl_3$, **E**) or ethyl cellulose solution (EC, 1 g, 10 %w/w in $CHCl_3$, **F**) or cellulose acetate propionate solution (1 g, 10 %w/w in $CHCl_3$, **G**) or cellulose acetate butyrate solution (1 g, 10 %w/w in $CHCl_3$, **H**), freon (300 µl), THF (200 µl) and DBSA (0.53 mg, only for **E** and **F**) was prepared and knife-coated on the PEN-support (3 mil) which back side was also previously coated with Egyptian Blue suspension. Composition of the sensing materials is summarized in Table **1**. The resulting layer thickness of the sensors (**A-D**) including the Teflon membrane (50 µm) is about 65.5 µm.

Table 1: Composition of the sensing materials per 100 mg of host polymer.

Sensor	Indicator [mg]	Host polymer	DBSA [mg]	Additional polymer
A	DiClC12 [0.625]	D7	0.26	Silicone rubber
B	DiClC12 [0.625]	HT 15	0.26	Silicone rubber
C	DiClBut [1.25]	D7	0.53	Silicone rubber
D	DiClBut [1.25]	HT 15	0.53	Silicone rubber
E	DiClBut [0.25]	HT 15	0.53	-
F*	DiClBut [0.25]	EC	0.53	-
G*	DiClBut [0.25]	CAP	-	-
H*	DiClBut [0.25]	CAB	-	-

*See Supporting Information

In order to prepare fibre optic sensors, the sensor foils were punched out with a stainless steel ferrule and fixed on a distal end of an optical fibre (Fig.**S1**).

Instrumentation and measurement

DLR-referenced sensor measurements were performed with a commercially available FirestingO_2 reader (PyroScience GmbH, Aachen) in combination with plastic optical fibres (∅ 1 mm, 1 meter length, acquired from Ratioplast, Germany). The measurements were carried out with following settings: LED intensity of 30 %, an amplification of 400x, a measuring time

of 10 ms, a measuring interval of 4 seconds and a modulation frequency of 4000 Hz. Corrected fluorescence spectra were acquired on a Fluorolog3 spectrofluorometer (Horiba Jobin Yvon) equipped with a NIR-sensitive photomultiplier R2658 from Hamamatsu (300-1050 nm).

Results and Discussion

Choice of pH indicator

The sensing principle is based on the acid-base equilibrium between indicator and ammonia (pK_a value of 9.2 at pH 7). Consequently, the sensitivity of an ammonia sensor strongly depends on the apparent pK_a value of the pH indicator: the lower the pK_a value of the pH dye the more sensitive is the sensor. Here, BF_2-chelated tetraarylazadipyrromethene dyes[30] (aza-BODIPY, namely **DiClBut** and **DiClC12**, Fig. **1**) were chosen as pH indicators due to very low apparent pK_a values of 4.4 and 3.9, respectively. Strong acidity of the phenol receptor is induced by the electron-withdrawing effect of the two chlorine atoms at the *ortho*-position. As can be seen, the peripheral substituents allow fine tuning of the pK_a value due to electron-withdrawing (carboxamide group) or electron-donating (butoxy-group in *para*-position) character. The sensors utilize fluorescence quenching caused by deprotonated phenolate attributed to a photoinduced electron transfer (PET). Whereas protonated form (no ammonia) is highly fluorescent, the emission is virtually "switched off" in presence of the analyte. Additionally, the pH-sensitive aza-BODIPY dyes undergo pronounced bathochromic shift of the absorption upon deprotonation (50-70 nm) due to intramolecular charge transfer (ICT).

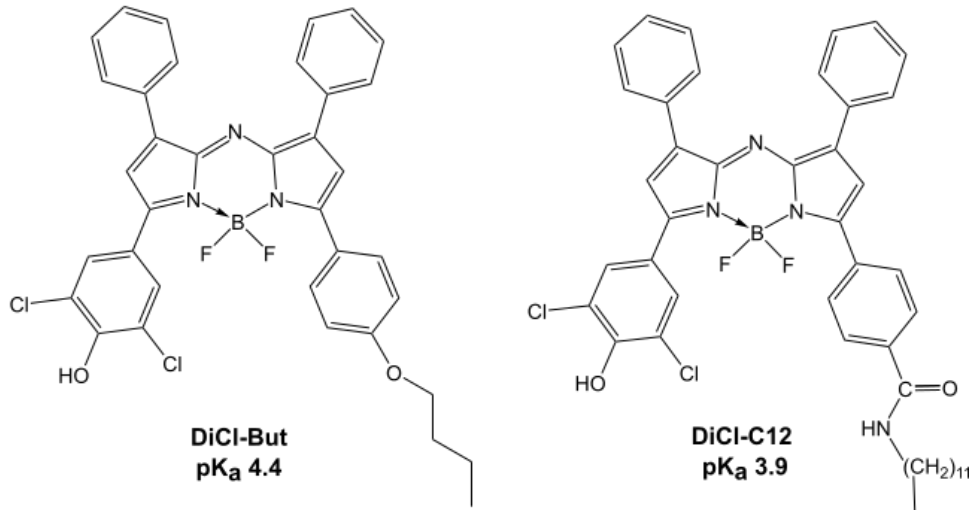

Figure 12: Chemical structures of aza-BODIPY dyes.

Aza-BODIPY dyes exhibit properties that outperform many other fluorophores. These dyes display good brightness[29] and show absorption and emission bands in the red and infrared (NIR) spectral region, respectively. Notably, aza-BODIPYs are exceptionally photostable which makes them ideal fluorophores for long-term measurements.

Dual-Lifetime Referencing (DLR)

Fluorescence intensity is an error-prone parameter which is highly influenced by a number of factors, such as intensity fluctuations of the excitation source, detector performance and artefacts originating from the optoelectronic system. Dual lifetime referencing (DLR) overcomes many problems associated with intensity-based measurements. This method requires a combination of an inert reference dye/inorganic phosphor with a long luminescence decay time and an analyte-sensitive fluorophore with overlapping absorption spectra.[39] Here, Egyptian blue was chosen as reference material due to its high photochemical inertness and spectral compatibility with the aza-BODIPY indicator dye. Both are efficiently excited with red LED (~624 nm) and emit in NIR part of the electromagnetic spectrum (see Figure **2**) making them compatible with a commercially available phase fluorometer (Firesting from PyroScience, Fig. S9). Both are simultaneously excited with a modulated light source and the intensity ratios of the two fluorophores is converted into an overall phase angle shift (phi). Conversion of the phase angle into cotangent values reflects direct proportionality to the indicators intensity. Alternatively, referenced ratiometric two wavelength measurement of the luminescence intensity is also possible.

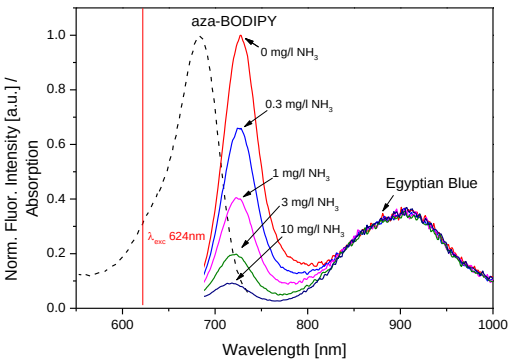

Figure 2: Emission (solid lines, λ_{exc} = 620 nm) and excitation (protonated form of aza-BODIPY, dotted line) spectra of sensor C based on DiClBut (λ_{max}=725 nm) as an indicator and Egyptian Blue (λ_{max}=900 nm) as a reference at different ammonia concentrations. Fluorescence emission of aza-BODIPY is quenched via PET (Photoinduced Electron Transfer) in presence of ammonia.

Sensor composition

Preliminary experiments revealed that without adding an acid to the sensor "cocktail" the indicator dye remains in its deprotonated state, resulting in no response to ammonia. Thus, non-volatile 4-dodecylbenzene sulfonic acid (DBSA) was added to all sensor mixtures in order to ensure full protonation of the aza-BODIPY dye.

First design of the ammonia sensor relied on an indicator dye dissolved in a polymeric matrix coated onto a transparent poly(ethylene naphthalate) (PEN) support and covered with a porous Teflon membrane to prevent interference from protons and other ionic species (Fig. **3a**, sensor **E**). In order to obtain good adhesion between the hydrophobic filter and the hydrophilic host polymer, (Freon, 1,1,2-trichloro-1,2,2-trifluoro-ethane) was added to the sensor formulation. The filters display remarkably high permeability for ammonia which relies on their porous structure. Moreover, the white and reflective membrane surface increases the signal intensity due to light scattering.

A number of different polymers were investigated for applicability as host materials including polyurethane hydrothane 15 (HT 15), polyurethane hydrogels Hydromed (D7 and D4), ethyl cellulose and various cellulose esters. HT 15 showed the best results regarding response and recovery times ($t_{90} \sim 5$ and 10 min, respectively) and sensitivity whereas cellulose acetate butyrate, cellulose acetate propionate and ethyl cellulose showed either low sensitivity or very slow response to ammonia (see SI, Fig. **S2-S4**). However, the ammonia sensor based on HT 15 exhibited pronounced signal drift (Figure **4a**). It is assumed that swelling of the hydrothane film results in its partial detachment from the PEN support or the Teflon membrane and penetration/condensation of water in resulted cavities, causing irreversible deprotonation of the indicator dye over time.

Hence, a new design concept was investigated in order to minimize the sensor drift. The indicator dye and Hydrothane were dissolved in an organic solvent (chloroform) and then cross-linkable polydimethylsiloxane was added. The obtained emulsion was knife-coated onto a PEN support and Teflon filter was subsequently laid onto the still wet film (see Figure **3b**). As a result of evaporation of the organic solvent and cross-linking of silicone primers, a dispersion of Hydrothane in silicone rubber was formed. Silicone rubber acts as additional permeation-selective membrane and dramatically improves the stability of the sensor.

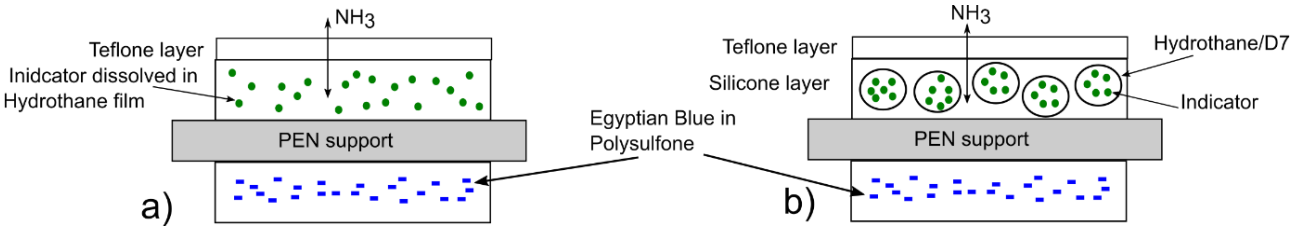

Figure 3: Cross-section of different sensor assemblies (not to scale): a) Indicator dye dissolved in HT 15 film only and b) indicator dye entrapped in HT 15/Silicone emulsion. Both sensors have a Teflon membrane filter on top.

Stability and sensitivity of the sensing materials

Fig. **4** shows the response and long term stability of the ammonia optodes based on the two sensor designs. It is evident, that the first design does not result in a stable material due to a strong drift (Fig. **4a**). Increase of the phase angle (particularly noticeable in the absence of ammonia) corresponds to the decrease of concentration of the fluorescent protonated form of the pH indicator. Such drift renders the sensors unsuitable for the long-term monitoring. This observation is in full agreement with a literature report.[12] On the contrary, the sensors exploring the second design are stable (Fig. **4b**). No noticeable drift and fully reversible response are observed for at least one week of continuous measurement. The test also underlines excellent photostability of the indicators: over 60,000 measurement points are acquired without photodegradation of the aza-BODIPY.

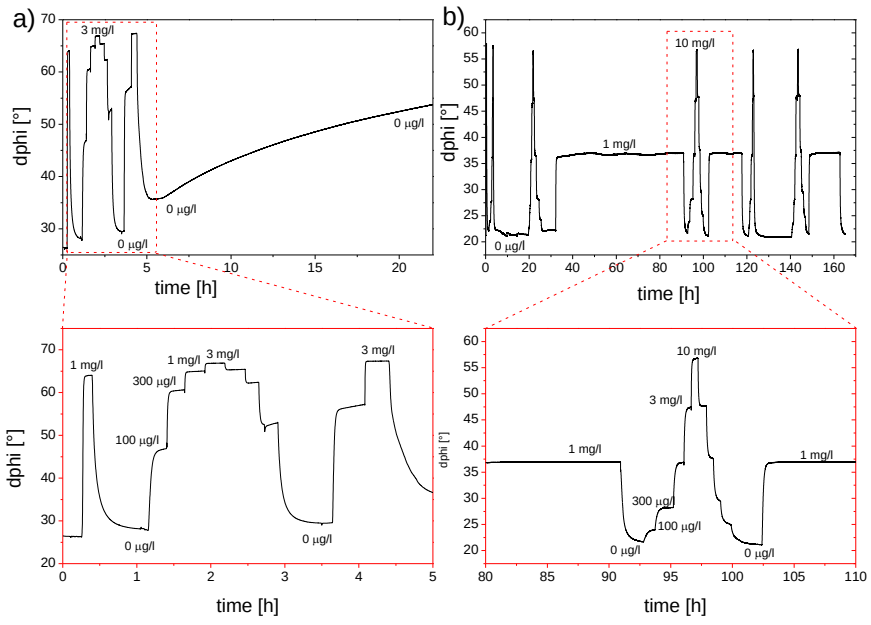

Figure 4: Response and long-term stability of ammonia optodes for different sensor assemblies: a) Sensor E: DiClBut dissolved in HT 15 film only. b) Sensor D: DiClBut indicator dye entrapped in HT 15/Silicon emulsion.

The sensing principle is based on the acid-base equilibrium between pH indicator and ammonia and is similar to optical pH probes. Consequently, plotting cot(phi) against the logarithm of the ammonia concentration yields a sigmoidal curve which can be ideally fitted by Boltzmann equation (1) ($R^2 \geq 99.6\%$, see Figure **5**):

$$y = A2 + \frac{A1-A2}{1+10^{\left(\frac{log(x)-x0}{dx}\right)}} \qquad \textbf{(1)}$$

A1 and A2 indicates the upper and lower plateau, x0 specifies the point of inflection and dx determines the slope of the curve. In order to investigate the tunability of the sensing properties, the sensor assembly shown in figure **3b** was also applied for **DiClBut** in hydrogel D7 as host polymer and for **DiClC12** (Fig. **1**) as indicator dye in both polymers (Fig. 5). D7 outperforms HT 15 in terms of detectable concentration ranges, especially in combination with **DiClC12** as indicator dye (lower pK_a value) which represents the most sensitive combination. In fact, **DiClBut** in HT (sensor **D**) and D7 (sensor **C**) show 50 % of the signal decrease at about 549 µg/l and 295 µg/l NH_3, respectively. More notably, 50% signal change for **DiClC12** in HT (**B**) and D7 (**A**) is achieved at concentrations as low as 66 µg/l and 23 µg/l, respectively (SI, Fig. **S5-S7**, Table **S2**). The LOD for the most sensitive sensor (**A**) was estimated to be 0.11 µg/l (SI, Fig. **S8**). Higher sensitivity of the D7-based sensors correlates well with better water uptake of the polymer compared to HT 15 (30 and 15%, respectively). It should be noted that trace ammonia sensing capabilities are of much importance e.g. for fish farming since dissolved ammonia is already toxic for aquatic organisms at concentrations above 25 µg/l. Similarly to the material **D**, the long-term operational stability of the sensor **A** is excellent (SI, Fig. **S9**). In fact, the sensor showed fully reversible response for over two weeks of continuous operation.

Current limitation of the sensors is their fairly long response and recovery times (t_{90}) which in case of sensor **A** were 2.7 h and 5.6 h, respectively, for a change in ammonia concentration between 10 µg/l to 100 µg/l (SI Fig. **S9**). Although the thickness of the sensing layer was calculated to be 15.5 µm, some of the sensing material may be entrapped inside of the pores of the Teflon filter, resulting in significant increase of the thickness. Faster responding sensors were obtained by simply reducing the sensing layer thickness to 7.8 µm (with identical sensor formulation). In fact, the response and recovery times decreased to 1 h and 2.7 h, respectively. It should be mentioned that the optoelectronic components of the FirestingO2 (which is originally designed for oxygen sensing) do not ideally match the spectral properties of the aza-BODIPY dyes so that neither the excitation is very efficient (λ = 624 nm, Fig. 2) nor the whole emission is collected due to the long-pass filter used. Therefore, optimization of the

optoelectronic components of the reader would allow significant improvement in the S/N ratio and therefore enable even thinner sensing layers. Such modification is expected to shift the response and recovery times well below 1 h. Other sensor designs (e.g. fiber-optic microsensors) may also result in further improvement.

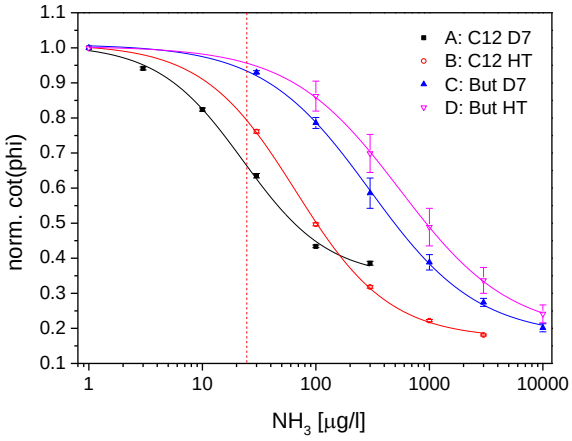

Figure 5: Calibration plots of ammonia sensors A, B, C and D, monitored at 25°C. The dashed red line displays the toxicity level of 25 µg/l for aquatic organisms

Cross-talk of pH and temperature

Ammonia sensing materials with immobilized pH sensitive indicators require a proton impermeable protection layer in order to avoid sensor response to pH changes of the aqueous test sample. Here, polyfluorinated membrane filters in combination with silicone rubber were chosen as proton barriers in the sensors. Potential cross-talk was tested at different pH values (4.0, 7.0 and 10.0) and none has been found (fig. **6**), even at pH values far beyond the indicator's pK_a value.

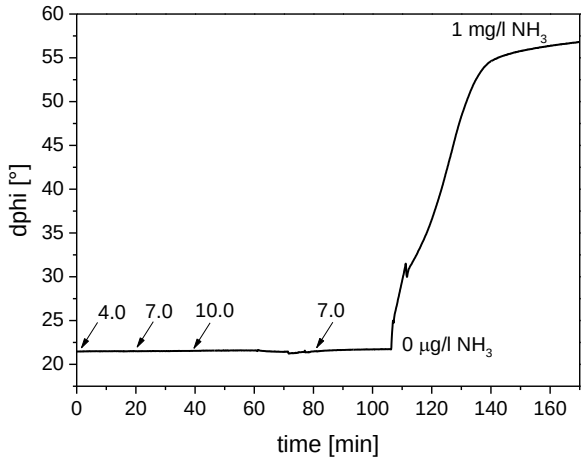

Figure 6: Effect of pH on response of the sensor **A**.

The ammonia sensing material displays a fairly strong temperature cross-talk. Figure **7** shows the calibration curves for 3 individual sensors of type **A** monitored at three different temperatures (10, 22.5 and 35 °C, SI fig. **S10**, Table **S3**). The ammonia concentration was recalculated for the shifted ammonia-ammonium equilibrium. A pronounced decrease in the sensitivity at higher temperatures is clearly visible. This behaviour is in good agreement with literature reports[15] and is attributed to decrease of ammonia solubility in the polymer. Some temperature cross-talk may originate from dependency of the fluorophore's emission, quantum yield and its pK_a value on temperature. The cot (phi) value is rising with increasing temperature. This can be explained by thermal quenching of the luminescence of Egyptian blue which affects the luminescence intensity and the decay time)[38] which both contribute to the overall phase shift in the DLR technique.

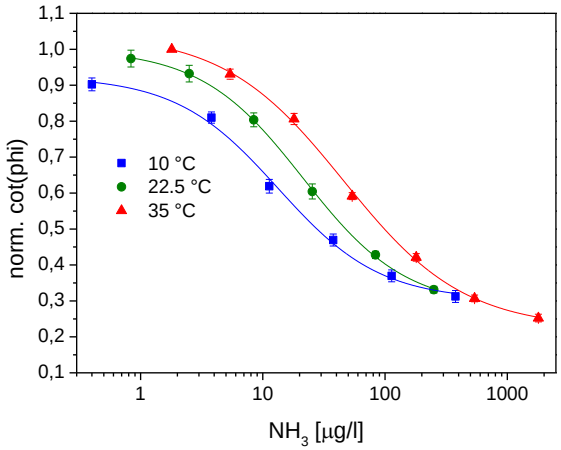

Figure 7: Calibration plots for the sensors of type A, monitored at three different temperatures (10, 22.5 and 35 °C).

To obtain a three-dimensional fit, the sigmoidal Boltzmann function was extended by only two temperature coefficients and following equation was used:

$$\cot(dphi) = \frac{A2+((A1+A1_t*(T-20))-A2)}{1+10^{\frac{\log(NH_3)-(x0+x0_t*(T-20))}{dx}}} \quad (2)$$

where $A1_t$ = 0.009402, $x0_t$ = 0.0191, A1 = 1.817, A2 = 0.4501, dx = 1.065, x0 = 1.336.

Application in wastewater treatment

Wastewater usually contains high levels of bound nitrogen (ammonia, nitrate, etc.) which encourages growth of algae, cyanobacteria or weeds. Thus, oxidation of nitrogen from ammonium/ammonia to nitrate (nitrification) and subsequent reduction of nitrate to nitrogen gas is a key process in wastewater treatment. Here, we demonstrate the applicability in environmental monitoring by measuring ammonia in sewage water from a wastewater treatment plant "Kläranlage Gössendorf" before and after the purification. For this purpose, the total ammonium content was determined via a photometric method (DIN EN 23406) and the concentration of free ammonia was calculated on the basis of pH measurement (at 25 °C). The concentration of free ammonia determined with sensor **B** was 1506 µg/l and 92.7 µg/l for the samples before and after the treatment, respectively. For comparison, the calculated ammonia concentrations obtained by the photometric method were 1221 and 90.0 µg/l, respectively. Whereas the lowest concentration determined by the optode shows a very good match with the reference method, the deviation is more significant for the higher concentration. This discrepancy can be explained by the fact that the resolution of the sensor between 1 and 3 mg/l

is very low (Fig. **5**). It should be mentioned here that optical pH sensors based on a single pH indicator also show a limited dynamic range (about 3 pH units). However, the dynamic range can be significantly extended by combining pH indicators with different pK_a values.[40] Analogously to this approach is it likely to be possible to obtain ammonia sensors with wider dynamic range by combining DiCl-But and DiCl-C12 indicators in the same matrix (e.g. Hydrothane). Extreme similarity of photophysical properties of both indicators is an important prerequisite for successful realization of this concept.

Conclusions

We presented a set of fibre-optic ammonia sensors based on highly photostable aza-BODIPY dyes which cover the concentration range of dissolved ammonia from 10 mg/l to trace concentration below 1 µg/l. Entrapment of the "sensing chemistry" in form of emulsion into silicone rubber dramatically increased the operational stability to at least several weeks of continuous measurement. The dual-lifetime referenced sensor utilizes inert Egyptian blue particles and is read-out with a compact phase fluorometer. The new sensors have high potential for a wide variety of biological, biotechnological and environmental applications such as fish farming or wastewater monitoring.

Acknowledgements

Financial support by the European Union FP7 SenseOCEAN - Marin Sensors for the 21st century (Grant agreement Number 614141) is gratefully acknowledged. The authors would like to thank Christoph Staudinger for the help with temperature compensation algorithm.

Supporting Material

Buffer Preparation

100 mM phosphate buffer solutions (pH 7.00) were prepared and an equivalent amount of ammonium chloride was dissolved in each buffer. The concentration of free ammonia is calculated by the Henderson-Hasselbalch equation,

$$pH = pK_a + log_{10} \frac{c[NH_3]}{c[NH_4^+]} \quad \textbf{(1)}$$

$$[NH_3] = [NH_4^+] \times 10^{(pH-pKa)}$$

pK_a of NH_4Cl = 9.24 at pH 7:

$$log[NH_3] = log[NH_4^+] - 2.44$$

The temperature dependency of the ammonia-ammonium equilibrium was calculated by the Gibbs free energy.

$$\Delta G = R \times T \times lnK \quad \textbf{(2)}$$

Table S1. Concentration of free ammonia in buffer solutions (100 mM phosphate buffer) containing NH_4Cl.

NH_4Cl mg/l	NH_4^+ (total) mg/l	NH_3 mg/l 10°C, pH 7.06	NH_3 mg/l 25°C, pH 7.00	NH_3 mg/l 35°C, pH 6.96
0.55	0.18	0.0004	0.001	0.0018
1.67	0.53	0.0011	0.003	0.0054
5.55	1.77	0.0038	0.010	0.0180
16.66	5.30	0.0113	0.030	0.0539
55.51	17.67	0.0377	0.100	0.1799
166.59	53.03	0.1132	0.300	0.5397
555.33	176.77	0.3773	1.00	1.799
1665.95	530.30	1.1318	3.00	5.397
5551.06	1767.00	3.773	10.00	17.99

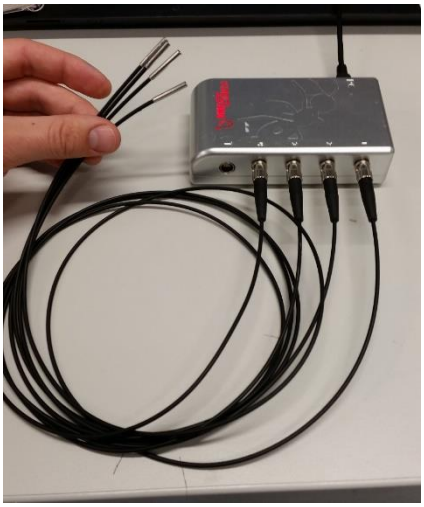

Figure S1: Photographic image of fibre-optic ammonia sensors connected to a four-channel phase oxygen meter.

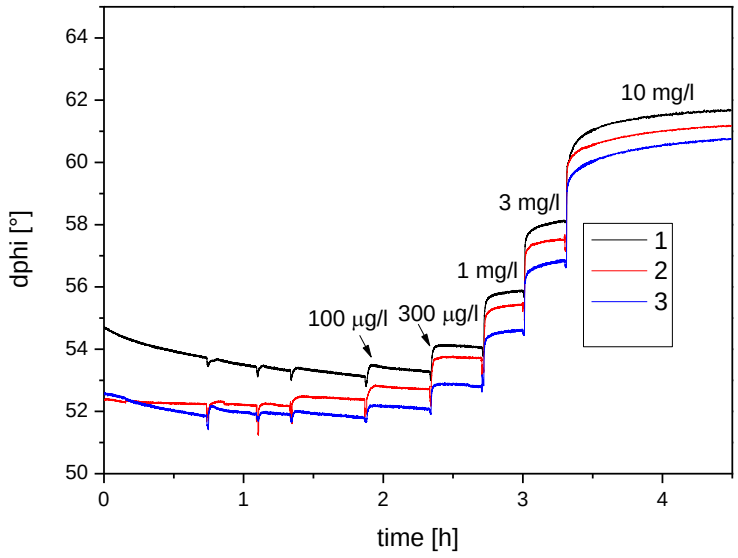

Figure S2: Time-resolved signal response (phase shift) of sensor **F** (ethyl cellulose as host polymer) at different ammonia concentrations at 25 °C.

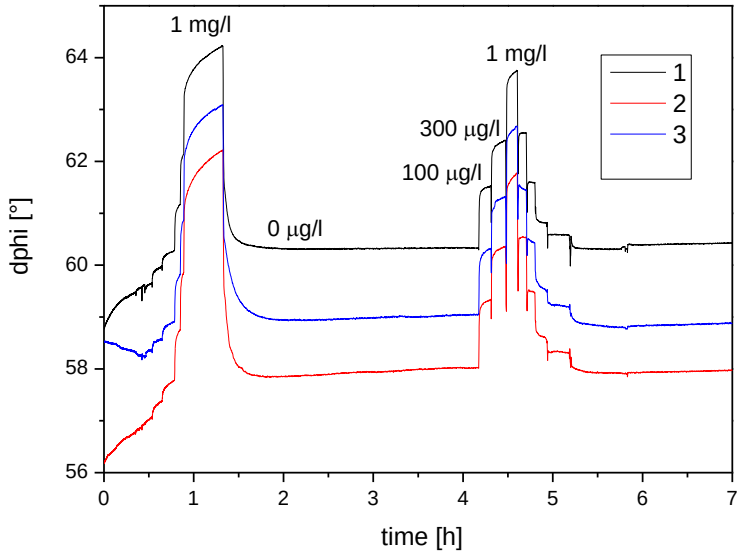

Figure S3: Time-resolved signal response (phase shift) of sensor **G** (cellulose acetate propionate as host polymer) at different ammonia concentrations at 25 °C.

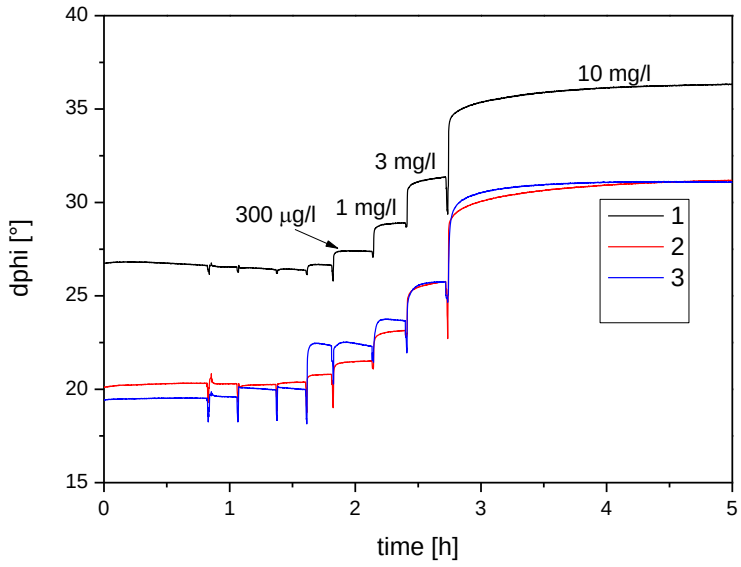

Figure S4: Time-resolved signal response (phase shift) of sensor **H** (cellulose acetate butyrate as host polymer) at different ammonia concentrations at 25 °C.

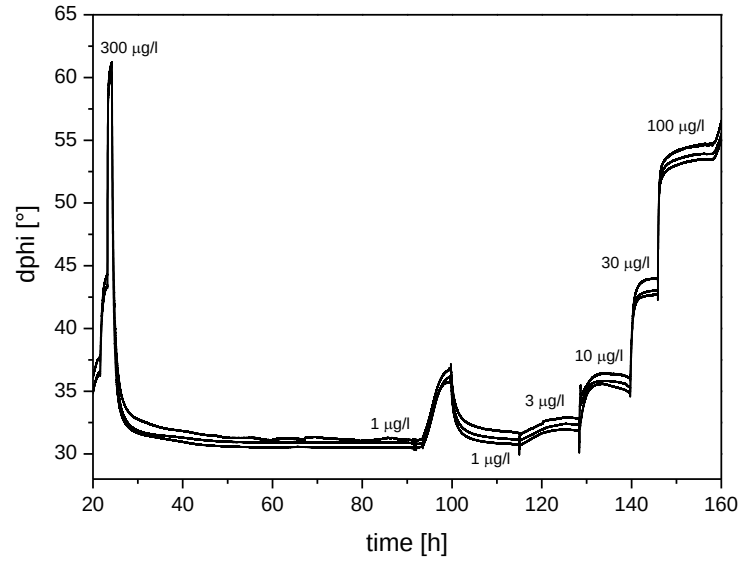

Figure S5: Response (phase shift) of sensor **A** to different ammonia concentrations at 25 °C.

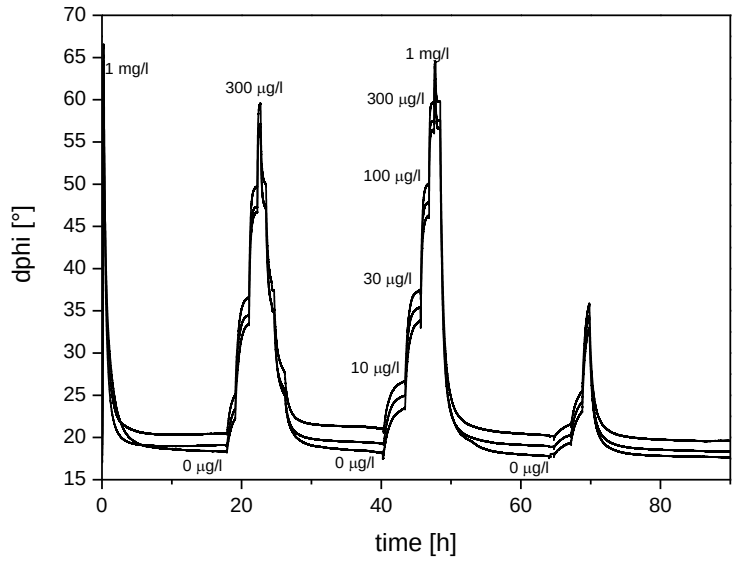

Figure S6: Response (phase shift) of sensor B to different ammonia concentrations at 25 °C.

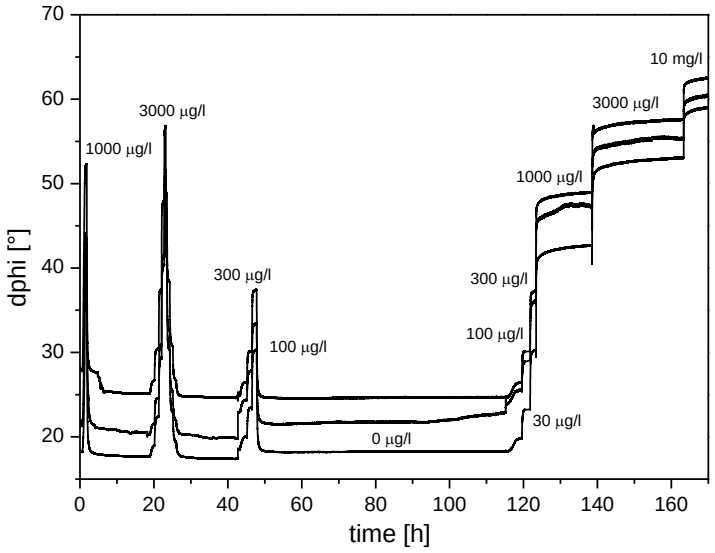

Figure S7: Response (phase shift) of sensor C to different ammonia concentrations at 25 °C.

Table S2: Fit parameters (sigmoidal curve, Boltzmann fit) for ammonia sensors at 25 °C.

Modell	Boltzmann		
Equation	y = A2 + (A1-A2)/(1 + exp((log10(x)-x0)/dx))		
χ^2	2,55E-04	5,80E-05	1,07E-04
Kor. R^2	0,99622	0,99945	0,99895
		Value	SD
Sensor **A**	A1	1,00956	0,02118
	A2	0,34538	0,0276
	x0	1,35953	0,04802
	dx	0,37658	0,05305
Sensor **B**	A1	1,01091	0,00858
	A2	0,17157	0,00824
	x0	1,82347	0,01696
	dx	0,41223	0,01744
Sensor **C**	A1	1,01007	0,01057
	A2	0,17685	0,01433
	x0	2,47665	0,02804
	dx	0,47306	0,02569
Sensor **D**	A1	1,0042	0,0054
	A2	0,18667	0,00999
	x0	2,73987	0,01787
	dx	0,48573	0,01511

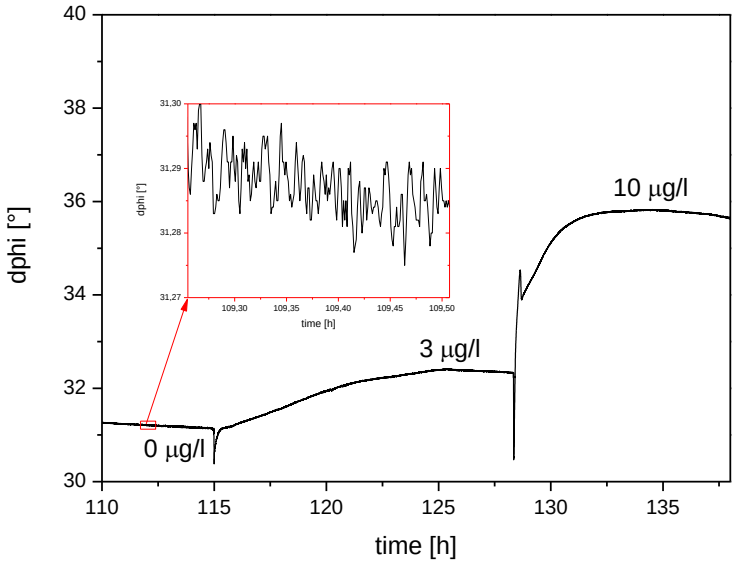

Figure S8: Estimation of LOD of Sensor A.

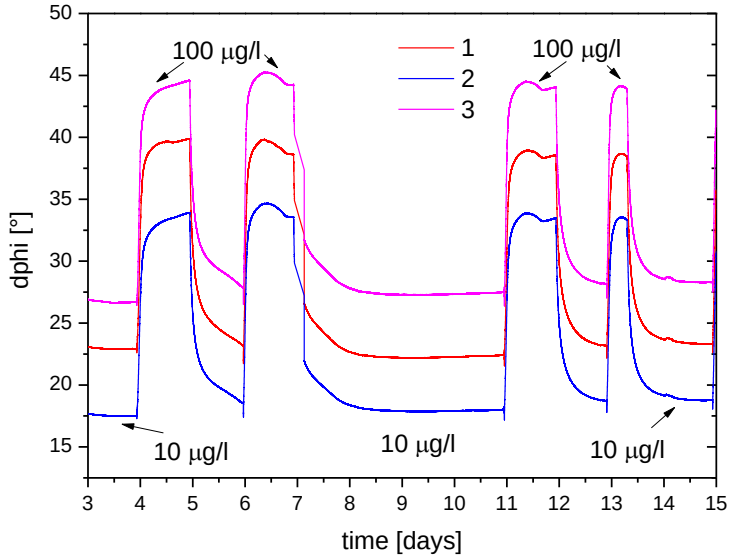

Figure S9: Response of sensor A between 10 and 100 µgl/l ammonia at 25°C monitored for 12 days**.**

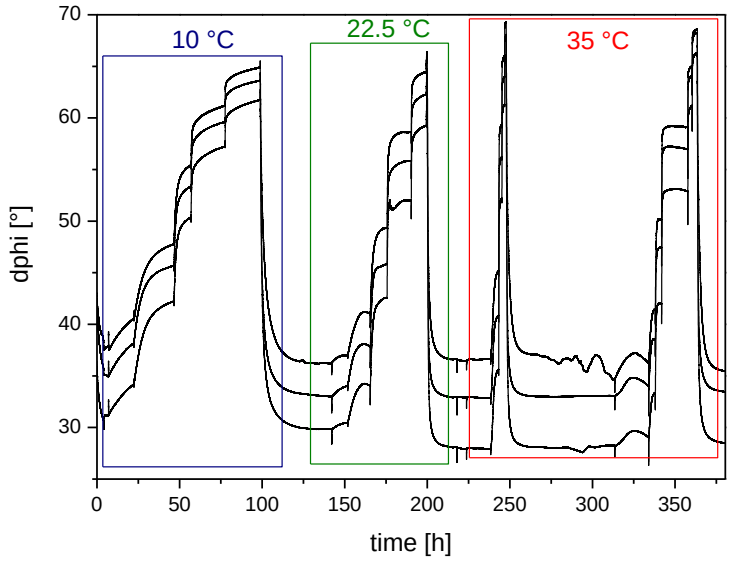

Figure S10: Signal response (phase shift) of sensor A to different ammonia concentrations, monitored at three temperatures (10, 22.5 and 35 °C).

Table S3: Parameters of the sigmoidal curve (Boltzmann Fit) of Sensor A.

Modell	Boltzmann		
Equation	y = A2 + (A1-A2)/(1 + exp((log10(x)-x0)/dx))		
χ^2	3,47E-04	2,78E-05	7,55E-05
R^2	0,99144	0,99939	0,99862
		Wert	Standardfehler
10 °C	A1	1,01663	0,02375
	A2	0,50113	0,02261
	x0	1,01626	0,06955
	dx	0,39917	0,06972
22.5 °C	A1	1,01969	0,0077
	A2	0,45737	0,01011
	x0	1,27515	0,02066
	dx	0,40351	0,02352
35 °C	A1	1,03211	0,01516
	A2	0,40849	0,01171
	x0	1,64224	0,03323
	dx	0,47126	0,037

Chapter 3

Photostable upconverting and downconverting pH sensors based on combination of a colorimetric NIR indicator and stable inorganic phosphors as secondary emitters

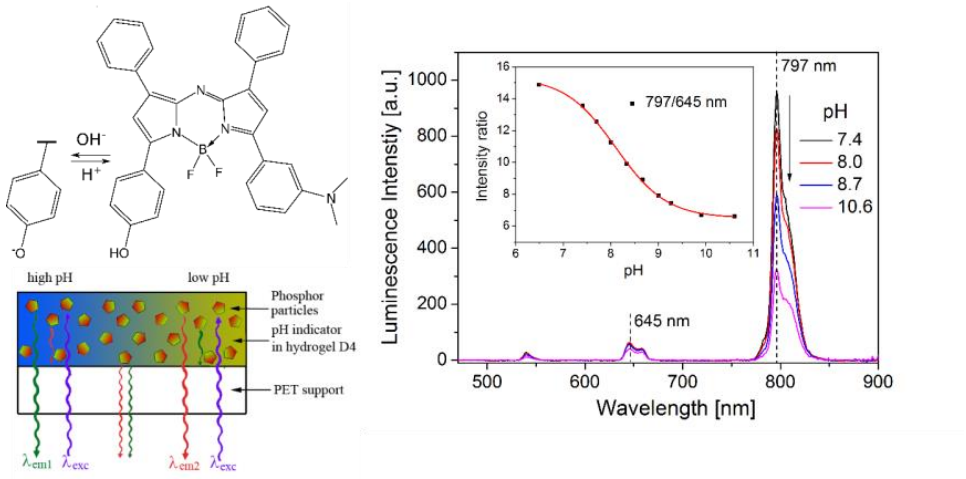

Photostable upconverting and downconverting pH sensors based on combination of a colorimetric NIR indicator and stable inorganic phosphors as secondary emitters

This paper was submitted in Sensors and Actuators: B. Chemical

Martin Strobl, Torsten Mayr, Ingo Klimant and Sergey M. Borisov

New robust optical pH sensors rely on a combination of a photochemically stable NIR colorimetric aza-BODIPY dye and inorganic phosphors. Inner-filter effect is utilized to convert the colorimetric changes into a luminescence response. Chromium(III)-activated gadolinium aluminium borate and Egyptian Blue were used as inert reference phosphors, enabling two-wavelength ratiometric read-out in the emission and excitation modes, respectively. Additionally, we synthetized dually-emitting upconverting particles (UCPs) based on lanthanide-doped molybdates ($NaCaY_{1-x}La_x(MoO_4)_3$, La = Yb(III), Ho(III) and Tm(III)) featuring anti-Stokes emission peaks in the red/NIR spectral region (645/800 nm). Upon NIR excitation (980 nm) the NIR emission of the upconverting particles is modulated by the pH indicator, whereas the red emission serves as a reference. Importantly, the spectral properties of the pH sensor based on UCPs are fully compatible with the biological optical window.

Keywords: pH, optical sensor, inorganic phosphor, upconversion, luminescence, inner-filter effect

Introduction

In the last decade, optical sensors have found wide-spread application for determination of pH in various fields of science and technology, including biochemistry, biotechnology [63,64], medical diagnostics or biomedical research [65–67]. Especially fluorescent pH sensors have attracted considerable attention due to their high sensitivity, versatility of formats (planar optodes, fibre-optic sensors, nanosensors) and well-established referencing read-out systems such as two-wavelength ratiometric measurement or dual-lifetime referencing [3,68]. However, several undesirable effects can severely compromise the response of fluorescent sensors, most prominently self-quenching of the analyte-sensitive fluorophore or quenching by fluorescence quenchers. Here, robust absorption-based indicators may overcome these issues. However, it should be kept in mind that response of absorption sensors is more difficult to quantify due to possible light losses deriving from additional reflectance/absorption from optical components, e.g. optical fibres.

The response of colorimetric pH indicators can be converted into a fluorescent response either by exploring FRET from a luminescent donor to the pH indicator [69–72] or *via* inner-filter effect [73,74]. Whereas the first approach introduces additional risks associated with (self)quenching of the donor and cross-talk to oxygen (if the luminescence lifetime of the donor is sufficiently long), the second approach is a more robust and allows application of highly photostable inorganic emitters. In this two-wavelength ratiometric sensing scheme the emission spectrum of an inert phosphor overlaps with the absorption of at least one form of the pH indicator and, depending on pH, the luminescence of the phosphor is reabsorbed by the indicator [73].

Photon upconversion is a process in which an anti-Stokes emission (visible range) is generated after excitation in the near-infrared region (980 nm) [34,35]. The crucial advantages of NIR-excitation is excellent penetration of excitation light, absence of photodamage of biological matter and virtually complete elimination of auto-fluorescence of biomolecules [75]. In the upconverting phosphors (UCPs), the Yb^{3+} ion is used as sensitizer which is excited by NIR light (e.g. a 980 nm laser diode) and the energy is transferred to activator ions such as Er^{3+}, Ho^{3+} or Tm^{3+}. The anti-Stokes shift of the UCPs strongly depends on the choice of lanthanide dopants. Whereas the Er^{3+}-doped materials emit in the green part of the electromagnetic spectrum, those doped with Ho^{3+} or Tm^{3+} generate a strong emission in the red or near-infrared spectral region, respectively. Due to the above advantages, light upconverting materials are not only of high interest for bioimaging and encoding applications [37,38] but also as components of optical sensing materials [76] including pH sensors. For instance, inner-filter effect based ratiometric pH sensors with upconverting capabilities have been reported [77–79]. However to the best of our knowledge, so far only UCPs which generate green or/and red anti-Stokes emission where used to design pH sensors [77–82]. Unfortunately, utilization of green emission for analytical purposes cancels some benefits provided by the upconverting phosphors since this emission is efficiently absorbed/scattered by tissues and blood.

Among all those colorimetric indicators presented in literature, there is surprising scarcity of pH indicators exhibiting absorption bands in the red/NIR-spectral region. Here, BF_2-chelated tetraarylazadipyrromethene dyes (aza-BODIPYs) [2,24,83,84] represent promising candidates due to their remarkable photostability, high molar absorption coefficients (80 000 $M^{-1}cm^{-1}$) and accessibility to structural modifications. However, aza-BODIPY dyes are known to be highly fluorescent, which is a disadvantage for the inner-filter effect based read-out due to the bias introduced by the pH-dependent emission. To the best of our knowledge, pH-sensitive aza-BODIPY indicators, exhibiting no fluorescence emission, have not been reported so far.

In this contribution, we synthesized an aza-BODIPY dye with completely "switched off" emission within its dynamic range which shows pronounced bathochromic shift of the NIR absorption upon deprotonation. This colorimetric aza-BODIPY dye is combined with inorganic phosphors ((photo)chemically stable chromium(III) activated gadolinium aluminium borate [85] or Egyptian Blue [32]) to result in luminescent dually wavelength referenced optical sensors. Moreover, we prepared a dually emitting red/NIR phosphor (650/800 nm) by doping $NaCaY(MoO_4)_3$ host [86] with Yb^{3+}, Ho^{3+} and Tm^{3+} and combined it with the new pH indicator to obtain a ratiometric pH upconversion-based sensor operating in a biological optical window.

Experimental Section

Materials

3'Dimethylaminoacetophenone, diisopropylethylamine, benzaldehyde and boron trifluoride diethyl etherate were purchased from TCI Europe (www.tcieurope.de) and 4'-hydroxychalcone was bought from ABCR (www.abcr.com). MOPS buffer, nitromethane and anhydrous sodium sulfate were purchased from Sigma Aldrich (www.sigmaaldrich.com). Deuterated chloroform ($CDCl_3$) and dimethyl sulfoxide (DMSO-d_6) were obtained from Euriso-top (www.euriso-top.com). All other solvents (synthesis grade) as well as sodium chloride and the buffer salts (MES, HEPES, and CHES) were purchased from Carl Roth (www.carlroth.com/de). Silica-gel (0.04-0.063 mm) was bought from Acros (www.acros.com). Polyurethane hydrogel (Hydromed D4) was purchased from AdvanSource biomaterials (www.advbiomaterials.com). Poly-(ethylene glycol terephthalate) support (PET) was from Pütz (www.puetz-folien.com). Microcristalline powder of chromium-doped gadolinium aluminium borate (Gr-GAB, 5 mol% doping with respect to aluminium) was synthesized as described elsewhere [33]. Silanized Egyptian Blue was prepared according to literature procedure [32]. For the synthesis of upconversion particles, sodium carbonate (99.9 %) was obtained from VWR (at.vwr.com/store/) and calcium carbonate ($\geq$ 99%) was bought from Fluka. Thulium(III) oxide (99.9 %), yttrium(III) oxide (99.99%), holmium(III) oxide (99.9 %) and molybdenum(VI) oxide (99.999 %) were purchased from ABCR. Ytterbium(III) oxide (99.9 %) was from Heraeus (www.heraeus.com/de).

Methods

Absorption measurements were performed on a Cary 50 UV-VIS spectrophotometer (Varian, Palo Alto). Fluorescence measurements for the pH sensors were performed on a Fluorolog3

spectrofluorimeter (Horiba J. Y.), equipped with a NIR-sensitive photomultiplier R2658 from Hamamatsu (300-1050 nm). Upconversion fluorescence spectra were recorded on a Hitachi-F-7000 spectrofluorometer at reduced scan rate (240 nm/min), equipped with a R9876 photomultiplier (Hamamatsu) in combination with an external 980-nm continuous wave laser (30 mW, Picotronic GmbH) as excitation source. All fluorescence spectra were corrected for detector response. In order to diminish background noise, a bandpass filter and a lens was installed between the laser diode and pH sensor foil and a Calfex^{TM} filter was positioned in front of the photomultiplier. The pH of the buffer solution (MES, HEPES, CHES) was adjusted with a pH meter using a glass electrode (InoLab pH/ion, WTW GmbH & Co. KG). The pH meter was calibrated at 25 °C with standard buffers of pH 7.01 and pH 4.01 (WTW GmbH & Co. KG). Ionic strength (IS = 150 mM) of the buffers was adjusted by using sodium chloride as the background electrolyte. The NMR spectroscopic experiments were performed on a 300 MHz instrument (Bruker) in DMSO-d_6 or $CDCl_3$ with TMS (tetramethylsilane) as a standard. Chemical shifts (δ) are given in parts per million (ppm) relative to TMS and coupling constants *J* are stated in Hz. The upconversion particles were finely ground in a planetary micro mill (Pulverisette 6, Fritsch). Relative fluorescence quantum yields were determined by using tetra-tert-butyl-29H,31H-phthalocyanine as a standard (ϕ = 0.44, Fluka) according to Demas and Crosby [87].

Preparation of upconversion phosphor particles

For **UCP 1** ($NaCaY_{0.2}Yb_{0.73}Ho_{0.07}(MoO_4)_3$), sodium carbonate (1 eq, 397 mg, 3.58 mmol), calcium carbonate (1 eq, 716 mg, 7.2 mmol), yttrium(III) oxide (0.2 eq, 162 mg, 0.72 mmol), ytterbium(III) oxide (0.73 eq, 1.029 g, 2.6 mmol), Ho_2O_3 (95 mg, 0.07 eq, 0.25 mmol) , molybdenum(VI) oxide (3 eq, 3.091 g, 21.5 mmol) and ethanol (3 ml) were homogenously mixed in an agate mortar with a pestle. The mixture was transferred in a crucible and heated in a muffle furnace at 500 °C for 5 h. Then, the solid was reground in an agate mortar and sintered at 950 °C for 5 h. The obtained product was finely ground in a ball mill. **UCP 2** ($NaCaY_{0.2}Yb_{0.73}Tm_{0.07}(MoO_4)_3$) was prepared analogously, but using Tm_2O_3 (96 mg, 0.07 eq, 0.25 mmol) instead. **UCP 3** ($NaCaY_{0.2}Yb_{0.7}Tm_{0.05}Ho_{0.05}$ $(MoO_4)_3$) was prepared with Y_2O_3 (987 mg, 0.7 eq, 2.5 mmol), Tm_2O_3 (69 mg, 0.05 eq, 0.17 mmol) and Ho_2O_3 (108 mg, 0.05 eq, 0.13 mmol) and amounts of all other components identical to those used for **UCP 1**. For **UCP 4** ($NaCaY_{0.2}Yb_{0.7}Tm_{0.02}Ho_{0.08}$ $(MoO_4)_3$) (27 mg, 0.02 eq, 0.07 mmol) of Tm_2O_3 and 108 mg (0.08 eq, 0.28 mmol) of Ho_2O_3 were used instead.

Dye synthesis

1–(4-hydroxyphenyl)-4-nitro-3-phenylbutan-1-one were synthesized according to Jokic *et al.*[81] and 1-(4-butoxyphenyl)-4-nitro-3-phenylbutan-1-one was prepared according to literature procedure [88].

(Z)-4-(5-((5-(4-butoxyphenyl)-3-phenyl-2H-pyrrol-2-ylidene)amino)-1-(difluoroboraneyl)-4-phenyl-1H-pyrrol-2-yl)-2-nitrophenol (2)

(E)-1-(4-hydroxy-3-nitrophenyl)-3-phenylprop-2-en-1-one [269.1] ***2a***

A solution of 4-hydroxy-3-nitroacetophenone (1 eq, 3 g, 16 mmol) benzaldehyde (1 eq, 1.68 ml, $\rho = 1.05$ g*cm^{-3}) and potassium hydroxide (3 eq, 2.79 g in 10 ml H_2O, 22.4 mmol) in ethanol (50 ml) was stirred at room temperature for 12 hours. During the course of the reaction the product partly precipitated from the reaction mixture. Then, the reaction solution was acidified with hydrochloric acid (1M HCl) and the solid was collected on a filter and washed with distilled water to afford the title compound. Yield: 3.62 g, **81.2 %.**

1-(4-hydroxy-3-nitrophenyl)-4-nitro-3-phenylbutan-1-one [330.1] ***2b***

Compound **2a** (1 eq, 3 g, 11 mmol) was dissolved in ethanol (50 ml); nitromethane (20 eq, 12.08 ml, 22 mmol, $\rho = 1.127$ g*cm^{-3}) and potassium hydroxide (1.4 eq, 876 mg, 15 mmol) were added and the reaction was heated under reflux for 3.5 hours. After cooling to room temperature, the solvent was removed in vacuum. The resulting oily residue was acidified with 1 M HCl and was partitioned between ethyl acetate and distilled water in a separating funnel. The organic layer was separated, dried over sodium sulfate and evaporated under reduced pressure. Yield: 3.04 g, **82.6 %**.

(Z)-4-(5-((5-(4-butoxyphenyl)-3-phenyl-2H-pyrrol-2-ylidene)amino)-4-phenyl-1H-pyrrol-2-yl)-2-nitrophenol [582.2] ***2c***

(1–(butoxyphenyl)-4-nitro-3-phenylbutan-1-one (1 eq, 2.37 g, 6.9 mmol), (1–(4-hydroxy-3-nitrophenyl)-4-nitro-3-phenylbutan-1-one (1 eq, 2.31 g, 6.9 mmol) and ammonium acetate (35 eq, 18.86 g, 242 mmol) were dissolved in butanol (40 ml) and the solution was heated under reflux for 12 h while stirring. After, the solvent was removed in vacuum; the obtained solid was washed with water and purified by flash chromatography with 3% THF/CH_2Cl_2 (after eluting symmetrical by-product with 100 % CH_2Cl_2). The final product was recrystallized from hexane/tetrahydrofuran mixture. Yield: 980 mg, **25.0 %**.

BF_2 chelate of (Z)-4-(5-((5-(4-butoxyphenyl)-3-phenyl-2H-pyrrol-2-ylidene)amino)-4-phenyl-1H-pyrrol-2-yl)-2-nitrophenol [630.2] ***2***

2c (1 eq, 339 mg, 0.58 mmol) was dissolved in dry CH_2Cl_2 (40 ml) N,N-diisopropylethylamine (DIPEA, 10 eq, 1.12 ml, 5.8 mmol, $\rho = 0.67$ g*cm^{-3}) was added into the solution. Afterwards boron trifluoride diethyl etherate (15 eq, 1.10 ml, 8.7 mmol, $\rho = 1.12$ g*cm^{-3}) was added under N_2-atmosphere and the reaction was stirred overnight. The impurities were removed by shaking the solution with water three times after which the dichloromethane fraction was dried over sodium sulphate. The crude solid was purified by column chromatography on silica gel in CH_2Cl_2. The product was obtained by gradually increasing the polarity by addition of THF. The solvent was removed under reduced pressure. Further purification was achieved by crystallization from hexane/tetrahydrofuran to give the final product. Yield: 275 mg, **75.0 %**.

^{1}H NMR (300 MHz, DMSO-*d6*) δ: 8.26-8.16 (m, 7H), 7.66 (s, 1H), 7.54-7.48 (m, 8H), 7.18-7.12 (m, 3H), 4.15-4.11 (t, *J* = 7.86 Hz, 2H), 1.77-1.70 (m, 2H), 1.53-1.44 (m, 2H), 0.98-0.93 (t, *J* = 7.3 Hz, 3H)

MALDI-TOF *m/z* found 630.2220 calculated 630.2256.

(Z)-4-(1-(difluoroboraneyl)-5-((5-(3-(dimethylamino)phenyl)-3-phenyl-2H-pyrrol-2-ylidene)amino)-4-phenyl-1H-pyrrol-2-yl)phenol (3)

(E)-1-(3-(dimethylamino)phenyl)-3-phenylprop-2-en-1-one [251.1] ***3a***

Compound **3a** was prepared analogously to **2a** but using 3'-dimethylaminoacetophenone (1 eq, 2.607 g), benzaldehyde (1 eq, 1.68 ml, $\rho = 1.05$ g*cm^{-3}), potassium hydroxide (3 eq, 2.68 g in 10 ml H_2O) and ethanol (50 ml) instead. Yield: 3.90 g, **97.3 %**.

1-(3-(dimethylamino)phenyl)-4-nitro-3-phenylbutan-1-one [312.1] ***3b***

Compound **3b** was prepared analogously to **2b** but using compound **3a** (1 eq, 2.303 g), in ethanol (50 ml), nitromethane (20 eq, 9.9 ml, $\rho = 1.127$ g*cm^{-3}) and potassium hydroxide (0.7 eq, 347 mg) instead and heating the solution under reflux for 3.5 hours. Yield: 2.74 g, **95.8 %**.

4-((5Z)-5-(5-(3-(dimethylamino)phenyl)-3-phenyl-2H-pyrrol-2-ylideneamino)-4-phenyl-1H-pyrrol-2-yl)phenol [508.2] ***3c***

Compound **3b** (1 eq, 1.77 g), (1–(4-hydroxyphenyl)-4-nitro-3-phenylbutan-1-one (1 eq, 1.62 g) and ammonium acetate (35 eq, 15.29 g) were dissolved in butanol (50 ml) and the solution was heated under reflux for 12 h while stirring. After, the solvent was removed in vacuum, the

obtained solid was washed with water and purified by flash chromatography with 2%THF/CH_2Cl_2 (after eluting symmetrical by-product with 100% CH_2Cl_2). The final product was crystalized from hexane/tetrahydrofuran mixture. Yield: 980 mg, **34.0 %**.

BF_2 chelate of 4-((5Z)-5-(5-(3-(dimethylamino)phenyl)-3-phenyl-2H-pyrrol-2-ylideneamino)-4-phenyl-1H-pyrrol-2-yl)phenol [556.2] ***3***

Compound **3** was prepared analogously to **2** but using **3c** (1 eq, 943 mg), dry CH_2Cl_2 (40 ml), N,N-diisopropylethylamine (DIPEA, 10 eq, 3.1 ml, ρ = 0.67 g*cm^{-3}) and boron trifluoride diethyl etherate (15 eq, 3.4 ml, ρ = 1.12 g*cm^{-3}) instead. After column chromatography further purification was achieved by crystallization from dichloromethane/cyclohexane mixture to give the final product as reddish powder. Yield: 400 mg, **38.7 %**.

^{1}H NMR (300 MHz, DMSO-*d6*) δ: 8.21-8.14 (m, 5H), 7.83-7.74 (m, 2H), 7.56-7.21 (m, 10H), 6.97-6.81 (m, 3H), 2.99 (s, 6H)

MALDI-TOF *m/z* found 557.2924 calculated 556.2252.

Preparation of sensing materials

For Sensor **A**, aza-BODIPY dye **3** (2 mg, 2 % w/w with respect to polymer) hydrogel D4 (100 mg) and **UCP 4** (100 mg) were dissolved/dispersed in tetrahydrofuran (1 ml) and knife-coated on a dust-free PET (polyethylene terephthalate) support by using a bar film applicator. The resulting layer thickness of all sensors was 7.5 µm. For sensor **B**, aza-BODIPY dye **3** (3 mg, 3 % w/w with respect to polymer), hydrogel D4 (100 mg) and microcrystalline Cr-GAB (100 mg) and tetrahydrofuran (1 ml) were used instead. Sensor **C** was prepared similarly, but using silanized microcrystalline Egyptian Blue powder (100 mg) instead of Cr-GAB.

Synthesis and properties of absorption-based aza-BODIPY indicators

In the first approach we attempted to design a non-fluorescent aza-BODIPY dye by introducing a nitro-group in the *ortho*-positon of the pH-sensitive phenol receptor (Figure **1**). Usually, nitro-substituted fluorophores exhibit drastically lowered emission intensity/quantum yield, resulting from a combination of physical and chemical factors [18,89,90]. The fluorescence quantum yield (φ = 0.07) for compound **2**, however, was found to be only 2-fold lower compared to the non-modified aza-BODIPY dye (φ = 0.15, **1**) [84].

Hence a new design concept was investigated where a dimethylamino-group as second PET-group was introduced (Figure **1,** dye **3**). Due to very low pK_a value of the aromatic amines,

complete quenching at neutral pH was expected. It is known that introduction of amino-functionalities in the *para*-positon of the aryl-rings 3 and 4 [26] or of the aryl rings 1 and 2 [24] results in significant changes in the absorption properties of the aza-BODIPY chromophore which also retains fluorescence at least for one of the dye forms. On the other hand, a hydroxy-group introduced in the *meta*-position of the ring 4 was demonstrated to have negligible effect on the absorption properties of the chromophore independent on pH [84]. Thus, the dimethylamino-group was introduced in the same position (dye **3**).

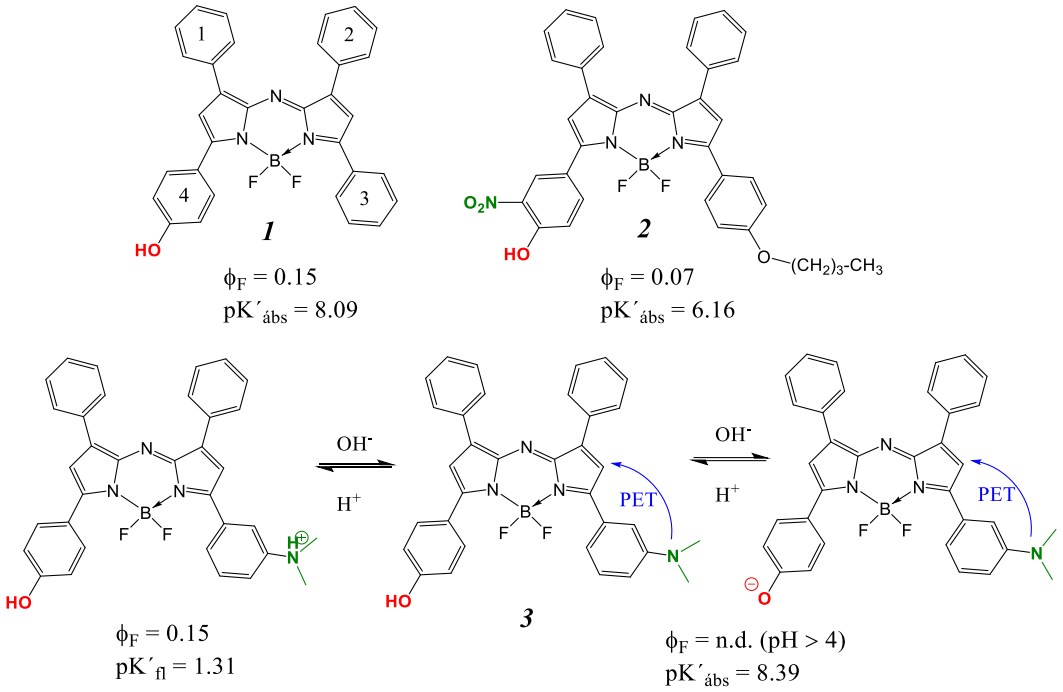

Figure 13) Chemical structures of aza-BODIPY dyes: 1) non-modified aza-BODIPY dye with phenol receptor [84]. 2) Nitro-substituted aza-BODIPY. 3) aza-BODIPY functionalized with dimethylamino moiety, acting as a permanent quencher at pH> 4.

The new aza-BODIPY compounds were physically entrapped in hydrogel D4 and their spectroscopic and pH sensing properties were investigated. As expected, the pK_a value of **2** (6.16) is drastically lowered by the electron-withdrawing nitro-group at the *ortho*-position of the phenol receptor when compared to the dye without nitro-group (9.05) [2]. Despite moderate quantum yield the new dye may be suitable for application in fluorescent pH sensors.

In contrast, introduction of the dimethylamino-group (**3**) as peripheral moiety results only in minor change of the pK_a-value (8.37, Figure **2b**) compared to aza-BODIPY dye possessing only a phenol receptor (pK_a = 8.35) [84]. It should be mentioned, that the pK_a value can be easily tuned by substitution of one or two chlorine atoms at the pH sensitive phenol group [2] thus providing

the possibility of adapting the pH response to a particular application. Notably, the aza-BODIPY dye exhibits distinct pH dependent absorption changes (Figure **2a**) due to intramolecular charge transfer, since the OH group of the phenol receptor is located in the p-position in respect to the BODIPY chromophore. The absorption maximum of the protonated form is located at 683 nm and bathochromically shifts to 753 nm upon deprotonation (Figure **2a**). The molar absorption coefficient ε of **3** is about 77 550 $M^{-1}cm^{-1}$ in tetrahydrofuran and is similar to other aza-BODIPYs [2,84]. As can be seen in Figure **2c**, the dye is virtually not fluorescent at pH ≥ 4 (Figure **2c**), but the fluorescence emission is "switched on" at very low pH due to protonation of dimethylamino-group (Figure **1a**) the sensor showing the apparent pK_a' value of 1.3. Hence, the pH dependent fluorescence emission of this indicator might be of interest for pH measurement in very acidic conditions such as typical for gastric environment [91]. The photostability of **3** was investigated under continuous illumination with an ultra-bright 642-nm LED array (light intensity: 91.7 $mW*cm^{-2}$) and compared with aza-BODIPY possessing only phenol receptor **1**. After 1 h of illumination, 5 % of **3** decomposed, whereas only 2 % of non-modified dye **1** degraded within this time frame. The electron-donating character of the dimethylamino substituent seems to be responsible for the decreased photostability. Nevertheless, the new indicator retains its remarkable photostability, making them highly suitable for long-term measurements.

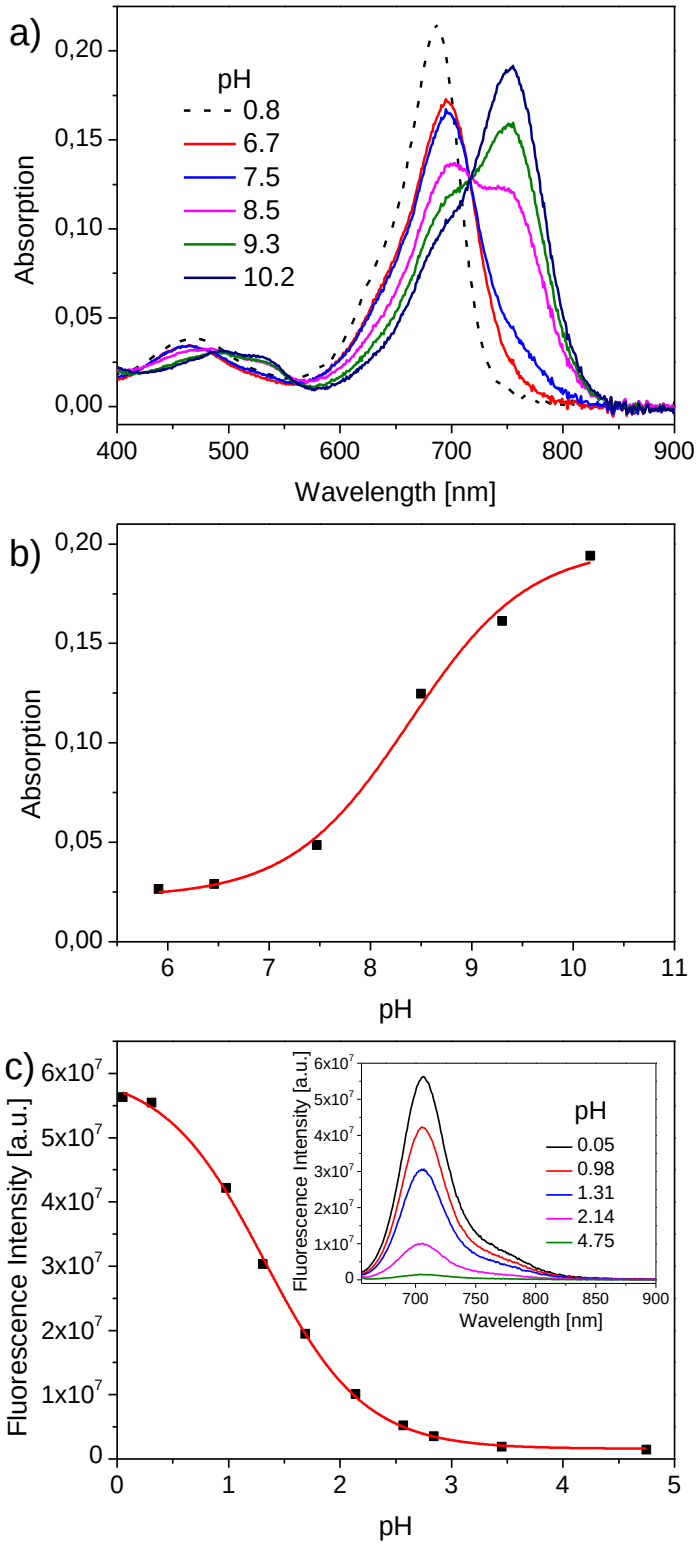

Figure 2) Spectral and pH sensing properties of 3 in Hydrogel D4. **a)** pH dependency of the absorption spectra; **b)** corresponding calibration curve, for absorption at 753 nm (pKa =8.37); **c)** pH dependent fluorescence emission (λexc =640 nm) in highly acidic media: calibration curve and fluorescence spectra (insert).

Referencing scheme and sensor design

As was mentioned above, the colorimetric response of the pH indicator is converted into luminescence changes by making use of the inner-filter effect read-out. In the first scheme (Figure **3a** and **3b**), the emission of a secondary emitter is partly reabsorbed by the indicator. The two-layer system (Figure **3a**) offers the highest degree of modulation since all the light emitted in the direction of the photodetector passes through the pH-sensing layer. However, a two layer system is rather challenging in manufacture since variations in the thicknesses of both layers significantly affect the calibration. Partial dissolution of the first layer upon coating of the second one should also be considered. In the one layer design (Figure **3b**) both the pH indicator and the phosphor are contained in the same layer. This concept offers significant advantages in respect to sensor manufacture and reproducibility. However, in case of the phosphor particles located close to the support the modulation of luminescence by the pH indicator is very limited. This limitation is partly overcome by light scattering in the sensing layer caused by the phosphor particles which efficiently increases the optical pathway.

Apart from modulation of the emission, modulation of the luminescence excitation is also possible (Figure **3c**). In this scheme, the excitation spectrum of the phosphor overlaps with the absorption spectrum of one or both forms of the indicator, resulting in pH dependent reduction of the excitation light intensity for a certain wavelength. On the other hand, the sensing layer is optically transparent for the emission light.

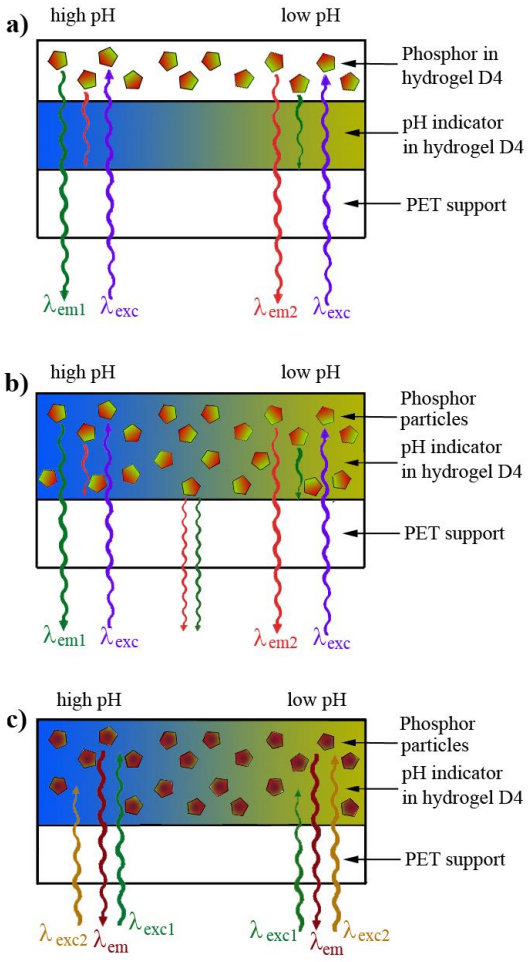

Figure 3) Sensor designs (cross-sections) of referenced pH sensors exploring modulation of the emission (a and b) and modulation of the excitation (c).

Ratiometric pH sensors based on Upconverting Phosphors

Among numerous UCPs presented in literature, lanthanide-doped molybdate ($NaCaY(MoO_4)_3$) [86] are rather interesting since they can be prepared in a simple solid state synthesis and allow high lanthanide doping without self-quenching. The same host was also demonstrated to be promising for design of downconverting phosphors with high Eu^{3+} doping [92]. All UCPs were doped with Yb^{3+} ions, acting as a sensitizer which enables excitation with NIR light (980 nm continuous wave laser). The $^2F_{7/2} \rightarrow {}^2F_{5/2}$ transition of Yb^{3+} is favorably resonant with many f-f transitions of Tm^{3+} and Ho^{3+}, enabling efficient sensitization of the upconverted luminescence [39]. *Co*-doping with Yb^{3+} and Ho^{3+} (**UCP 1**) generates a dual emission in the green (550 nm) and red (650 nm) range, originating from $^5S_2/{}^5F_4 \rightarrow {}^5I_8$ and $^5F_5 \rightarrow {}^5I_8$ transition, respectively (Figure **4a**). In case of the **UCP 2** *co*-doped with Yb^{3+} and Tm^{3+}, an intense NIR-emission band is observed (800 nm) and can be ascribed to the $^3H_4 \rightarrow {}^3H_6$ transition.

In order to obtain a dually emitting upconverting phosphor with emission maxima in red and near-infrared region, the molybdate host was doped with sensitizer Yb^{3+} and both Ho^{3+} and Tm^{3+} activators (Figure **4b,** insert). In case of equal concentration of both activators (**UCP 3**), the NIR emission is significantly stronger than the red one indicating possibility of energy transfer from Ho^{3+} to Tm^{3+}. However, the intensity of the two emission peaks can be easily adjusted by varying the doping ratio of Ho^{3+} and Tm^{3+} (**UCP 4,** $NaCaY_{0.2}Yb_{0.7}Tm_{0.02}Ho_{0.08}(MoO_4)_3$).

In order to obtain a referenced upconverting pH sensor, dually emitting red/NIR **UCPs 4** and the aza-BODIPY indicator **3** were *co*-entrapped into a hydrophilic hydrogel D4 layer (material **A**, corresponding to the scheme depicted in Figure **3b**). Whereas the absorption of both, the protonated and deprotonated form of the aza-BODIPY dye, overlaps with the emission peak at 645 nm, only the deprotonated form of the pH indicator matches the emission peak at 800 nm. Thus, the NIR emission is modulated by the pH changes being the most intense at lower pH values and the least intense in the basic media (Figure **4b**). The red emission of the UCPs is barely affected by pH and serves for referencing purposes. The pH calibration curve obtained for the luminescence intensity ratio (797/645) nm (Figure **4c**) has sigmoidal shape and the apparent pK_a' value is 8.12. It should be mentioned that the deprotonated form of the aza-BODIPY dye does not fully overlap with the near-infrared emission peak at 800 nm. However, since aza-BODIPY are highly accessible to structural modifications, additional bathochromic shift of the aza-BODIPY dye's absorption can be easily achieved by introduction of electron-

donating groups, e.g. alkoxy groups or increasing the rigidity of the chromophore. Such modification would result in even better modulation of the NIR luminescence of the upconverting particles.

Compared to the pH sensors based on combination of UCPs and colorimetric indicators described previously [77–79], the new sensor reported here offers significant advantages. First, the pH indicator dye is fairly lipophilic and does not show any leaching out of the hydrogel. In contrast, such indicators as bromothymol blue [77] or neutral red [78] are water-soluble which results in drift in aqueous media due to leaching of the pH indicator. Second, the reported sensors utilize dual green/red emission for analytical purposes which diminishes the advantages of UCPs particularly for sensing in biological matter. On the other hand, the sensor presented here makes use of NIR and red emission of the UCPs which are both located in the biological optical window.

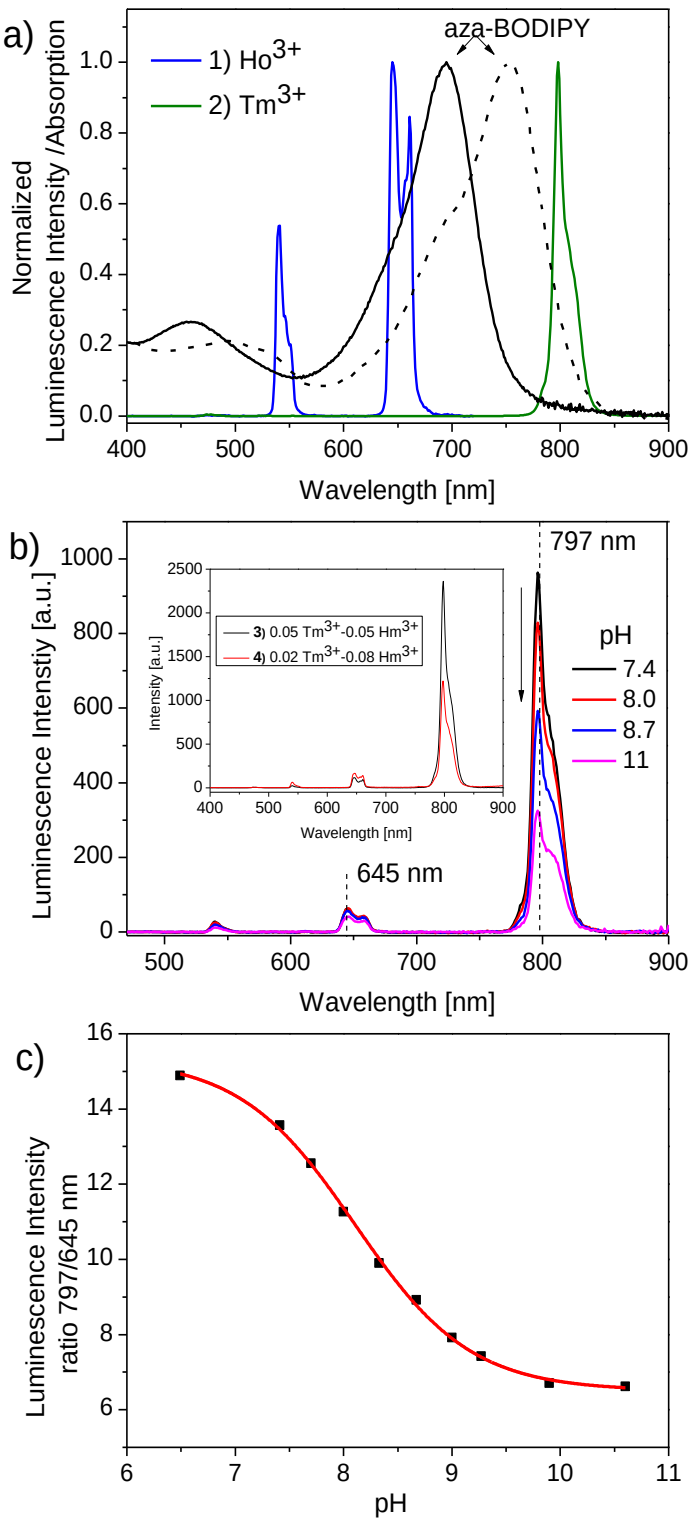

Figure 4a) Emission spectra of $NaCaY(MoO_4)_3$ phosphors doped with Yb^{3+} as a sensitizer and Ho^{3+} (**UCP 1**) or Tm^{3+} as an acceptor **(UCP 2**) upon excitation at 980 nm and absorption spectra of aza-BODIPY dye **3** in protonated (black line) and deprotonated (dotted line) forms. **b**) pH-dependent emission spectra of the sensor based on **UCP 4** (λ_{exc} 980 nm); insert: Emission spectra of the phosphors co-doped with both Tm^{3+} and Ho^{3+} (**UCP 3** and **4**). **c**) The corresponding calibration curve for the ratio of luminescence intensities at 797 and 645 nm.

Ratiometric read-out by using downconverting phosphors

Ratiometric read-out in the emission mode

The sensing material consists of the aza-BODIPY dye **3** and chromium(III)-activated gadolinium aluminium borate (Cr-GAB) particles, dissolved/dispersed in hydrogel D4 (sensor **B,** reference scheme corresponding to Figure **3b**). As seen in figure **5a**, the broad emission of Gr-GAB overlaps with the absorption spectra of the aza-BODIPY dye. Particularly, the two emission maxima of Gr-GAB (686 and 752 nm) perfectly match the absorption maxima of neutral and deprotonated forms of the indicator dye (683 and 742 nm, respectively). This leads to an opposing change in the intensities of the emission maxima of Gr-GAB, depending on pH (Figure **5b**). Plotting the signal ratio of the luminescence intensities of the emission peaks at 683 and 742 nm against pH results in a sigmoidally-shaped curve with a calculated apparent pK_a´ value of 8.01 (Figure **5c**).

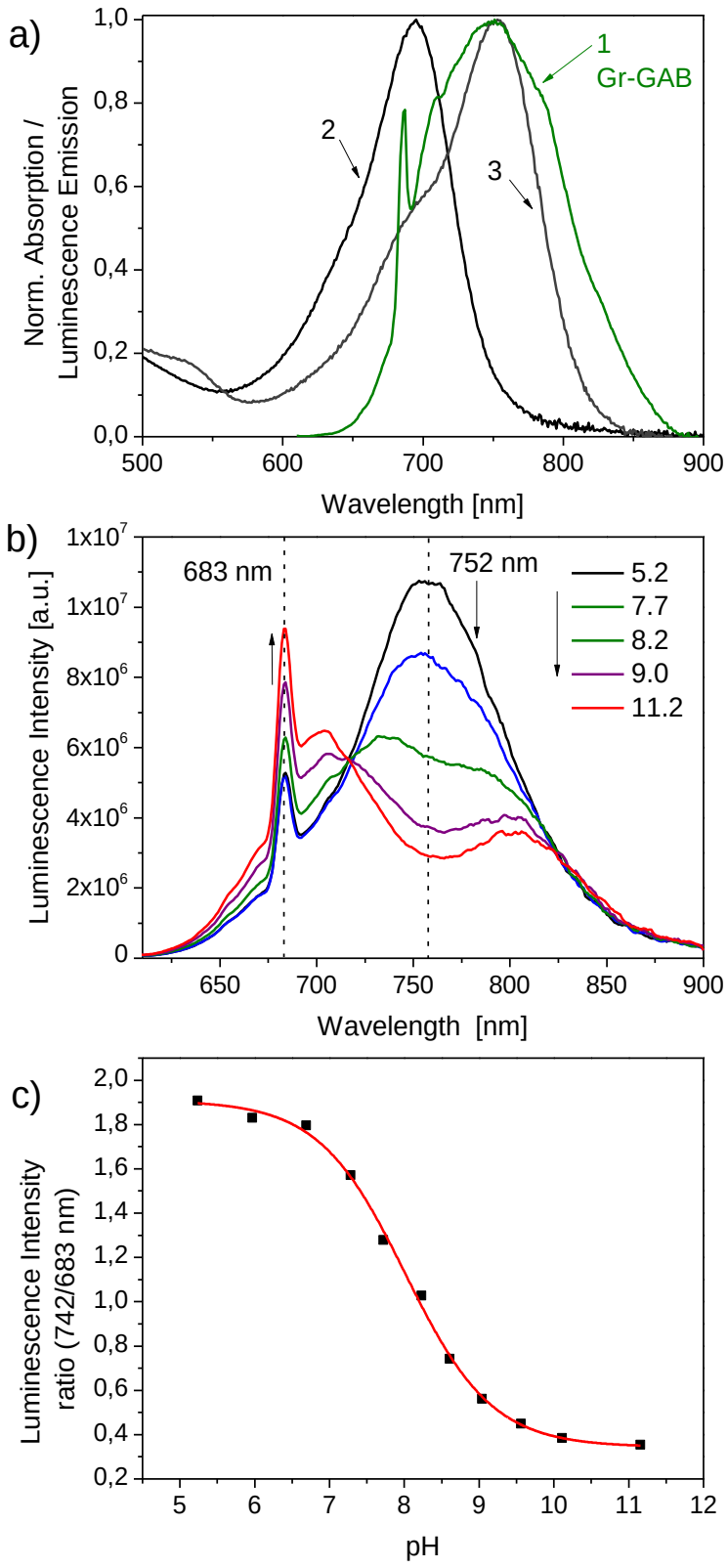

Figure 5) Ratiometric pH sensing in the emission mode. **a**) Spectral properties of the pH sensing material components: emission spectrum of Cr-GAB powder (1, λ_{exc}= 590 nm) and absorption spectra of the pH indicator 3 in the protonated (**2**) and deprotonated (**3**) forms. **b**) pH-dependent emission spectra of the sensor. **c**) Calibration curve for ratiometric read-out at two emission wavelengths (742 and 683 nm).

Ratiometric excitation read-out

In this approach the sensing material consists of the aza-BODIPY dye **3** and silanized Egyptian Blue phosphor particles immobilized in hydrogel D4 (sensor **C**, sensor design corresponding to Figure **3c**). As can be observed in figure **6a**, the luminescence excitation spectrum of Egyptian blue partly overlaps with the absorption of the protonated and deprotonated forms of the aza-BODIPY dye. Consequently, the excitation light intensity is modulated by the absorption of the pH-sensitive aza-BODIDPY dye, resulting in ratiometric response (Figure **6b** and **6c**). Notably, the luminescence emission (λ_{max} 920 nm) is not absorbed by any form of the indicator. It should be mentioned that the spectral overlap in this read-out scheme is not ideal. A different phosphor with bathochromically shifted excitation spectrum would be more suitable for referencing this long-wave absorbing aza-BODIPY dye.

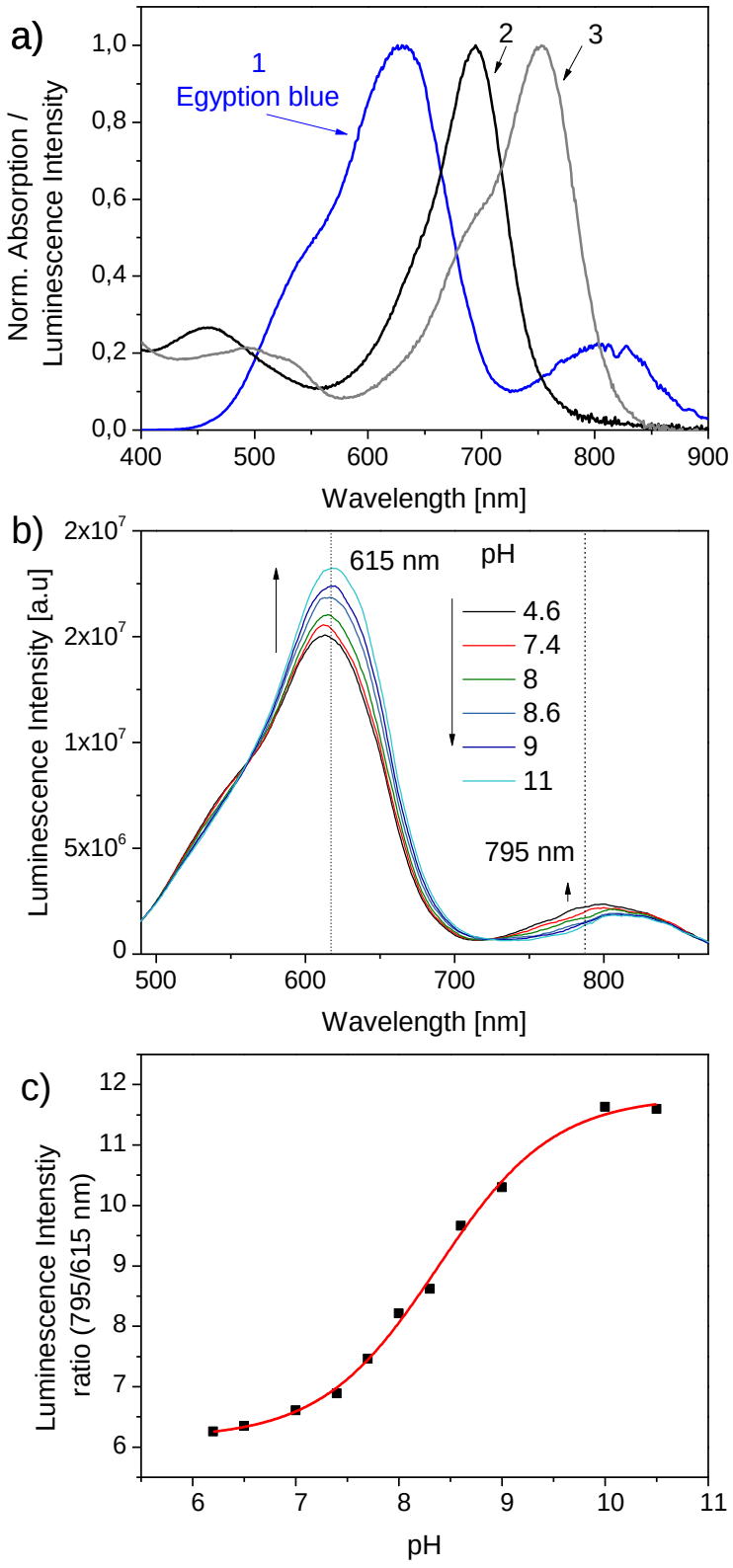

Figure 6). Ratiometric pH sensing in the excitation mode. a) Spectral properties of the pH sensing material components: excitation spectrum of Egyptian blue powder (1, λexc = 920 nm); absorption spectra of the pH indicator 3 in the protonated (2) and deprotonated (3) forms. b) pH-dependent emission spectra of the sensor. c) Calibration curve for ratiometric read-out at two excitation wavelengths (615 and 795 nm).

Conclusions

We successfully synthetized a NIR absorption-based aza-BODIPY pH indicator which shows virtually no fluorescence at pH > 4. Entrapment of the dye into hydrophilic hydrogel D4 along with phosphor particles results in a wide range of referenced luminescent pH sensing materials. The ratiometric response is obtained *via* modulation of the phosphor emission or excitation *via* inner-filter effect. Thereby, the sensors presented are not prone to interferences deriving from fluorescence quenchers and do not suffer from self-quenching of the indicator which is typical for fluorescent sensors. The referenced pH sensing materials also benefit from the exceptional (photo)chemical stability of the inorganic phosphors (Cr-GAB and Egyptian Blue) and the excellent photostability of the colorimetric aza-BODIPY dye. Moreover, when referencing with dually-emitting UCPs, doped with Yb^{3+} as a sensitizer and Tm^{3+} and Ho^{3+} as activators, long-wavelength excitation (980 nm) and ratiometric read-out detection utilizing red and near-infrared luminescence enable deep light penetration into (biological) matter since both excitation and emission are located in the biological optical window. Thus, the new sensor overcomes main drawback of the state-of-the art pH sensors based on upconverting phosphors.

Acknowledgements. Financial support by the European Union FP7 Project Sense Ocean (Grant Agreement Number 614141) and COST action CM1403 "The European Upconversion Network: From the Design of Photon-Upconverting Nanomaterials to Biomedical Applications" is gratefully acknowledged.

Chapter 4

Highly Photostable NIR Indicators for Optical Carbon Dioxide Sensors

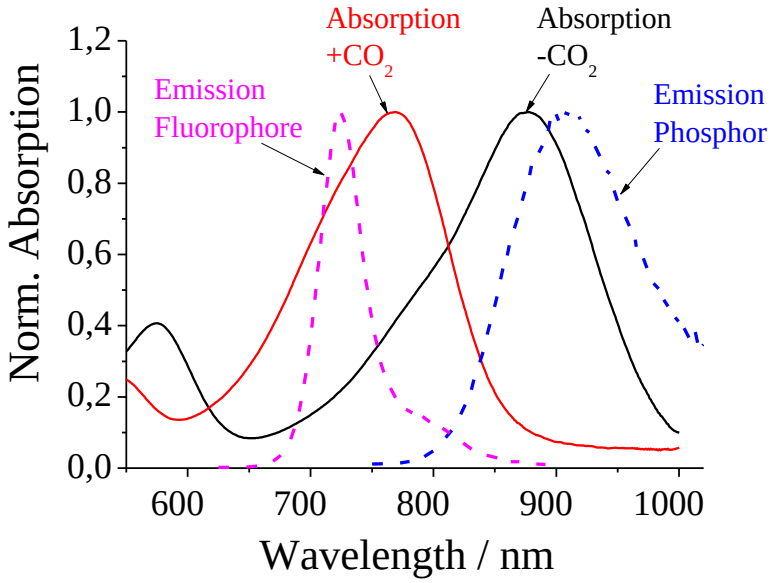

Highly Photostable NIR Indicators for Optical Carbon Dioxide Sensors

This chapter was published in **J. Mater. Chem. C**, 2015, 3, 5474-5483; doi: 10.1039/C5TC00346F

Authors: Susanne Schutting, Tijana Jokic, **Martin Strobl**, Sergey M. Borisov, Dirk de Beer and Ingo Klimant

A new class of pH-sensitive indicator dyes for optical carbon dioxide sensors based on di-OH-aza-BODIPYs is presented. These colorimetric indicators show absorption maxima in the near infrared range (λ_{max} 670–700 nm for the neutral form, λ_{max} 725–760 nm for the mono-anionic form, λ_{max} 785–830 nm for the di-anionic form), high molar absorption coefficients of up to 77 000 M^{-1} cm^{-1} and unmatched photostability. Depending on the electron-withdrawing or electron-donating effect of the substituents the pK_a values are tuneable (8.7–10.7). Therefore, optical carbon dioxide sensors based on the presented dyes cover diverse dynamic ranges (0.007–2 kPa; 0.18–20 kPa and 0.2–100 kPa), which enables different applications varying from marine science and environmental monitoring to food packaging. The sensors are outstandingly photostable in the absence and presence of carbon dioxide and can be read out via *absorption or* via *the luminescence-based ratiometric scheme using the absorption-modulated inner-filter effect. Monitoring of the carbon dioxide production/consumption of a Hebe plant is demonstrated.*

Introduction

Carbon dioxide is one of the most important parameters besides pH and oxygen in many scientific and industrial fields, such as medicine[93–95], marine science[96–99], food packaging[100], bio processing[101,102] or environmental and industrial monitoring[103]. Therefore, an appropriate detection method is necessary. Routine techniques like infrared (IR) spectroscopy, gas chromatography (GC) or the Severinghaus electrode are well established, but suffer from different drawbacks[104,105]. For instance IR spectroscopy is mainly used for gas samples[106,107], because of strong interferences of water and the Severinghaus electrode is strongly affected by osmotic effects. A promising alternative tool are carbon dioxide chemosensors[16-23], where so called "plastic type" sensors are the most common ones[24-31]. The core of this type of sensor is a pH-sensitive indicator dye. It is embedded in a polymer matrix together with a base (mainly a quaternary ammonium base) and responds to carbon dioxide by changing its spectral properties according to the grade of protonation. Read-out of these sensors can be carried out

via absorption or luminescence intensity. In case of a fluorescent indicator dye referencing of the fluorescence intensity is needed. This can be realized by using an analyte-insensitive reference dye with different spectral properties to the indicator, either a different emission spectrum or a different luminescence decay time. Although necessary in many cases, the addition of reference materials can cause dramatic ratio changes when photobleaching of one dye (reference or indicator) or both occurs. Therefore, self-referencing indicator dyes are highly desired for ratiometric read-out. However, only a few self-referencing dyes (absorption and fluorescence intensity) where published so far[32-38]. Optical carbon dioxide sensors are also from great interest in biological applications. Here, indicators with absorption/fluorescence intensity maxima in the infrared (IR) or near-infrared (NIR) region are preferred, because of several advantages, e.g. low light scattering, background signals from organic matter are dramatically diminished and one can use low-cost excitation sources. Recently our group presented pH-sensitive BF_2-chelated tetraarylazadipyrromethene indicators (aza-BODIPYs)[38] for optical pH sensors. This indicator class represents an interesting alternative to state-of-the-art dyes for biological applications like SNARF indicators[39] or cyanine dyes[40,41]. The aza-BODIPYs showed absorption/fluorescence intensity spectra in the near-infrared region and were excellently photostable. Although pH-sensitive, these dyes could not be used for optical carbon dioxide sensors. Here, the formation of the ion pair was irreversible and the indicator could not be protonated anymore, even at 100% CO_2. Chemical modification led to symmetrical aza-BODIPYs with two de-/protonizeable hydroxyl groups. In this study we present a new class of pH-sensitive indicator dyes suitable for optical carbon dioxide sensors, the di-OH-aza-BODIPYs. It will be shown, that the pK_a values of the di-OH-aza-BODIPYs can be tuned by using different substituents with either electron-withdrawing or –donating effect. The dyes are excellently photostable and show absorption maxima in the near-infrared region. Luminescence based ratiometric read-out can be realized via absorption modulated inner filter effect[42-45]. An application example demonstrating the carbon dioxide production/consumption of a Hebe plant is presented in the last section of this contribution.

Experimental

Materials. Ethyl cellulose (EC49, ethoxyl content 49%), thymol-blue (A.C.S. reagent), m-cresol-purple (indicator grade), poly(styrene-co-divinylbenzene) microspheres (8 µm mean particle size; PS-microparticles), 3´-chloro-4´-hydroxyacetophenone, ammonium acetate, benzaldehyde, N,N-diisopropylethylamine (DIPEA), dry dichloromethane, boron trifluoride

diethyl etherate, MOPS buffer salt, sodium sulphate (anhydrous) and tetraoctylammonium hydroxide solution (TOAOH, 20% in methanol) were obtained from Sigma-Aldrich (www.sigmaaldrich.com). Deuterated dimethyl sulfoxide (DMSO-*d6*) was purchased from Euriso-top (www.eurisotop.com). Perfluordecalin (98%; cis and trans), 1-butanol (99%, BuOH) and nitromethane were received from ABCR (Germany, www.abcr.de), Hyflon AD 60 (Type: Copolymer MDO (polymer of 2,2,4-trifluoromethoxy-1,3-dioxole) and TFE (ethylene tetrafluoride)) from Solvay (www.solvay.com). Nitrogen, 2% oxygen in nitrogen, 5% carbon dioxide in nitrogen, 0.2% carbon dioxide in nitrogen, argon and carbon dioxide (all of 99.999% purity) were obtained from Air Liquide (Austria, www.airliquide.at). Toluene, ethanol (EtOH), tetrahydrofuran (THF), hydrochloric acid (37%), dichloromethane (DCM) and hexane were purchased from VWR (Austria, www.vwr.com). 3´-methyl-4-hydroxyacetophenone, 4´-butoxyacetophenone and 2-fluoro-4-hydroxyacetophenone were from TCI Europe (www.tcichemicals.com). Poly(ethylene terephthalate) (PET) support Melinex 505 was obtained from Pütz (Germany, www.puetz-folien.com). Potassium chloride, potassium carbonate (pro analysi), potassium hydroxide (KOH) and Silica gel 60 (0.063-0.200 mm) were received from Merck (www.merck.at). Sodium hydroxide, the buffer salts CHES, MES and CAPS and ethyl acetate were purchased from Roth (www.carlroth.com). De-ionized water was filtered via a Barnstead NANOpure ultrapure water system. 1-(4-hydroxyphenyl)-4-nitro-3-phenylbutan-1-one (compound 1b) was synthesized according to Jokic et al.[38]. Silanized Egyptian Blue particles were prepared according to the literature procedure.[46]

Synthesis of 3,7-bis(4-butoxyphenyl)-5,5-difluoro-1,9-diphenyl-5H-4λ⁴,5λ⁴-dipyrrolo-[1,2-c:2`,1`-f][1,3,5,2]triazaborinine (di-butoxy-complex)

*(E)-1-(4-butoxyphenyl)-3-phenylprop-2-en-1-one (compound **a**):* 4'-butoxyacetophenone (1 eq, 2.00 g, 10.4 mmol) was dissolved in absolute ethanol (15 ml). Benzaldehyde (1 eq, 1060 µL, 10.6 mmol) and potassium hydroxide (3 eq, 1.79 g, 31.9 mmol in 5 ml H_2O) were added to the solution and the reaction was stirred at room temperature for 12 hours. Then, the reaction solution/suspension was acidified with 0.1 M HCl and the resulting precipitate was collected by filtration and was washed with water three times (3x 100 ml). The precipitate was dried by using the rotary evaporator and was used for the next step without further purification (2.78 g, 95.2 %).

*1-(4-butoxyphenyl)-4-nitro-3-phenylbutan-1-one (compound **b**):* A solution of (E)-1-(4-butoxyphenyl)-3-phenylprop-2-en-1-one (1 eq, 2.78 g, 9.9 mmol), nitromethane (20 eq, 10.7

ml, 198 mmol) and KOH (0.3 eq, 0.17 g, 3.0 mmol) in 30 ml ethanol absolute was heated under reflux for 12 hours. After cooling to room temperature the solvent was removed by using a rotary evaporator. The resulting oily residue was acidified with 0.1 M HCl and was partitioned with ethyl acetate and water in a separating funnel. The organic layer was separated, dried over sodium sulfate and the solvent removed under reduced pressure (2.96 g, 87.3 %).

(5Z)-5-(4-butoxyphenyl)-N-(5-(4-butoxyphenyl)-3-phenyl-2H-pyrrol-2-ylidene)-3-phenyl-1H-pyrrol-2-amine: Compound **b** (1 eq, 2.5 g, 4.21 mmol) and ammonium acetate (35 eq, 11,37 g, 147.5 mmol) were dissolved in 50 ml 1-butanol and the reaction solution was heated under reflux for 24 hours. The reaction was cooled to room temperature and the solvent removed under reduced pressure. Then, the solid was redissolved in DCM and washed with water three times (3x 100 ml). The crude solid was purified by column chromatography on silica gel eluting with DCM/cyclohexane (1:1 v/v). The product was recrystallized from a hexane/THF mixture to give blue metallic crystals (983 mg, 45.4 %). ^{1}H NMR (300 MHz, $CDCl_3$) δ 8.06 (d, *J* =7.1 Hz, 4 H), 7.88-7.83 (m, 4 H), 7.44-7.31 (m, 6 H), 7.11 (s, 2 H), 7.02 (d, *J* = 8.8 Hz, 4 H), 4.06 (t, *J* = 6.5 Hz, 4 H), 1.91-1.72 (qu, *J* = 8.5 Hz, 4 H), 1.6-1.48 (m, 4 H), 1.01 (t, *J* = 7.4 Hz, 6 H).

3,7-bis(4-butoxyphenyl)-5,5-difluoro-1,9-diphenyl-5H-4λ^4,5λ^4-dipyrrolo-[1,2-c:2`,1`-f][1,3,5,2]triazaborinine. Compound **c** (1 eq., 300 mg, 0.51 mmol) was dissolved in 200 ml dry DCM. *N*,*N*-diisopropylethylamine (DIPEA, 10 eq, 839 µl, 5.06 mmol) and boron trifluoride diethyl etherate (15 eq, 953 µl, 7.58 mmol) were added and the reaction solution was stirred under nitrogen for 12 hours. The green solution was washed with water three times (3 x 200ml) and dried over anhydrous sodium sulfate. The crude product was purified by column chromatography on silica-gel eluting with DCM/cyclohexane (1:1 v/v). The product was recrystallized from a hexane-THF mixture to give red metallic needles (599 mg, 55.4%). ^{1}H NMR (300 MHz, $CDCl_3$) δ 8.09 - 8.05 (m, 8 H), 7.49 - 7.38 (m, 6 H), 7.04 - 6.98 (m, 6 H), 4.07 – 4.02 (t, *J* = 6.4 Hz, 4 H), 1.58 – 1.45 (qu, *J* = 14.4 Hz, 4 H), 1.62 – 1.42 (m, 4 H), 1.02 – 0.97 (t, *J* = 7.4 Hz, 6 H) DI-EI-TOF: m/z of $[M]^+$ found 641.3007, calculated 641.3032.

Synthesis of 4,4`-(5,5-difluoro-1,9-diphenyl-5H-4λ$^4$,5λ$^4$-dipyrrolo-[1,2-c:2`,1`-f][1,3,5,2]triazaborinine-diyl)bis(2-chlorophenol) (di-Cl-di-OH-complex)

*1-(3-chloro-4-hydroxyphenyl)-3-phenylpropenone (compound **1a**):* 3´-chloro-4´-hydroxyacetophenone (1 eq, 2 g, 11.7 mmol) and benzaldehyde (1 eq, 1.24 g, 11.7 mmol) were dissolved in 10 ml ethanol absolute. 10 ml of aqueous potassium hydroxide solution (3 eq, 1.96 g, 35.1 mmol) were added dropwise. The resulting solution was stirred for 8-12 hours, during

which the product precipitated as the potassium salt. The solution/suspension was poured into 10 ml hydrochloric acid (1 M) and further concentrated hydrochloric acid was added until the solution was acidic. The obtained yellow solid was washed with water and used for further synthesis without purification (2.7 g, 77%).

*1-(3-chloro-4-hydroxyphenyl)-4-nitro-3-phenylbutan-1-one (compound **1b**):* A solution of compound 1a (1 eq, 2 g, 7.7 mmol), nitromethane (20 eq, 8.35 ml, 154.7 mmol) and potassium hydroxide (1.2 eq, 0.52 g, 9.28 mmol) in 10 ml ethanol was heated at 60°C under reflux for 12 hours. After cooling to room temperature, the solvent was removed in vacuo and the oily residue obtained was acidified with hydrochloric acid (4 M) and partitioned between ethyl acetate (50 ml) and de-ionized water (50 ml). The organic layer was separated, dried over sodium sulfate (anhydrous) and evaporated under reduced pressure. The obtained product was used for further synthesis without purification (2.4 g; 73%).

*[5-(3-chloro-4-hydroxyphenyl)-3-phenyl-1H-pyrrol-2-yl]-[5-(3-chloro-4-hydroxyphenyl)-3-phenylpyrrol-2-ylidene]amine (compound **1c**):* Compound **1b** (1 eq, 2.02 g, 8.76 mmol) and ammonium acetate (35 eq, 19.03 g, 307 mmol) in 50 ml 1-butanol were heated under reflux for 24 hours. The reaction was cooled to room temperature, salt was removed by extraction with de-ionized water/DCM and the product was purified by column chromatography on silica gel eluting with 5% ethyl acetate/DCM (after eluting impurities with hexane, 20% DCM/hexane, 1% ethyl acetate/DCM and 2% ethyl acetate/DCM) to yield [5-(3-chloro-4-hydroxyphenyl)-3-phenyl-1H-pyrrol-2-yl]-[5-(3-chloro-4-hydroxyphenyl)-3-phenylpyrrol-2-ylidene]amine as a blue-black solid. The product was recrystallized from a hexane/THF mixture to give green metallic crystals (0.097 g, 5.77%). ^{1}H NMR (300 MHz, DMSO-d_6) δ 8.09 (d, J = 7.6 Hz, 6H), 7.90 (d, J = 8.5 Hz, 2H), 7.62 (s, 2H), 7.54 – 7.32 (m, 6H), 7.19 (d, J = 8.5 Hz, 2H). Electron impact-direct insertion-time of flight (EI-DI-TOF) m/z [MH^+] found 549.1007, calculated 549.1011.

4,4`-(5,5-difluoro-1,9-diphenyl-5H-4λ$^4$,5λ$^4$-dipyrrolo-[1,2-c:2`,1`-f][1,3,5,2]triazaborinine-3,7-diyl)bis(2-chlorophenol) (di-Cl-di-OH-complex). Compound **1c** (0.017 g, 0.07 mmol) was dissolved in 50 ml of dry DCM, treated with diisopropylethylamine (10 eq, 0.053 ml, 0.32 mmol) and boron trifluoride diethyletherate (15 eq, 0.061 ml, 0.48 mmol) and stirred under argon for 24 hours. Purification was carried out via column chromatography on silica gel eluting with 2% ethanol/DCM (after eluting impurities with DCM). Recrystallization from hexane/THF gave the final product di-Cl-di-OH-complex as a red metallic solid (0.008 g, 44%).

^{1}H NMR (300 MHz, DMSO-d_6) δ 8.29 (s, 2H), 8.16 (d, J = 7.0 Hz, 4H), 8.03 (d, J = 8.7 Hz, 2H), 7.65 (s, 2H), 7.60 – 7.41 (m, 6H), 7.13 (d, J = 8.7 Hz, 2H). EI-DI-TOF: m/z [MH^+] found 597.0968, calculated 597.0999.

Synthesis of 4,4`-(5,5-difluoro-1,9-diphenyl-5H-4λ$^4$,5λ$^4$-dipyrrolo-[1,2-c:2`,1`-f][1,3,5,2]triazaborinine-3,7-diyl)bis(3-fluorophenol) (di-F-di-OH-complex).

The synthesis was performed analogously to that of the di-Cl-di-OH-complex, but starting from 2´-fluoro-4´-hydroxyacetophenone. (728 mg) Steps 1 and 2 yielded 1.033 g (90.2%) and 1.28 g (99.4%) of the crude product, respectively. After synthesis step 3, the crude product was purified by column chromatography on silica gel eluting with 4 % THF/DCM to yield [5-(2-fluoro-4-hydroxyphenyl)-3-phenyl-1H-pyrrol-2-yl]-[5-(2-fluoro-4-hydroxyphenyl)-3-phenylpyrrol-2-ylidene]amine as a blue-black solid. The product was recrystallized from a hexane/THF mixture to give green metallic crystals (0.23 g, 20.9%). ^{1}H NMR (300 MHz, DMSO-d_6) δ 8.04-8.06 (d, J = 7.0 Hz, 6H), 7.35-7.47 (m, 8H), 6.78-6.86 (m, 4H). DI-EI-TOF: m/z of [M]+ found 517.1626, calculated 517.1602.

*4,4`-(5,5-difluoro-1,9-diphenyl-5H-4λ$^4$,5λ$^4$-dipyrrolo-[1,2-c:2`,1`-f][1,3,5,2]triazaborinine-3,7-diyl)bis(3-fluorophenol) (di-F-di-OH-complex).* 4,4`-(5,5-difluoro-1,9-diphenyl-5H-4λ^4,5λ^4-dipyrrolo-[1,2-c:2`,1`-f][1,3,5,2]triazaborinine-3,7-diyl)bis(3-fluorophenol) (di-F-di-OH-complex). was synthesized using the same procedure. Purification was carried out *via* column chromatography on silica gel eluting with 4 % THF/DCM. Recrystallization from hexane-THF gave the final product di-F-di-OH-complex as a red metallic solid (0.044 g, 19.6%). ^{1}H NMR (300 MHz, DMSO-d6) δ 8.12 (d, J = 7.0 Hz, 4H), 7.82 (t, J = 8.7 Hz, 2H), 7.56-7.48 (q, J = 9.4, 7.9 Hz, 6H), 7.31 (d, J = 3.4 Hz, 2H), 6.77 (d, J = 10.7 Hz, 4H). DI-EI-TOF: m/z of [M]+ found 565.1615, calc. 565.1591.

Synthesis of 4,4`-(5,5-difluoro-1,9-diphenyl-5H-4λ$^4$,5λ$^4$-dipyrrolo-[1,2-c:2`,1`-f][1,3,5,2]triazaborinine-3,7-diyl)diphenol (di-OH-complex).

Compound **3a** 1-(4-hydroxyphenyl)-3-phenylpropenone was commercially available. Further synthesis steps were performed analogously to the synthesis steps of the di-Cl-di-OH-complex. Synthesis of compound **3b** gave 2.06 g (80%) of the crude product, starting from 2.02 g of 4'-hydroxychalcones. The crude 3c was purified by column chromatography on silica gel eluting with 4% THF/DCM to yield [5-(4-hydroxyphenyl)-3-phenyl-1H-pyrrol-2-yl]-[5-(4-hydroxyphenyl)-3-phenylpyrrol-2-ylidene]amine as a blue-black solid. The product was

recrystallized from a hexane-THF mixture to give metallic green crystals (0.41 g, 49%). ^{1}H NMR (300 MHz, DMSO-d6), δ 8.09 (d, *J* = 7.3 Hz, 4H), 7.93 (d, *J* = 8.6 Hz, 4H), 7.53 (s, 2H), 7.42 (m, 6H), 7.01 (d, *J* = 8.6 Hz, 4H). EI-DI-TOF: m/z [MH^+] found 481.1773, calc. 481.179.

*Purification of 4,4`-(5,5-difluoro-1,9-diphenyl-5H-4λ$^4$,5λ$^4$-dipyrrolo-[1,2-c:2`,1`-f][1,3,5,2]triazaborinine-3,7-diyl)diphenol.* Purification of 4,4`-(5,5-difluoro-1,9-diphenyl-5H-4λ^4,5λ^4-dipyrrolo-[1,2-c:2`,1`-f][1,3,5,2]triazaborinine-3,7-diyl)diphenol was carried out *via* column chromatography on silica gel eluting with DCM/ethyl acetate (4:1). Recrystallization from hexane-THF gave the final product di-OH-complex as a metallic red solid (0.26 g, 70%). ^{1}H NMR (300 MHz, DMSO-d6) δ 8.13 (dd, J = 18.6, 8.0 Hz, 8H), 7.65 – 7.39 (m, 8H), 6.95 (d, J = 8.8 Hz, 4H). EI-DI-TOF m/z [MH^+] found 529.1786, calc. 529.1779.

Synthesis of 4,4`-(5,5-difluoro-1,9-diphenyl-5H-4λ$^4$,5λ$^4$-dipyrrolo-[1,2-c:2`,1`-f][1,3,5,2]triazaborinine-3,7-diyl)bis(2-methylphenol) (di-CH_3-di-OH-complex).

The synthesis was carried out analogously to that of the di-Cl-di-OH-complex, starting from 3´-methyl-4´-hydroxyacetophenone. Steps 1 and 2 yielded 3.5 g (93%) and 1.33 g (53%) of the crude product, respectively. After synthesis step 3, the crude product was purified by column chromatography on silica gel eluting with 5 % ethyl acetate/DCM (after eluting impurities with hexane/DCM 1:1, DCM) to yield **4c** as a blue-black solid. The product was recrystallized from a hexane-THF mixture to give green metallic crystals (0.174 g, 5.8%). ^{1}H NMR (300 MHz, DMSO-d_6) δ 8.10 (d, *J* = 7.3 Hz, 4H), 7.91 – 7.75 (m, 4H), 7.57 – 7.33 (m, 8H), 7.00 (d, *J* = 8.4 Hz, 2H), 2.29 (s, 6H). EI-DI-TOF: m/z [MH^+] found 509.2086, calc. 509.2103.

*Purification of 4,4`-(5,5-difluoro-1,9-diphenyl-5H-4λ$^4$,5λ$^4$-dipyrrolo-[1,2-c:2`,1`-f][1,3,5,2]triazaborinine-3,7-diyl)bis(2-methylphenol).* Purification of 4,4`-(5,5-difluoro-1,9-diphenyl-5H-4λ^4,5λ^4-dipyrrolo-[1,2-c:2`,1`-f][1,3,5,2]triazaborinine-3,7-diyl)bis(2-methylphenol) was carried out via column chromatography on silica gel eluting with 5% ethyl acetate/DCM (after eluting impurities with DCM, 1% ethyl acetate/DCM and 2% ethyl acetate/DCM). Recrystallization from hexane/THF gave the final product di-CH_3-di-OH-complex as a red metallic solid (0.04 g, 40%). ^{1}H NMR (300 MHz, DMSO-d_6) δ 8.16 (d, *J* = 7.2 Hz, 4H), 8.08 – 7.90 (m, 4H), 7.52 (m, 8H), 6.95 (d, *J* = 8.5 Hz, 2H), 2.22 (s, 6H). Electron impact-direct insertion-time of flight (EI-DI-TOF) m/z [MH^+] found 557.21, calc. 557.209.

Staining of PS-microparticles. 0.50 g PS-particles were dispersed in a solution of 5 mg (1%w/w in respect to the PS-particles) di-butoxy-complex in 10 ml tetrahydrofuran (THF) and

stirred for 1.5 hours. Then 8 ml of de-ionized water were added dropwise. After 10 min of stirring the dispersion was transferred rapidly into a beaker with 50 ml of de-ionized water. The dispersion was again stirred for 10 min. Then the particles were filtered through a cellulose filter and rewashed with 20 ml ethanol. Afterwards the particles were transferred into a milling cup, were grinded in a planet mill, washed with ethanol and dried.

Sensor preparation. A cocktail containing 100 mg ethyl cellulose and 1 mg dye (1% w/w in respect to the polymer) dissolved in a toluene: ethanol mixture (6:4 v/v) was purged with carbon dioxide gas. Afterwards 100 µl tetraoctylammonium hydroxide solution (20% w/w TOAOH in MeOH) were added. The cocktail was knife-coated on a dust-free PET support. A sensing film of ~7 µm thickness was obtained after evaporation of the solvent. For luminescence-based measurements a second layer was added to the absorption-based sensing foils. Here, 0.180 g Hyflon AD 60 were dissolved in 2.820 g perfluordecalin, which was washed prior to use with 1 mol/l potassium carbonate solution). Afterwards 0.360 g Egyptian Blue powder (200% w/w with respect to the polymer) and 0.054 g stained PS-particles (30% w/w in respect to the polymer) were dispersed homogeneously in the Hyflon solution. The thickness of this layer after evaporation of the solvent was estimated to be ~4.5 µm.

Methods

^{1}H NMR spectra were recorded on a 300 MHz instrument (Bruker) in DMSO-d_6 with TMS as standard. Absorption spectra were recorded on a Cary 50 UV-vis spectrophotometer (Varian). The determination of the molar absorption coefficient was carried out as an average of three independent measurements. Fluorescence spectra were recorded on a Fluorolog3 fluorescence spectrometer (Horiba) equipped with a NIR-sensitive photomultiplier R2658 from Hamamatsu (300-1050 nm). Photobleaching experiments were performed by irradiating the sensor foils in a glass cuvette with the light of a high-power 10 W LED array (λ_{max} 458 nm, 3 LEDs, LED-TECH.de) operated at 6 W input power. A lens (Edmund Optics) was used to focus the light of the LED array on the glass cuvette (photon flux: ~3900 µmol s^{-1} m^{-2} as determined with a Li-250A light meter from Li-COR). The photodegradation profiles were obtained by monitoring the absorption spectra of a sensor foil based on the respective dye. The cuvette was flushed with either carbon dioxide gas for the neutral form, or with nitrogen for the di-anionic form and sealed. Thymol-blue and m-cresol-purple were used for comparison. In case of the anionic form of thymol-blue, m-cresol-purple, the di-OH-complex and the di-CH_3-di-OH-complex (di-anionic forms) sodium hydroxide was placed at the bottom of the cuvette to capture carbon

dioxide traces. Gas calibration mixtures were obtained using a gas mixing device from MKS (www.mksinst.com). The gas mixture was humidified to about 85% relative humidity, using silica gel soaked with a saturated potassium chloride solution, prior to entering the calibration chamber. Temperature was controlled by a cryostat ThermoHaake DC50. Dyed particles were filtered through cellulose filters type 113A from Roth (www.carlroth.com). Particle milling was carried out using an 80 ml milling cup, zirconia spheres (Ø 5 mm) and a Pulverisette 6 planet mill from Fritsch (www.fritsch.de). For the determination of the pKa values two independent titration curves using aqueous buffer/ethanol mixtures (1:1) were measured and the average value of the point of inflection obtained was used. For the production/consumption measurements of carbon dioxide two Firesting-Mini devices and an oxygen trace sensor from Pyroscience (www.pyro-science.com) were used. For illumination of the sample was performed with 3 commercially available halogen bulb lamps with an averaged photon flux of ~ 217 µmol s^{-1} m^2 per lamp (determined with a Li-250A light meter from Li-COR, www.licor.com). The plant was positioned in a glass desiccator, which was flushed with a gas mixture of 2% oxygen in nitrogen.

Results and Discussion

As reported by Jokic et al.[108] there are two ways for the preparation of azadipyrromethenes to obtain either unsymmetrical[47] or symmetrical[48] chromophores. The previously published asymmetrical dyes bearing one hydroxyl group were proved to be promising pH indicators.[38] Unfortunately, they were found to be unsuitable for optical carbon dioxide sensors. The ion pair built between the hydroxyl group and the tetraoctylammonium base was comparatively strong. Even after exposure of the sensors to pure carbon dioxide, the amount of CO_2 was not enough to achieve re-protonation of the indicators and only after exposure to strong acid vapours (*e.g.* hydrochloric acid) the indicators were irreversibly re-protonable.

Dissociation of both hydroxyl groups in symmetrical azadipyrromethenes was expected to be more difficult compared to the mono-hydroxy derivatives since two ion pairs with bulky cations would be built upon deprotonation. Therefore, this new class of pH indicators potentially suitable for CO_2 sensing was investigated. The starting point of our synthesis were diaryl-α,β-unsaturated ketones (chalcones) either commercially available or readily made by an aldol condensation of the corresponding aldehydes and acetophenone (Scheme 1). The Michael addition of nitromethane to the chalcones, using KOH as a base, yields 1,3-diaryl-4-nitrobutan-1-ones in essentially quantitative yields.

Scheme 1. 4-step-synthesis scheme for the di-OH-aza-BODIPY-complexes.

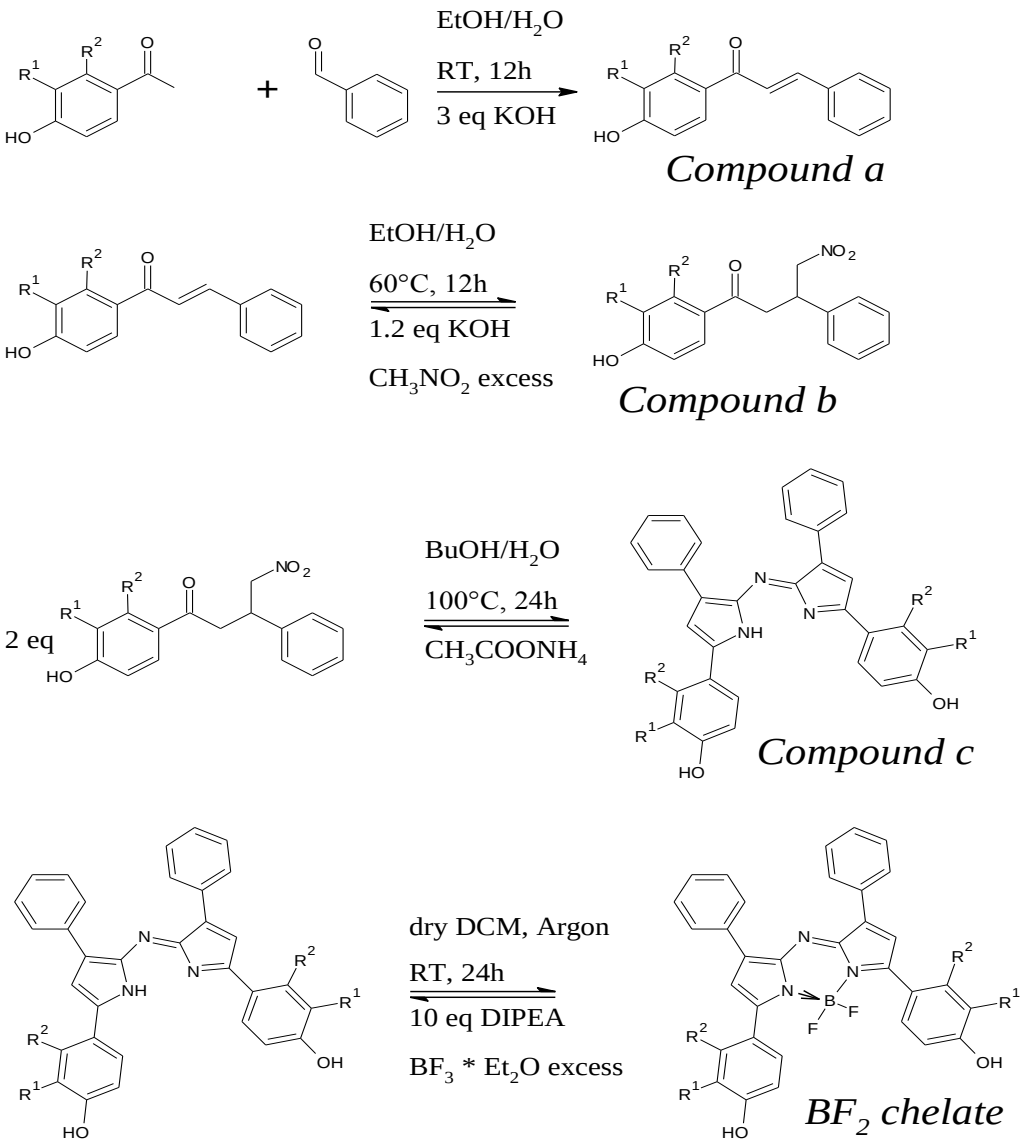

di-OH-complex: $R^1 = R^2 = H$

di-F-di-OH-complex: $R^1 = H$, $R^2 = F$

di-Cl-di-OH-complex: $R^1 = Cl$, $R^2 = H$

di-CH_3-di-OH-complex: $R^1 = CH_3$, $R^2 = H$

Photophysical properties

Dissolved in an ethanol/aqueous buffer mixture (1:1) all di-OH-aza-BODIPY dyes showed absorption spectra corresponding to the two protonation steps of the hydroxyl groups (Fig. 1). The neutral forms showed maxima at 670-700 nm and the mono-anionic forms at 725-760 nm. The di-anionic forms were again bathochromically shifted for approximately 60 nm (λ_{max} 785-

830 nm). Generally, the di-CH_3-di-OH-complex bearing electron-donating methyl groups showed absorption maxima shifted to higher wavelengths compared to the non-substituted di-OH-complex (Table 1). In contrast, complexes bearing electron-withdrawing groups displayed absorption maxima at shorter wavelengths.

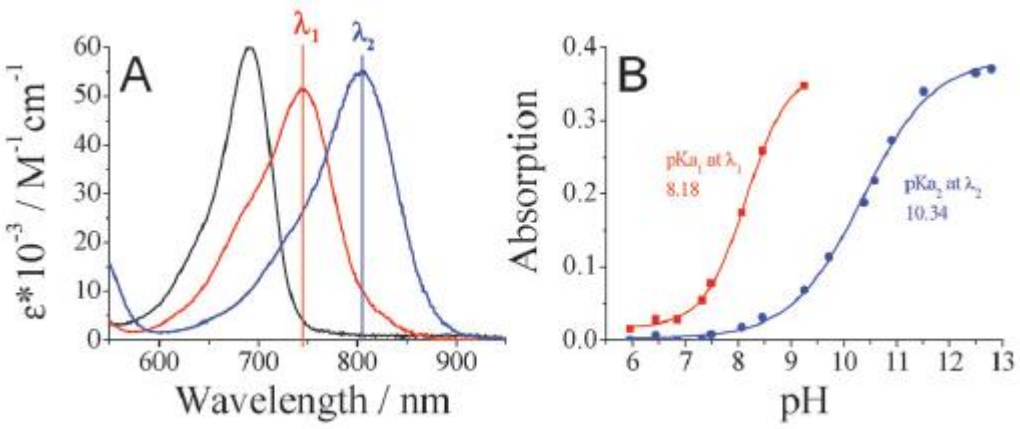

Fig. 1 (A) Absorption spectra of the neutral (black line, pH 6.4), the mono-anionic (red line, pH 9.3) and the di-anionic (blue line, pH 12.8) forms of the di-OH-complex dissolved in the ethanol/aqueous buffer mixture (1:1) at 25°C and (B) the titration curves for pKa_1 determined at 745 nm (red) and pKa_2 at 805 nm (blue), respectively.

An overview of the spectroscopic properties of the presented dyes is given in Table 1. Molar absorption coefficients are rather high: 55000-77000 $M^{-1}cm^{-1}$ than for. pK_a determination was carried out in a mixture of ethanol/aqueous buffer solution (1:1). For all di-OH-aza-BODIPY dyes two protonation steps can be observed (table 1). Here, the complex with electron-donating methyl groups in the *ortho*-position to the hydroxyl groups showed the highest pK_a values, followed by the non-substituted di-OH-complex. Electron-withdrawing chlorine atoms located in the proximity of the hydroxyl groups (ortho-position) have the strongest impact on the pK_a values, whereas the electron-withdrawing effect of fluorine atoms in the *meta*-position is significantly lower.

Table 1. Absorption maxima, molar absorption coefficients (ε) and pK_a values of the di-OH-aza-BODIPY-complexes dissolved in ethanol/aqueous buffer mixture (1:1), as well as the absorption maxima for optical CO_2 sensors (EC49) based on the respective aza-BODIPY-complexes.

	neutral form		**mono-anionic form**			**di-anionic form**	
	λmax (ε*10^{-3}) EtOH/aqu. buffer 1:1 [nm (M^{-1}cm^{-1})]	**pKa$_1$** EtOH/ aqu. buffer 1:1	**λmax (ε*10^{-3})** EtOH/aqu. buffer 1:1 [nm (M^{-1}cm^{-1})]	**λmax** EC49 [nm]	**pKa$_2$** EtOH/ aqu. buffer 1:1	**λmax (ε*10^{-3})** EtOH/aqu. buffer 1:1 [nm (M^{-1}cm^{-1})]	**λmax** EC49 [nm]
di-CH$_3$-di-OH	701 (76.8)	8.40	762 (65.5)	775	10.68	827 (70.7)	908
di-OH	692 (59.9)	8.18	745 (51.3)	772	10.34	805 (55.2)	876
di-F-di-OH	669 (51.1)	7.32	725 (46.7)	760	9.35	784 (52.8)	860
di-Cl-di-OH	688 (61.4)	6.52	752 (52.6)	781	8.72	808 (57.9)	890

Carbon dioxide sensors

The pH-sensitive di-OH-aza-BODIPY dyes were embedded in an ethyl cellulose matrix (EC49) along with tetraoctylammonium hydroxide as base to obtain optical carbon dioxide sensors. Clearly, the sensors showed well observable spectral changes in the near infrared (NIR) range according to the protonation of the di-anionic form giving the mono-anionic form (Fig. 2). The neutral forms of the di-OH-complexes showed slight fluorescence in solution, and the sensors based on the indicators did not show detectable fluorescence, neither for the mono-

anionic nor for the di-anionic form. Compared to the measurements in solution the CO_2 sensors based on the di-OH-aza-BODIPY dyes showed significantly bathochromically shifted absorption spectra with maxima at 760-780 nm for their mono-anionic forms and maxima at 860-910 nm for their di-anionic forms. Generally, a similar trend for the absorption maxima of the CO_2 sensors based on the respective complexes was observed (Table 1). Here, the shift between the mono-anionic and the di-anionic form was enlarged to over 100 nm. This fact is advantageous for optical sensors, because peak separation becomes easier.

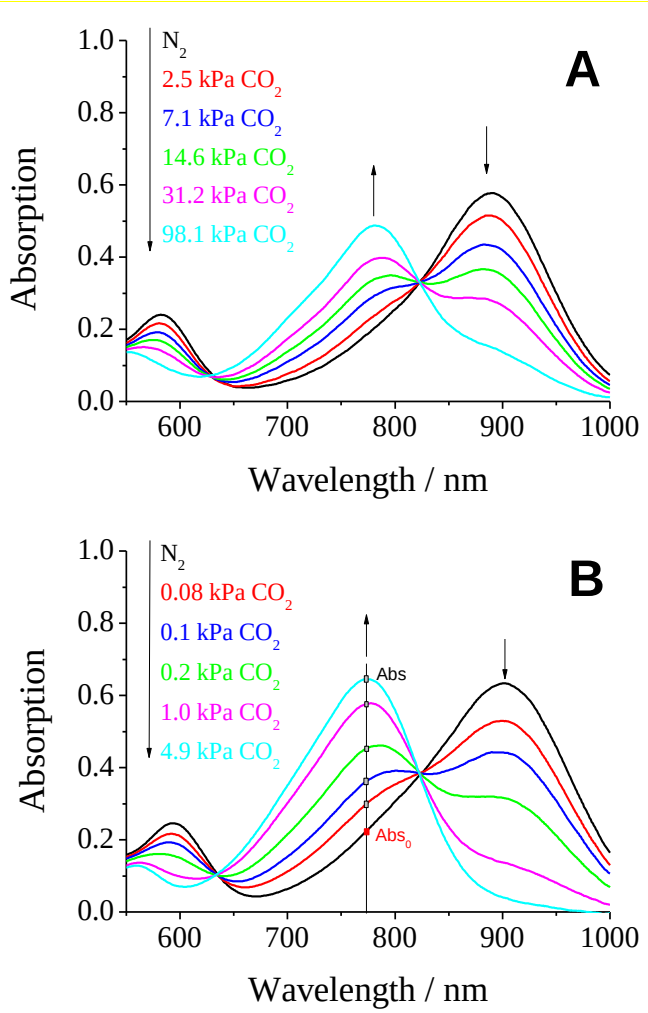

Fig. 2 Absorption spectra of optical carbon dioxide sensors based on (A) the di-Cl-di-OH-complex and (B) the di-CH_3-di-OH-complex in EC49 (base: TOAOH) at 25 °C at various pCO_2 values.

Despite the fact that all di-OH-aza-BODIPY dyes showed two protonation steps in aqueous solution, only one protonation step was observed in optical sensors based on these indicators. In fact, in the absence of carbon dioxide both hydroxyl groups build ion pairs with the quarternary ammonium base and the spectra for the di-anionic forms are observable. The mono-anionic form is built in the presence of carbon dioxide and is stable even at 100% CO_2. Spectra

of the neutral forms are not observable anymore (Fig. 2). Therefore, the pK_{a2} values measured in solution are most relevant for optical carbon dioxide sensors based on the di-OH-aza-BODIPY dyes. Indeed, these values correlate very well to the sensitivities of the optical CO_2 sensors (Table 1 and Fig. 3). The sensitivity increases in the following order: di-Cl-di-OH < di-F-di-OH < di-OH < di-CH_3-di-OH. Notably, for the most sensitive sensor based on di-CH3-di-OH about 25% of the overall signal change is observed already at atmospheric pCO_2 which is, to the best of our knowledge, one of the highest sensitivities reported so far. Di-F-di-OH and di-Cl-di-OH complexes bearing electron-withdrawing groups displayed diminished pK_{a2} values of 9.35 and 8.72, respectively, and enabled measurements up to 100% CO_2. These great differences in sensitivity lead to a broad range of applications, varying from food packaging and capnography for di-F-di-OH and di-Cl-di-OH complexes to environmental monitoring for di-OH and di-CH_3-di-OH complexes.

Fig. 3 shows the increasing absorption absorption of the mono-anionic form in relation to the absorption at 0 kPa (Abs-Abs_0) carbon dioxide (see Fig. B). The higher the sensitivity of the sensor, the steeper the respective calibration curves, as shown in Fig. 3, and the lower the amount of carbon dioxide necessary to fully protonate the sensor. Sensors based on the di-Cl-di-OH-complex and the di-F-di-OH-complex showed limits of detection (LOD) of 0.19 kPa and 0.18 kPa, respectively. However, determining the LOD value for very sensitive sensors can be very challenging. For measurements of low levels of carbon dioxide the measuring system (gas mixer, gas lines, flow cell, etc.) has to be completely decarbonized, which is very difficult to achieve in reality. Especially for atmospheric levels of pCO_2 (0.04 kPa ≈ 400 ppm in the gas phase ≈ 13.6 μmol^{-1} in water at 298.15 K) and below, traces of environmental carbon dioxide disturbed the measurements for sensors based on the di-CH_3-di-OH-complex and the di-OH-complex. Hence, the determined LODs for these two complexes (0.11 kPa for di-OH and 0.007 kPa for di-CH_3-di-OH) were only rough estimations.

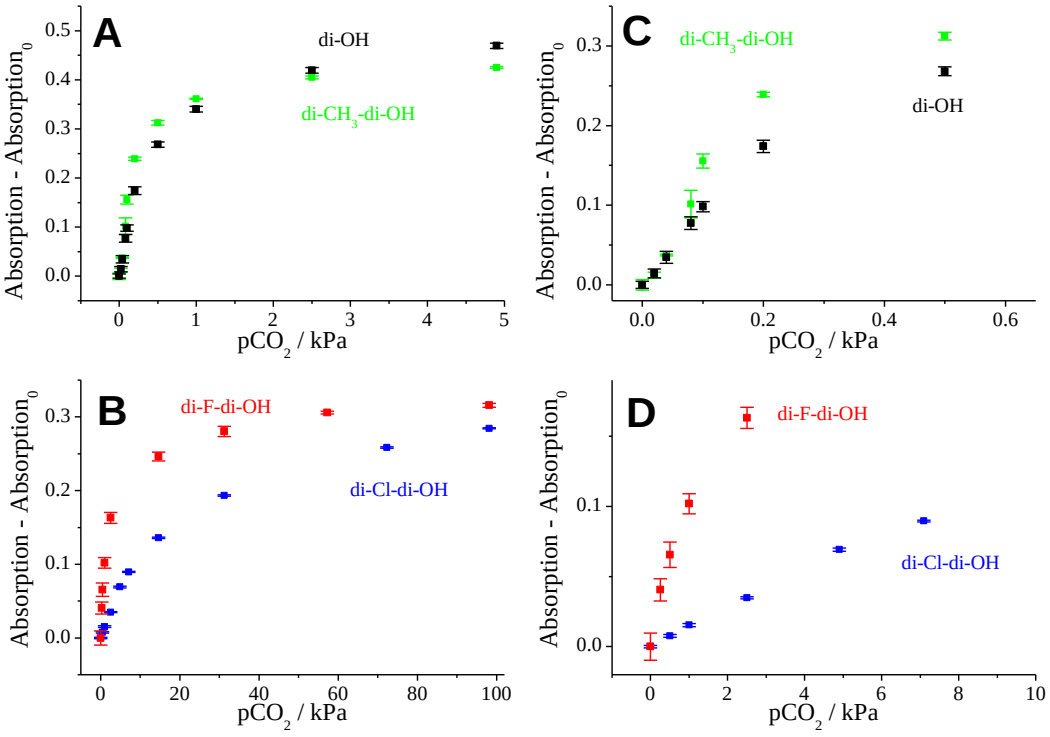

Fig. 3 (A) Calibration curves (absorption – absorption at 0 kPa of the mono-anionic form) for the carbon dioxide sensors based on di-OH-complex (black) and di-CH_3-di-OH-complex (green) and (B) di-Cl-di-OH-complex (blue) and di-F-di-OH-complex (red) 25°C under humid conditions with the respective "zoom-in" sections (C and D).

Photodegradation profiles of the carbon dioxide sensors were obtained from the absorption spectra after illuminating the sensor foils with a high-power LED array (λ_{max} 458 nm). For comparison, the state-of-the-art indicator dyes such as *m*-cresol-purple, thymol-blue and HPTS were used (ESI, Fig. S1). The photostability of both the mono-anionic and the di-anionic form were investigated. Therefore, the cuvette was filled either with pure carbon dioxide (mono-anionic form) or with pure nitrogen (di-anionic form). Clearly, all of the di-OH-aza-BODIPY dyes showed outstanding better photostability, much better than the reference indicators embedded in the same ethyl cellulose matrix. After 1.5 hours of illumination the presented dyes showed hardly any photobleaching effects for both the mono-anionic and di-anionic forms, whereas m-cresol-purple (neutral form), thymol-blue (neutral form) and HPTS (only anionic form) were degraded to less than 80%. The anionic forms of m-cresol-purple and thymol-blue were even less photostable than there neutral forms (ESI, Fig. S1).

Luminescence-based ratiometric read-out using IFE (inner filter effect) based sensors

Read-out of the planar optodes and fibre-optic sensors based on colorimetric systems is significantly more challenging than that of the luminescent systems. The inner-filter effect (IFE) was made use of in order to enable read-out *via* luminescence. Additionally to the first layer containing the absorption-based indicator dye along with TOAOH in ethyl cellulose, a second layer containing the secondary emitters was used.[42] It included the pH-insensitive di-butoxy-complex entrapped in PS-particles as a fluorophore and Egyptian blue (EB) as a phosphor, both embedded in Hyflon AD 60. The absorption spectra of the di-OH-complex and the emission spectra of the secondary emitters are shown in Fig. 4A. Here the broad emission band of the phosphor (EB) overlaps with the absorption spectrum of the di-anionic form of the indicator and the emission band of the fluorophore (di-butoxy-aza-BODIPY-complex) overlaps with the absorption spectrum of the mono-anionic form of the indicator. The isobestic point of the di-OH-indicator is located at 610 nm and represents an ideal wavelength for exciting the secondary emitters matching the maxima of the red LEDs available (605, 617 nm). The fluorescence spectra of the sensor based on the combination of EB, the di-butoxy-complex and the non-substituted di-OH indicator are shown in Fig. 4B. Emission peaks in the absence (λ_{max} 913 nm) and presence (λ_{max} 738 nm) of carbon dioxide were well observable. Hence, luminescence-based ratiometric read-out becomes possible. This can be realized either by using two emission filters isolating the respective components or by measuring the luminescence phase shift. In fact, the phase shift for luminescent Egyptian blue is 55.8° at 2000 Hz and the phase shift of the fluorophore is 0 at this modulation frequency.

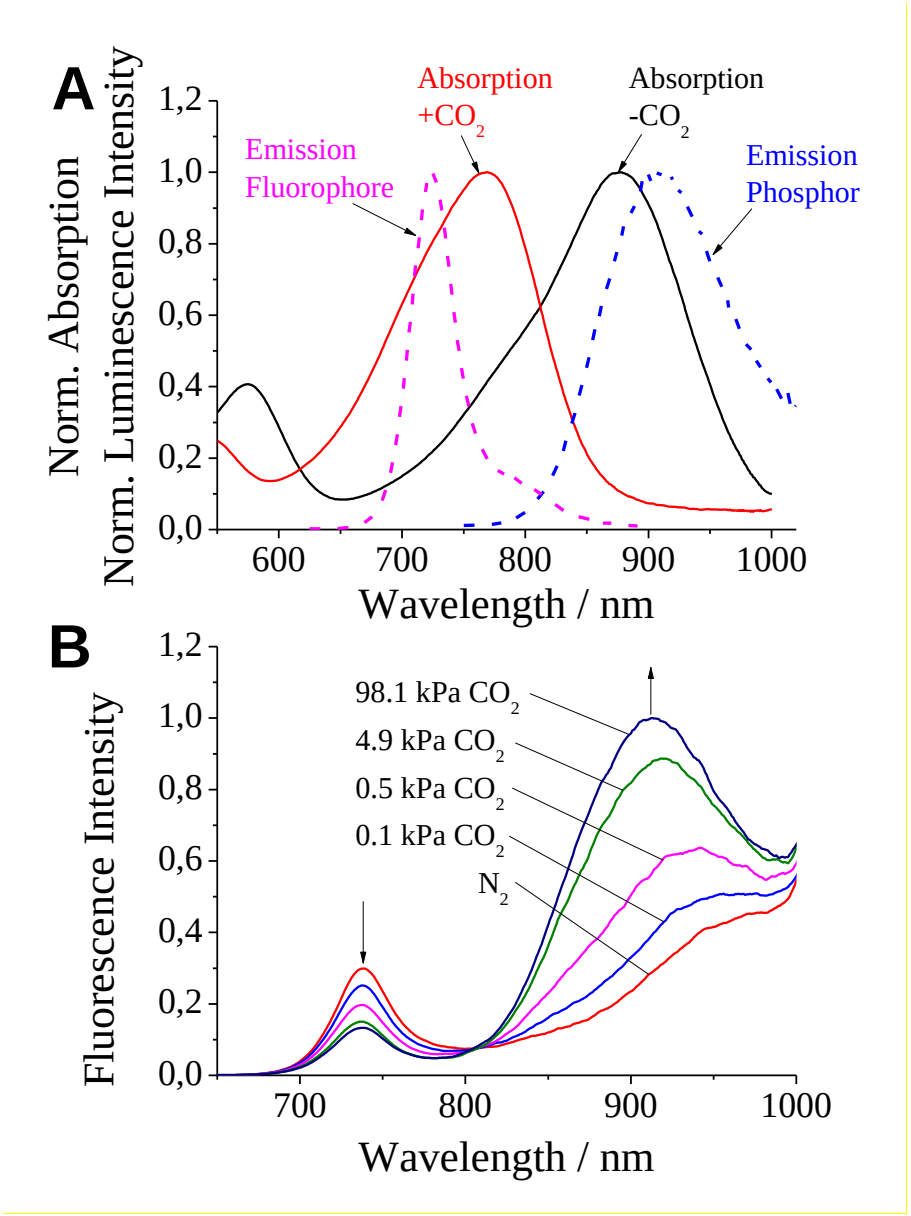

Figure 4. (A) Respective emission spectra (λ_{exc} 610 nm) of Egyptian Blue (EB; blue dashed line; "Emission Phosphor") and the di-butoxy-complex (dissolved in tetrahydrofuran; magenta dashed line; "Emission Fluorophore"); absorption spectra of the sensor based on the di-OH-complex in absence (black line) and in presence (red line) of carbon dioxide at 25°C. (B) Emission spectra (λ_{exc} 610 nm) of a carbon dioxide sensor based on the di-OH-complex and inner-filter-effect read-out at 25 °C under humidified conditions.

Carbon dioxide production/consumption of a Hebe plant. The applicability of the presented carbon dioxide sensors is demonstrated by showing the respiration of a Hebe pant. The Hebe plant in soil, a carbon dioxide sensor based on the di-CH_3-di-OH-complex and an oxygen trace sensor were placed in a desiccator. The desiccator was purged for 15 min with a gas mixture of 2% oxygen in nitrogen (in order to achieve better dynamics when measuring with an optical oxygen sensor compared to air saturation) and then closed tightly. During the measurement the

setup was alternately kept in darkness and illuminated for 30 min, respectively using three halogen lamps. According to these illumination sequences the production/consumption of carbon dioxide was observed (Fig. 5). In darkness an increase of carbon dioxide occurred due to respiration, whereas during illumination the concentration was decreased. Over the whole measurement more CO_2 was produced than consumed which may be due to stress-induced respiration of the Hebe plant. Corresponding to the applied light sequences also the oxygen concentration was affected. Note that over the whole experiment the oxygen concentration was increasing which can be explained by slow diffusion of oxygen into the dessicator. Surprisingly, oxygen concentration did not increase significantly during the light phase, but it increased abruptly immediately after the light was switched off, reaching a plateau after about 30 min (Fig. 5). This effect may be attributed to the storage of generated oxygen in the plant and its release in the beginning of the dark phase. After this time the equilibrium between oxygen consumption during respiration and oxygen diffusion from outside is reached. As can be seen, the same phenomenon is observed if both the light and dark cycles are extended to 60 min (see hours 2 to 4 in Fig. 5). The above plant behaviour is beyond the scope of the paper and calls for more detailed investigation.

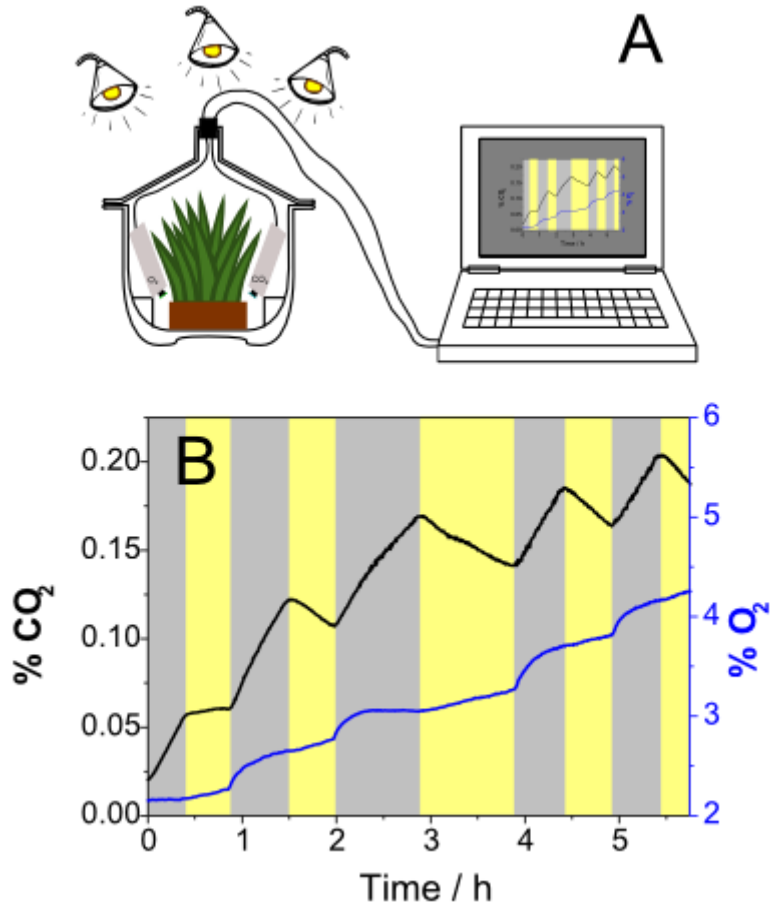

Fig. 5 (A) Experimental set-up and (B) carbon dioxide and oxygen dynamics in a dessicator containing a Hebe plant during illumination (yellow zones) and in darkness (gray zones).

Conclusion

A new class of colorimetric pH-sensitive indicators for carbon dioxide sensors has been presented. The di-OH-aza-BODIPY dyes show characteristic CO_2-dependent absorption spectra in the near-infrared region. In addition to the remarkable photostability of the indicators and the high molar absorption coefficients, the dynamic ranges of the sensors can be tuned via electron-donating and electron-withdrawing substituents. This enables a broad range of applications from environmental monitoring to food packaging or capnography. The sensors based on di-CH_3-di-OH-aza-BODIPYs are the most sensitive sensors ever reported and resolve well below atmospheric CO_2 levels. The absorption-modulated inner-filter effect was used to enable referenced luminescence-based ratiometric read-out. As an example the production/consumption of carbon dioxide of a Hebe plant was demonstrated.

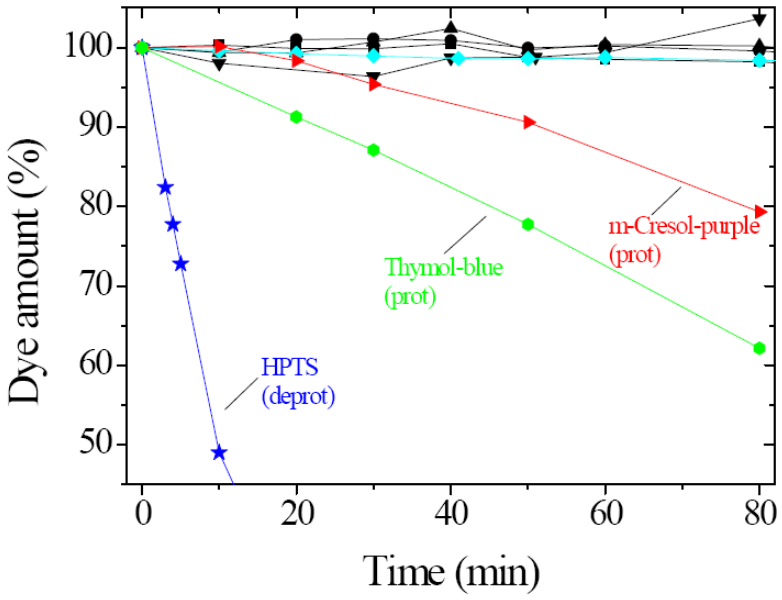

Figure S1. Photodegradation profiles for carbon dioxide sensors (EC49; base: TOAH; T=25 °C) based on the di-OH-aza-BODIPY dyes (black), m-cresol-purple (red triangles), thymol-blue (green dots) obtained from the absorption spectra of the respective neutral form and the absorption spectra of the deprotonated forms of the di-Cl-di-OH-complex (cyan) and HPTS(TOA)$_3$ (blue stars).

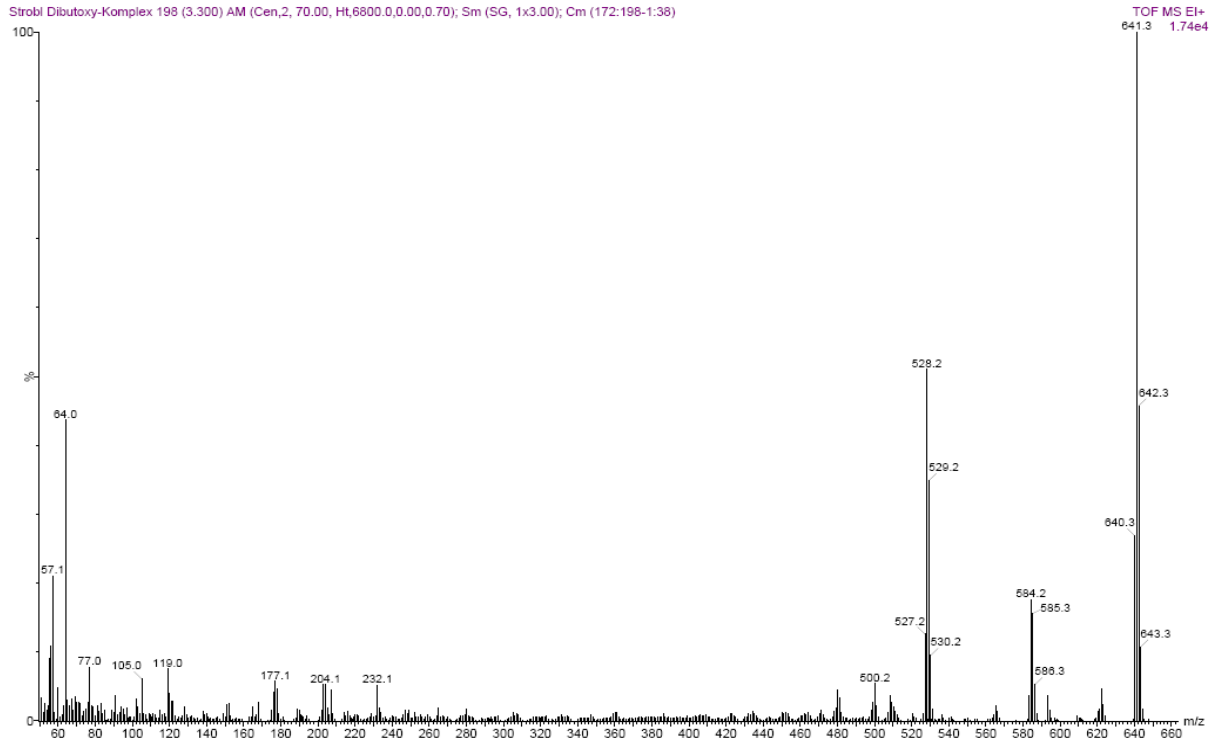

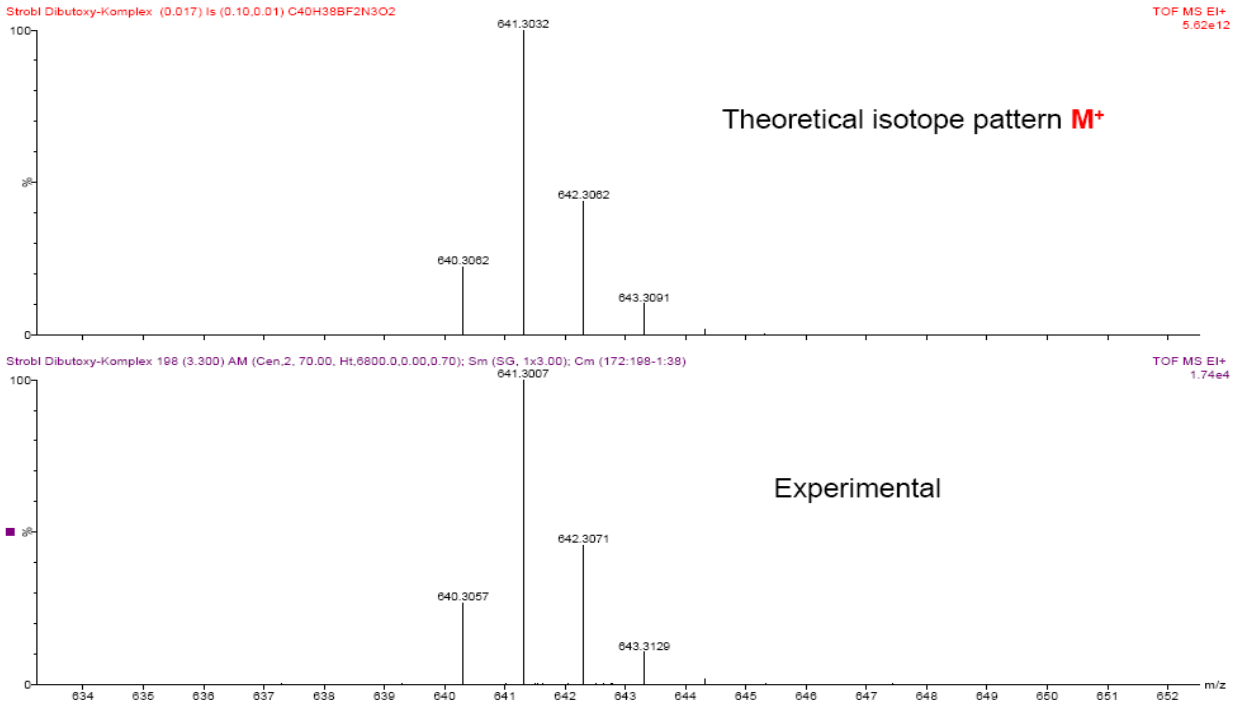

Figure S2. EI-DI Mass spectrum of 3,7-bis(4-butoxyphenyl)-5,5-difluoro-1,9-diphenyl-5H-4λ^4,5λ^4-dipyrrolo[1,2-c:2`,1`-*f*][1,3,5,2]triazaborinine (di-butoxy-complex).

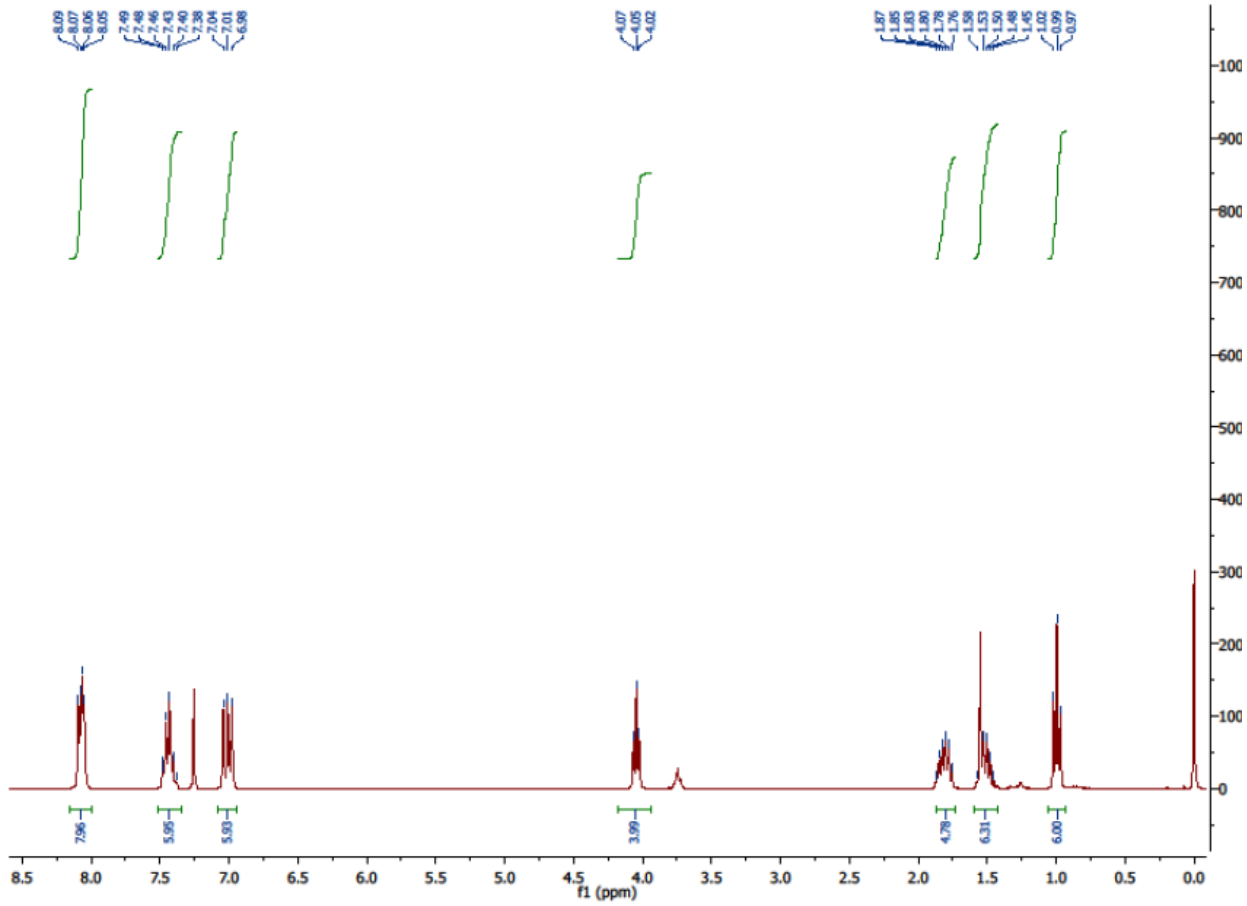

Figure S3. ^{1}H NMR of 3,7-bis(4-butoxyphenyl)-5,5-difluoro-1,9-diphenyl-5H-4λ^{4},5λ^{4}-dipyrrolo[1,2-c:2`,1`-*f*][1,3,5,2]triazaborinine (di-butoxy-complex).

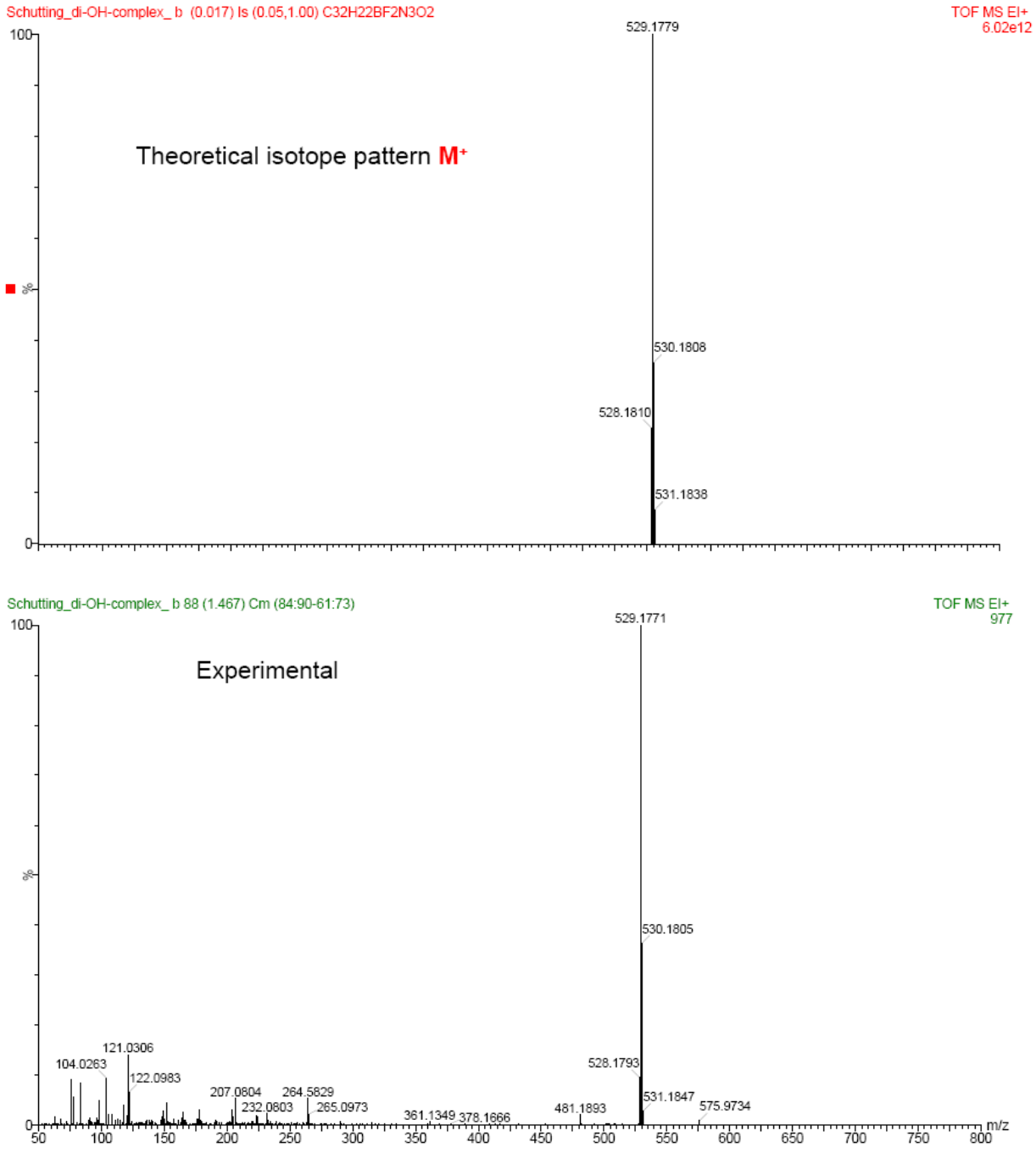

Figure S4. EI-DI Mass spectrum of 4,4`-(5,5-difluoro-1,9-diphenyl-5H-4λ$^{4}$,5λ$^{4}$-dipyrrolo[1,2-c:2`,1`-*f*][1,3,5,2]triazaborinine-3,7-diyl)diphenol (di-OH-complex).

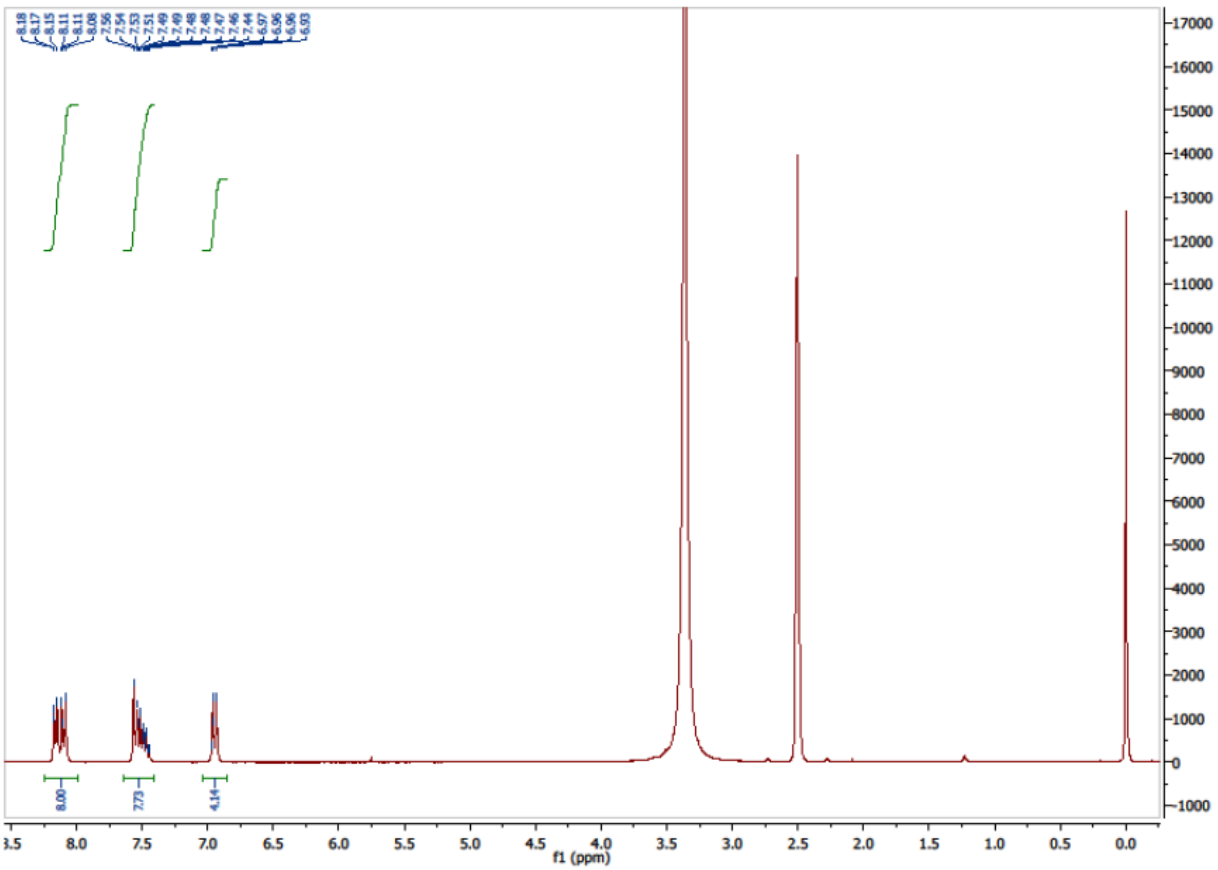

Figure S5. ^{1}H NMR of 4,4`-(5,5-difluoro-1,9-diphenyl-5H-4λ4,5λ4-dipyrrolo[1,2-c:2`,1`-*f*][1,3,5,2]triazaborinine-3,7-diyl)diphenol (di-OH-complex)

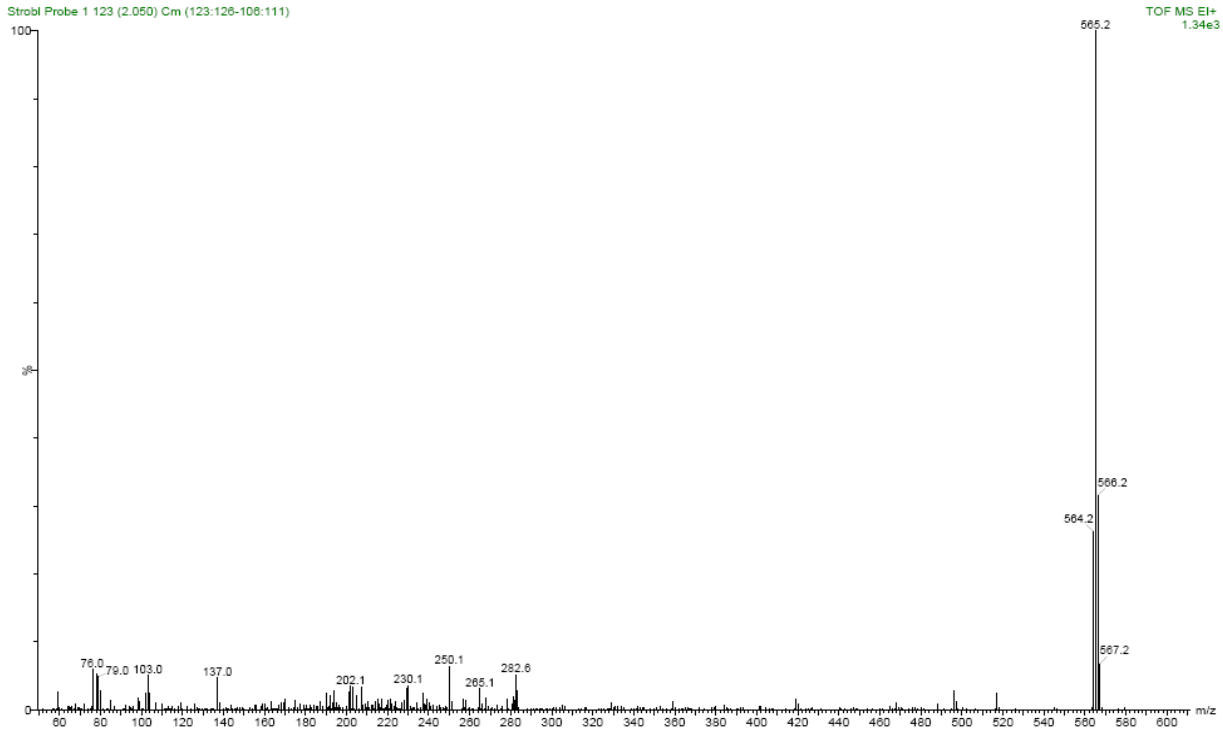

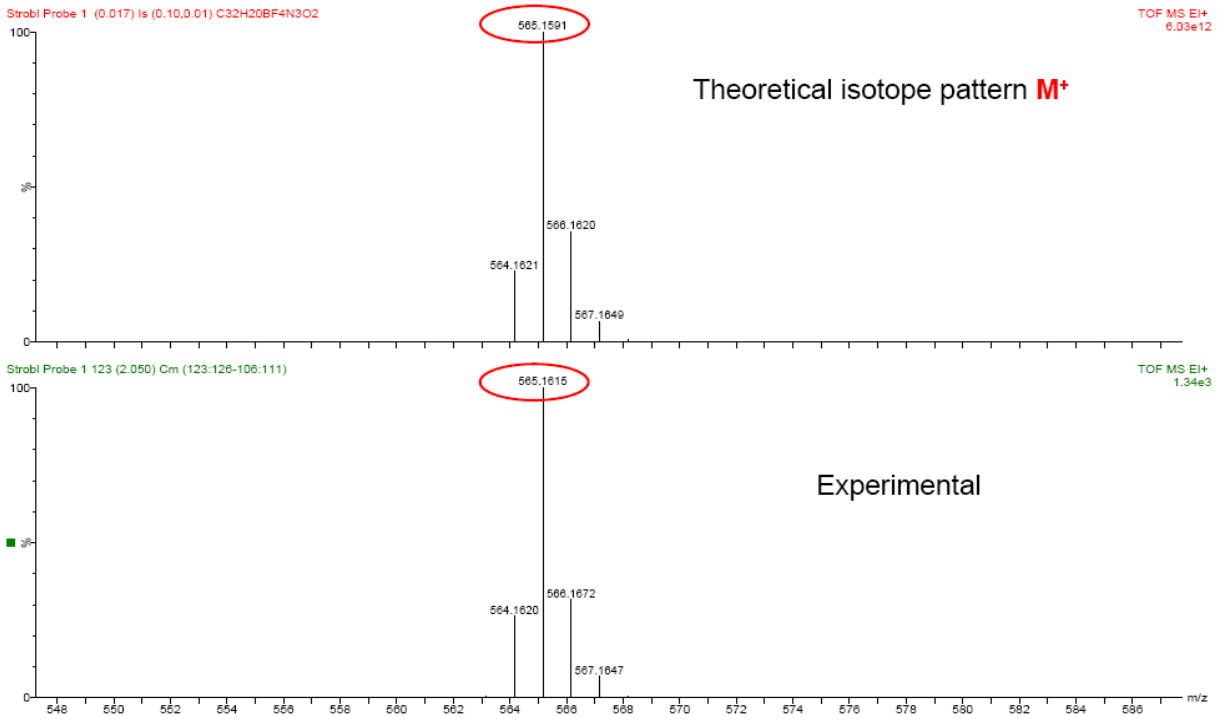

Figure S6. EI-DI Mass spectrum of 4,4`-(5,5-difluoro-1,9-diphenyl-5H-4λ$^4$,5λ$^4$-dipyrrolo[1,2-c:2`,1`-*f*][1,3,5,2]triazaborinine-3,7-diyl)bis(3-fluorophenol) (di-F-di-OH-complex).

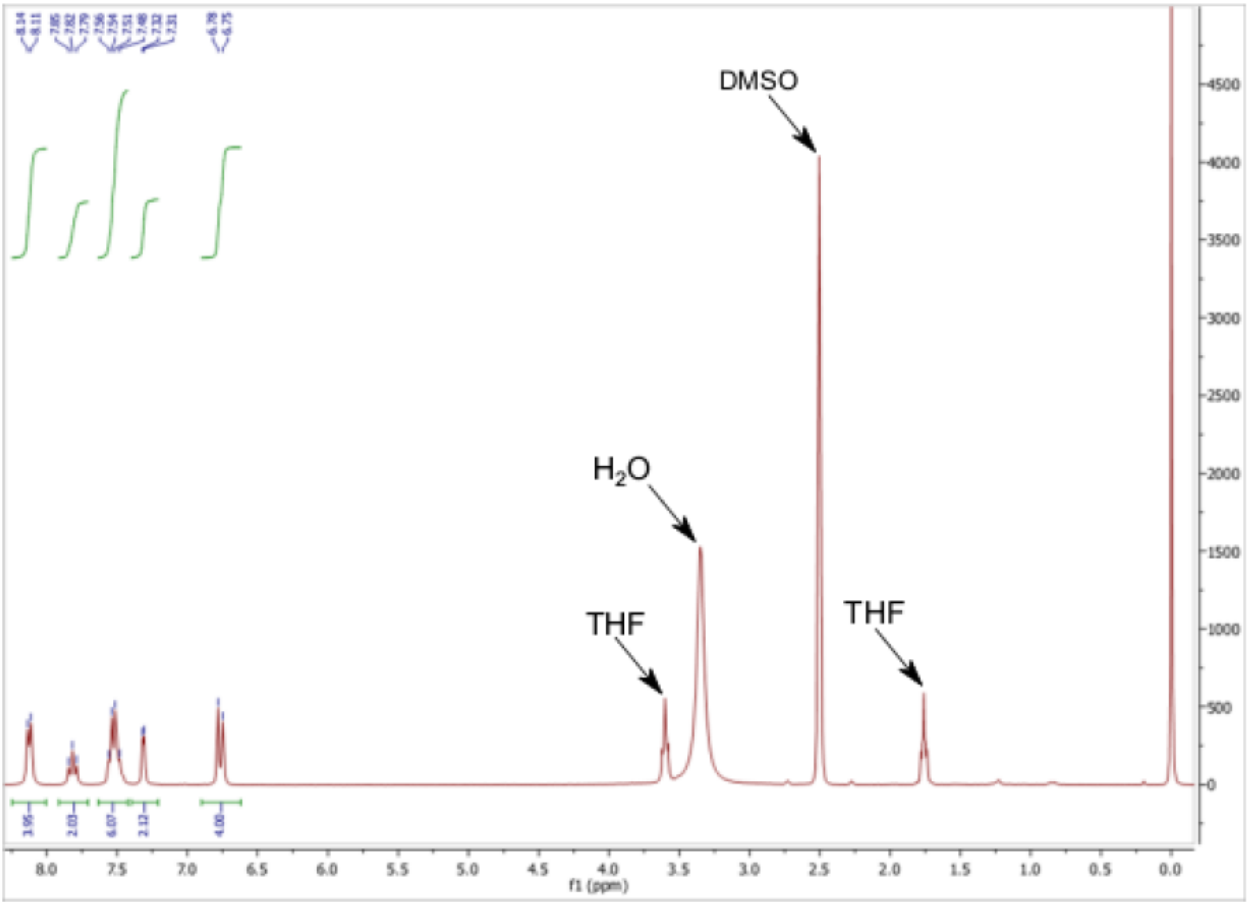

Figure S7. ^{1}H NMR of 4,4`-(5,5-difluoro-1,9-diphenyl-5H-4λ$^{4}$,5λ$^{4}$-dipyrrolo[1,2-c:2`,1`-*f*][1,3,5,2]triazaborinine-3,7-diyl)bis(3-fluorophenol) (di-F-di-OH-complex).

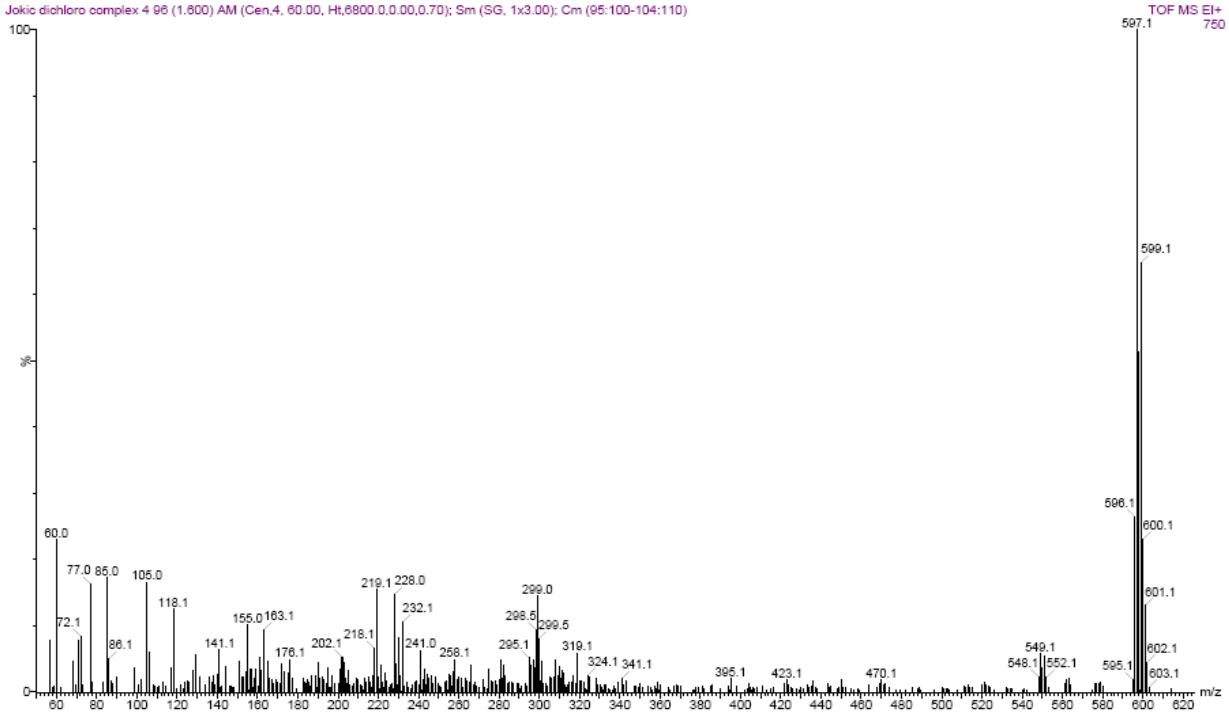

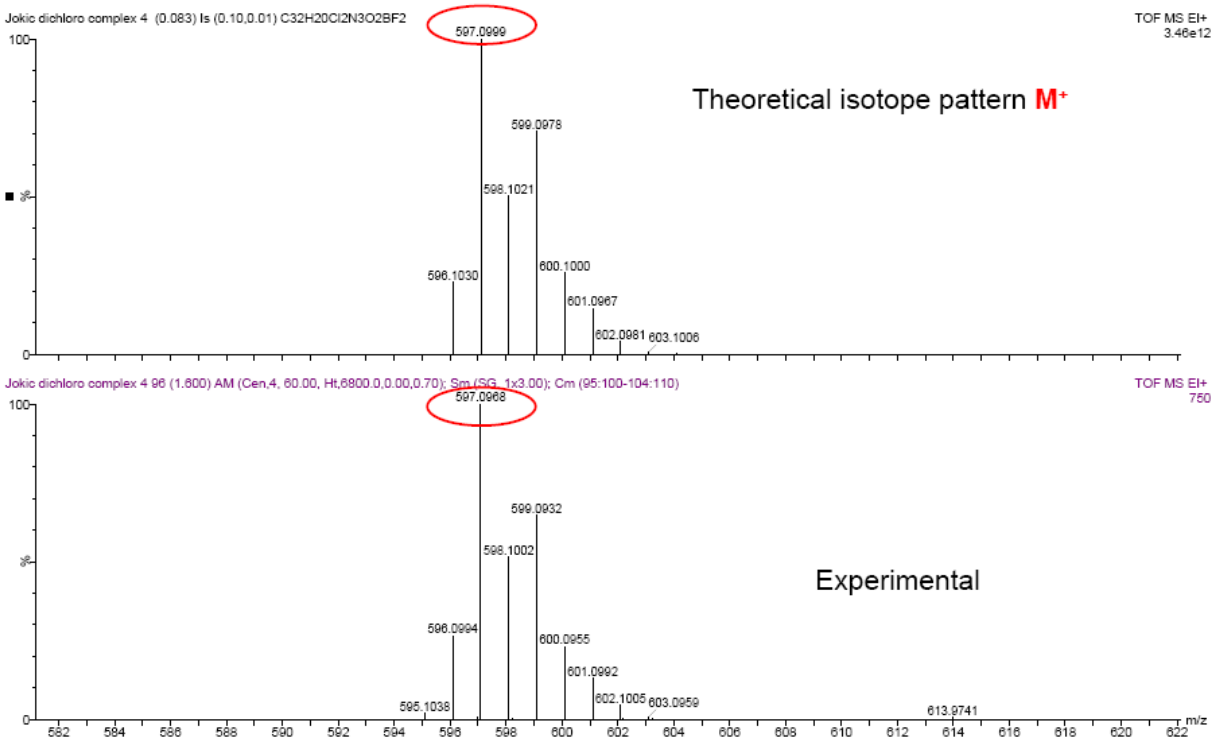

Figure S8. EI-DI Mass Spectrum of 4,4`-(5,5-difluoro-1,9-diphenyl-5*H*-4λ$^4$,5λ$^4$-dipyrrolo[1,2-c:2`,1`-*f*][1,3,5,2]triazaborinine-3,7-diyl)bis(2-chlorophenol) (di-Cl-di-OH-complex).

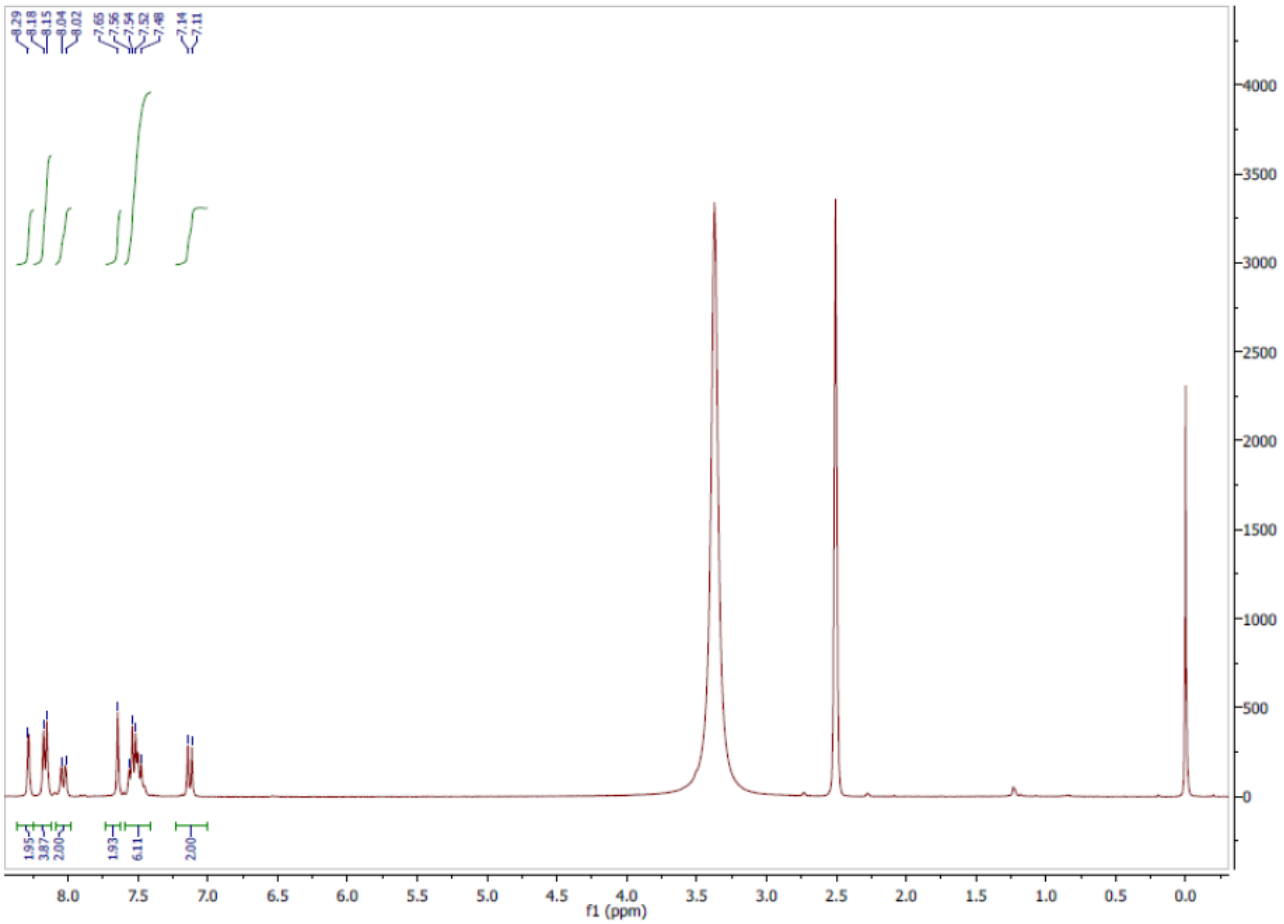

Figure S9. ^{1}H NMR of 4,4`-(5,5-difluoro-1,9-diphenyl-5*H*-4λ$^{4}$,5λ$^{4}$-dipyrrolo[1,2-c:2`,1`-*f*][1,3,5,2]triazaborinine-3,7-diyl)bis(2-chlorophenol) (di-Cl-di-OH-complex).

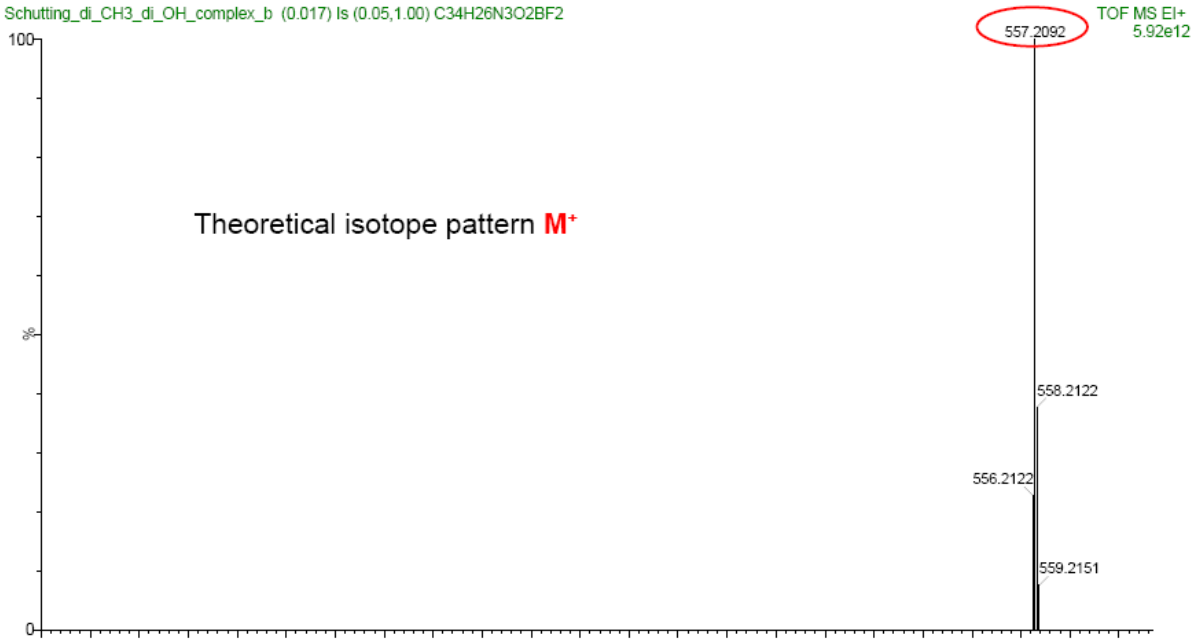

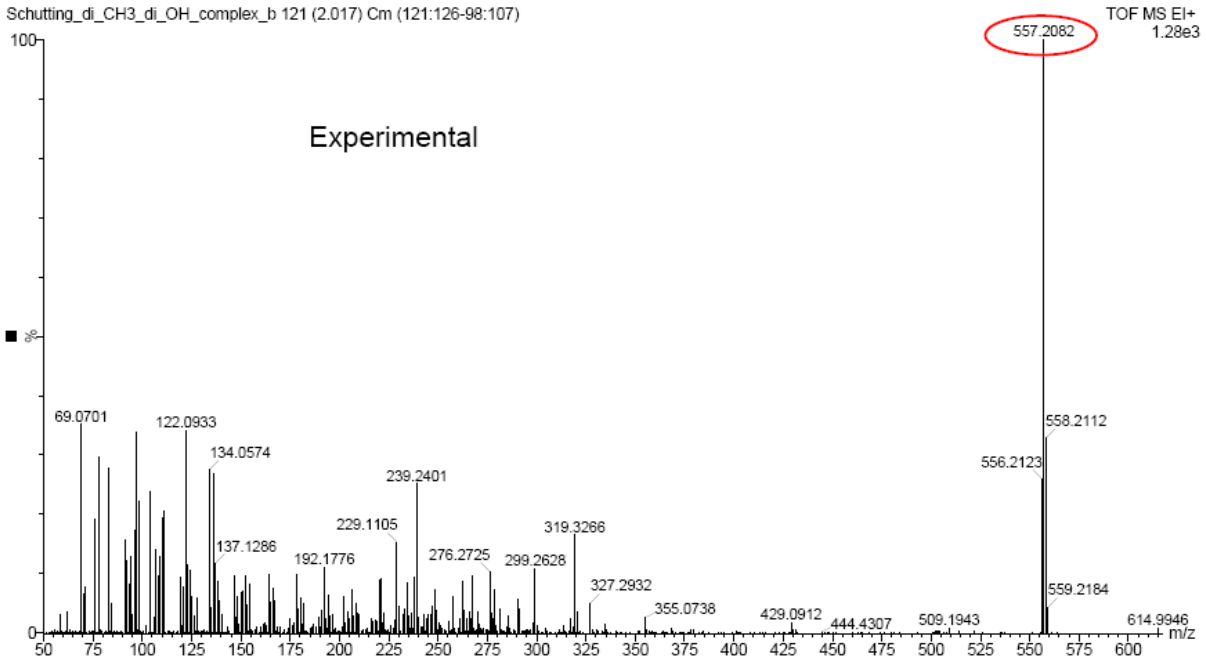

Figure S10. EI-DI Mass spectrum of 4,4`-(5,5-difluoro-1,9-diphenyl-5*H*-4λ$^4$,5λ$^4$-dipyrrolo[1,2-c:2`,1`-*f*][1,3,5,2]triazaborinine-3,7-diyl)bis(2-methylphenol) (di-CH_3-di-OH-complex).

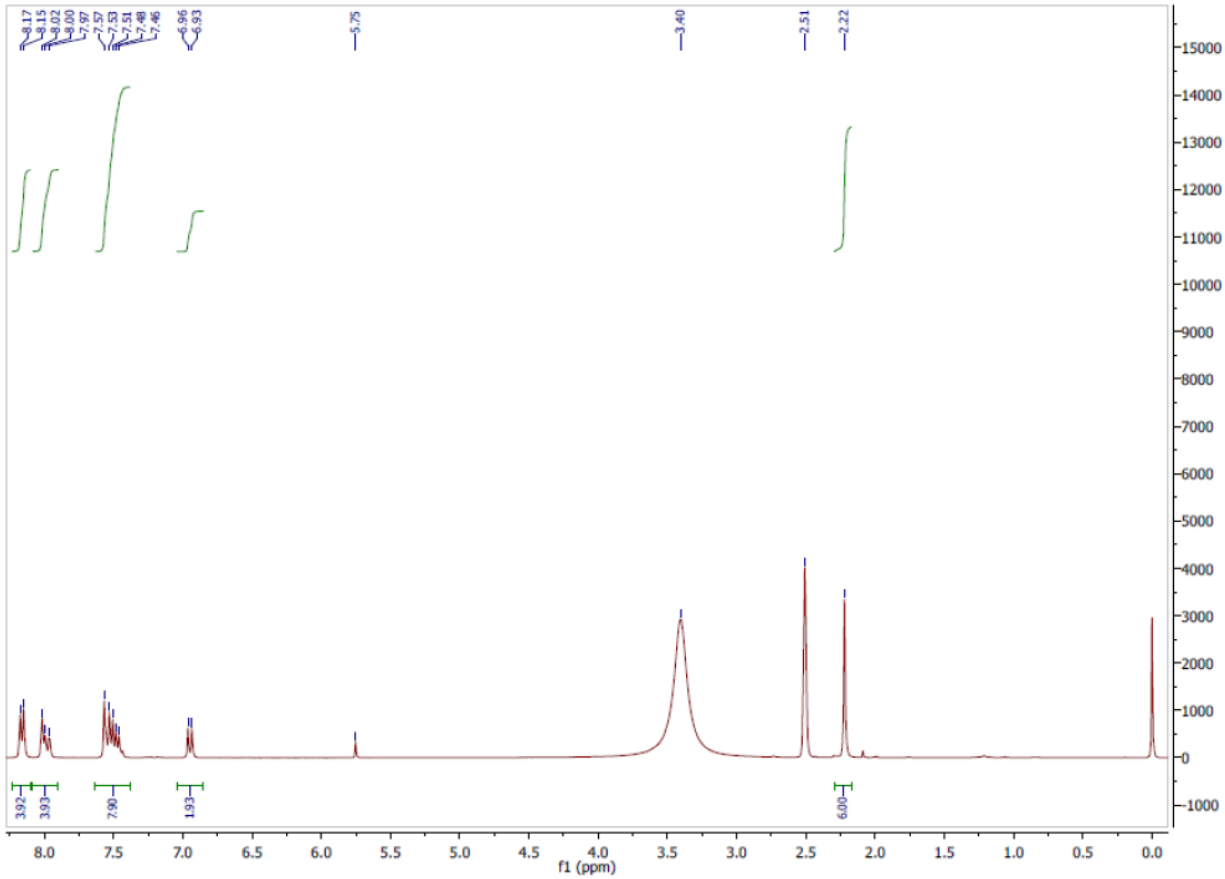

Figure S11. ^{1}H NMR of 4,4`-(5,5-difluoro-1,9-diphenyl-5*H*-4λ$^4$,5λ$^4$-dipyrrolo[1,2-c:2`,1`-*f*][1,3,5,2]triazaborinine-3,7-diyl)bis(2-methylphenol) (di-CH_3-di-OH-complex).

Brockmanngasse 58/17
Graz 8010, Austria
E-Mail: martin.strobl@tugraz.at

PERSONAL DATA:

- Date of Birth: 09.05.1987, Fürstenfeld
- Citizenship: Austria

EDUCATION:

09/2013 – 03/2017	**Graz UNIVERSITY of Technology** - Institute of Analytical Chemistry and Food Chemistry - Ph.D. candidate in the Applied Sensors Workgroup of Prof. Torsten Mayr - **Tasks**: Organic Synthesis of fluorescent indicator dyes. Development of optical sensors for determination of pH, pCO_2 and ammonia. Drafting of scientific reports and papers, Presentation of research results at conferences. Supervision of bachelor and master students.
10/2006 – 06/2013	**Graz UNIVERSITY of Technology** - Student at the Faculty of Chemistry - Bachelor thesis: Biocidal polymers (Institute for Chemistry and Technology of Materials) - Master Thesis: Covalent Coupling of Fluorescent pH Indicators, Supervisor: Prof. Dr. Ingo Klimant
08/2010 – 12/2010	**UNIVERSITY of LUND, Sweden** - ERASMUS - Exchange Student Program - Faculty of Chemistry
2005/06	**COMMUNITY SERVICE** Emergency Medical Technician
2001-2005	**HIGHSCHOOL, Jennersdorf**

Publications in peer reviewed journals

submitted in 12/2016	**Photostable upconverting and downconverting pH sensors based on combination of a colorimetric NIR indicator and stable inorganic phosphors as secondary emitters** **Strobl, M**., Mayr, T., Klimant, I. and Borisov, M. S. accepted in *Sensors and Actuators: B. Chemical*
submitted in 12/2016	**Trace ammonia sensors based on fluorescent NIR-emitting aza-BODIPY dyes** **Strobl, M.,** Walcher, A., Mayr, T., Klimant, I. and Borisov, M. S. accepted in *Analytical Chemistry*
11/2016	**Highly sensitive poisoning-resistant optical carbon dioxide sensors for environmental monitoring** Fritzsche, E., Gruber, P., Schutting, S., Fischer, P. J., **Strobl, M.,** Müller, D. J., Borisov, M. S. and Klimant, I. In: *Analytical Methods*. 2017, 9 55-65
09/2016	**Simultaneous determination of oxygen and pH inside microfluidic devices using core-shell nanosensors** Ehgartner, J., **Strobl, M.**, Bolivar, J. M., Rabl, D., Rothbauer, M., Ertl, P., Borisov, M. S. and Mayr, T. In: *Analytical chemistry*. 88, 19, p. 9796–9804
08/2016	**Fast pesticide detection inside microfluidic device with integrated optical pH, oxygen sensors and algal fluorescence** Tahirbegi, I. B., Ehgartner, J, Kasjanow, A., Paradiso, M., Bouwes, D. and Mayr, T. In: *Biosensors & bioelectronics*. 88, p. 188-195
08/2016	**Design and Application of an Optical Sensor for Simultaneous Imaging of pH and Dissolved O_2 with low Cross-Talk** Moßhammer, M., Strobl, M., Kühl, M., Klimant, I., Borisov, M. S. and Koren, K. In: *ACS Sensors* 2016, 1, 681-687
09/2015	**NIR-Emitting aza-BODIPY dyes – new building blocks for broad-range optical pH sensors** **Strobl, M**., Rappitsch, T., Borisov M. S., Mayr T. and Klimant, I. In: *Analyst* 2015, 140, 7150-7153

04/2015	**NIR optical carbon dioxide sensors based on highly photostable dihydroxy-aza-BODIPY dyes** Schutting, S., Jokic, T., **Strobl, M**., Borisov M. S., de Beer, D. and Klimant, I., In: *Journal of Materials Chemistry C* 2015, 3, 5474-5483

Participation in Conferences and Congresses

03/2016	**EUROPT[R]ODE** XII Conference on Optical Sensors and Biosensors, Graz, Austria
10/2015	**Young-Chem2015** 13th International Congress of Young Chemists, Krakow, Poland Oral presentation: *NIR-emitting aza-BODIPY dye – New Building Blocks for Broad-range Optical pH Sensors*
09/2015	**MAF 14** 14th Conference on Methods and Application of Fluorescence, Würzburg, Germany
04/2014	**EUROPT[R]ODE** 13th Conference on Optical Sensors and Biosensors, Athens, Greece

Working Experience

2016-ongoing	Springer ***Journal Microchimica Acta***, Staff member of the Editorial team
2010-2016	**Teaching Assistant for various laboratory courses** (General Chemistry, Analytical Chemistry, Molecular Analytics and Spectroscopy)
07/2011-07/2013	**Cytec Company** in Werndorf, Summer job, Quality control

About me

Personal	Team-minded, flexible, industrious, optimistic
Language	German (native speaker), English (fluent), Swedish (A1 course)
Hobbies	Gym, Traveling, Cooking, Hiking, Nature and History Documentaries

References

1. Wencel, D., Abel, T. & McDonagh, C. Optical Chemical pH Sensors. *Anal. Chem.* **86,** 15–29 (2014).
2. Strobl, M., Rappitsch, T., Borisov, S. M., Mayr, T. & Klimant, I. NIR-emitting aza-BODIPY dyes – new building blocks for broad-range optical pH sensors. *Analyst* **140,** 7150–7153 (2015).
3. Klimant, I. *et al.* in *New Trends in Fluorescence Spectroscopy* (eds. Valeur, P. B. & Brochon, D. J.-C.) 257–274 (Springer Berlin Heidelberg, 2001). doi:10.1007/978-3-642-56853-4_13
4. Valeur, B. & Brochon, J.-C. *New Trends in Fluorescence Spectroscopy: Applications to Chemical and Life Sciences*. (Springer Science & Business Media, 2012).
5. Dafu, C. *et al.* Optical-fibre pH sensor. *Sens. Actuators B Chem.* **12,** 29–32 (1993).
6. Ehgartner, J. *et al.* Simultaneous Determination of Oxygen and pH Inside Microfluidic Devices Using Core–Shell Nanosensors. *Anal. Chem.* **88,** 9796–9804 (2016).
7. Weidgans, B. M., Krause, C., Klimant, I. & Wolfbeis, O. S. Fluorescent pH sensors with negligible sensitivity to ionic strength. *The Analyst* **129,** 645–650 (2004).
8. Staudinger, C. & Borisov, S. M. Long-wavelength analyte-sensitive luminescent probes and optical (bio)sensors. *Methods Appl. Fluoresc.* **3,** 042005 (2015).
9. Frangioni, J. V. In vivo near-infrared fluorescence imaging. *Curr. Opin. Chem. Biol.* **7,** 626–634 (2003).
10. Vinogradov, S. A. & Wilson, D. F. Electrostatic core shielding in dendritic polyglutamic porphyrins. *Chem. Weinh. Bergstr. Ger.* **6,** 2456–2461 (2000).
11. Finikova, O. *et al.* Porphyrin and Tetrabenzoporphyrin Dendrimers: Tunable Membrane-Impermeable Fluorescent pH Nanosensors. *J. Am. Chem. Soc.* **125,** 4882–4893 (2003).
12. Khalil, G. E. *et al.* meso-Tetraarylporpholactones as high pH sensors. *Analyst* **135,** 2125–2131 (2010).
13. Li, Y. *et al.* Hemicyanine-based High Resolution Ratiometric near-Infrared Fluorescent Probe for Monitoring pH Changes in Vivo. *Anal. Chem.* **87,** 2495–2503 (2015).
14. He, L., Lin, W., Xu, Q. & Wei, H. A Unique Type of Pyrrole-Based Cyanine Fluorophores with Turn-on and Ratiometric Fluorescence Signals at Different pH Regions for Sensing pH in Enzymes and Living Cells. *ACS Appl. Mater. Interfaces* **6,** 22326–22333 (2014).

15. Liu, W. *et al.* Reversible Near-Infrared pH Probes Based on Benzo[a]phenoxazine. *Anal. Chem.* **85,** 7419–7425 (2013).
16. Liu, X.-D. *et al.* A coumarin–indole-based near-infrared ratiometric pH probe for intracellular fluorescence imaging. *Analyst* **138,** 6542–6550 (2013).
17. Aigner, D., Borisov, S. M., Petritsch, P. & Klimant, I. Novel near infra-red fluorescent pH sensors based on 1-aminoperylene bisimides covalently grafted onto poly(acryloylmorpholine). *Chem. Commun.* **49,** 2139–2141 (2013).
18. Loudet, A. & Burgess, K. BODIPY Dyes and Their Derivatives: Syntheses and Spectroscopic Properties. *Chem. Rev.* **107,** 4891–4932 (2007).
19. Rurack, K., Kollmannsberger, M. & Daub, J. A highly efficient sensor molecule emitting in the near infrared (NIR): 3,5-distyryl-8-(p-dimethylaminophenyl)difluoroboradiaza-s-indacene. *New J. Chem.* **25,** 289–292 (2001).
20. Zhang, J. *et al.* Near-infrared fluorescent probes based on piperazine-functionalized BODIPY dyes for sensitive detection of lysosomal pH. *J. Mater. Chem. B* **3,** 2173–2184 (2015).
21. Descalzo, A. B. *et al.* Phenanthrene-Fused Boron−Dipyrromethenes as Bright Long-Wavelength Fluorophores. *Org. Lett.* **10,** 1581–1584 (2008).
22. Killoran, J., Allen, L., Gallagher, J. F., Gallagher, W. M. & O'Shea, D. F. Synthesis of BF2 chelates of tetraarylazadipyrromethenes and evidence for their photodynamic therapeutic behaviour. *Chem. Commun. Camb. Engl.* 1862–1863 (2002).
23. Allik, T. H., Hermes, R. E., Sathyamoorthi, G. & Boyer, J. H. Spectroscopy and laser performance of new BF2-complex dyes in solution. in **2115,** 240–248 (1994).
24. Killoran, J., McDonnell, S. O., Gallagher, J. F. & O'Shea, D. F. A substituted BF2-chelated tetraarylazadipyrromethene as an intrinsic dual chemosensor in the 650–850 nm spectral range. *New J. Chem.* **32,** 483–489 (2008).
25. Murtagh, J., Frimannsson, D. O. & O'Shea, D. F. Azide Conjugatable and pH Responsive Near-Infrared Fluorescent Imaging Probes. *Org. Lett.* **11,** 5386–5389 (2009).
26. McDonnell, S. O. & O'Shea, D. F. Near-Infrared Sensing Properties of Dimethlyamino-Substituted BF2−Azadipyrromethenes. *Org. Lett.* **8,** 3493–3496 (2006).
27. J. Hall, M., T. Allen, L. & F. O'Shea, D. PET modulated fluorescent sensing from the BF 2 chelated azadipyrromethene platform. *Org. Biomol. Chem.* **4,** 776–780 (2006).

28. Jokic, T. *et al.* Highly Photostable Near-Infrared Fluorescent pH Indicators and Sensors Based on BF 2 -Chelated Tetraarylazadipyrromethene Dyes. *Anal. Chem.* **84,** 6723–6730 (2012).
29. Valeur, B. & Berberan-Santos, M. N. in *Molecular Fluorescence* I–XXI (Wiley-VCH Verlag GmbH & Co. KGaA, 2012).
30. Borisov, S. M., Neurauter, G., Schroeder, C., Klimant, I. & Wolfbeis, O. S. Modified dual lifetime referencing method for simultaneous optical determination and sensing of two analytes. *Appl. Spectrosc.* **60,** 1167–1173 (2006).
31. Borisov, S. M., Gatterer, K. & Klimant, I. Red light-excitable dual lifetime referenced optical pH sensors with intrinsic temperature compensation. *Analyst* **135,** 1711–1717 (2010).
32. Borisov, S. M., Würth, C., Resch-Genger, U. & Klimant, I. New life of ancient pigments: application in high-performance optical sensing materials. *Anal. Chem.* **85,** 9371–9377 (2013).
33. Borisov, S. M., Gatterer, K., Bitschnau, B. & Klimant, I. Preparation and Characterization of Chromium(III)-Activated Yttrium Aluminum Borate: A New Thermographic Phosphor for Optical Sensing and Imaging at Ambient Temperatures. *J. Phys. Chem. C* **114,** 9118–9124 (2010).
34. Auzel, F. Upconversion and Anti-Stokes Processes with f and d Ions in Solids. *Chem. Rev.* **104,** 139–174 (2004).
35. Heer, S., Kömpe, K., Güdel, H.-U. & Haase, M. Highly Efficient Multicolour Upconversion Emission in Transparent Colloids of Lanthanide-Doped NaYF4 Nanocrystals. *Adv. Mater.* **16,** 2102–2105 (2004).
36. Chen, J. & Zhao, J. X. Upconversion Nanomaterials: Synthesis, Mechanism, and Applications in Sensing. *Sensors* **12,** 2414–2435 (2012).
37. Mader, H. S., Kele, P., Saleh, S. M. & Wolfbeis, O. S. Upconverting luminescent nanoparticles for use in bioconjugation and bioimaging. *Curr. Opin. Chem. Biol.* **14,** 582–596 (2010).
38. Gorris, H. H. & Wolfbeis, O. S. Photon-Upconverting Nanoparticles for Optical Encoding and Multiplexing of Cells, Biomolecules, and Microspheres. *Angew. Chem. Int. Ed.* **52,** 3584–3600 (2013).
39. Zhou, J., Liu, Q., Feng, W., Sun, Y. & Li, F. Upconversion Luminescent Materials: Advances and Applications. *Chem. Rev.* **115,** 395–465 (2015).

40. Jeevarajan, A. S., Vani, S., Taylor, T. D. & Anderson, M. M. Continuous pH monitoring in a perfused bioreactor system using an optical pH sensor. *Biotechnol. Bioeng.* **78,** 467–472 (2002).
41. John, G. T., Goelling, D., Klimant, I., Schneider, H. & Heinzle, E. PH-sensing 96-well microtitre plates for the characterization of acid production by dairy starter cultures. *J. Dairy Res.* **70,** 327–333 (2003).
42. Zhang, W. *et al.* A highly sensitive acidic pH fluorescent probe and its application to HepG2 cells. *Analyst* **134,** 367–371 (2009).
43. Tang, B. *et al.* A near-infrared neutral pH fluorescent probe for monitoring minor pH changes: imaging in living HepG2 and HL-7702 cells. *J. Am. Chem. Soc.* **131,** 3016–3023 (2009).
44. Wang, X.-D. & Wolfbeis, O. S. Fiber-Optic Chemical Sensors and Biosensors (2008–2012). *Anal. Chem.* **85,** 487–508 (2013).
45. Arregui, F. J., Otano, M., Fernandez-Valdivielso, C. & Matias, I. R. An experimental study about the utilization of Liquicoat® solutions for the fabrication of pH optical fiber sensors. *Sens. Actuators B Chem.* **87,** 289–295 (2002).
46. Wolfbeis, O. S. *Fiber optic chemical sensors and biosensors*. (CRC Press, 1991).
47. Aigner, D. *et al.* New fluorescent pH sensors based on covalently linkable PET rhodamines. *Talanta* **99,** 194–201 (2012).
48. Aigner, D. *et al.* Fluorescent materials for pH sensing and imaging based on novel 1,4-diketopyrrolo-[3,4-c]pyrrole dyes. *J. Mater. Chem. C* **1,** 5685–5693 (2013).
49. Aigner, D., Borisov, S. M. & Klimant, I. New fluorescent perylene bisimide indicators—a platform for broadband pH optodes. *Anal. Bioanal. Chem.* **400,** 2475–2485 (2011).
50. Lobnik, A., Oehme, I., Murkovic, I. & Wolfbeis, O. S. pH optical sensors based on sol–gels: Chemical doping versus covalent immobilization. *Anal. Chim. Acta* **367,** 159–165 (1998).
51. Shen, L., Lu, X., Tian, H. & Zhu, W. A Long Wavelength Fluorescent Hydrophilic Copolymer Based on Naphthalenediimide as pH Sensor with Broad Linear Response Range. *Macromolecules* **44,** 5612–5618 (2011).
52. Niu, C.-G., Gui, X.-Q., Zeng, G.-M. & Yuan, X.-Z. A ratiometric fluorescence sensor with broad dynamic range based on two pH-sensitive fluorophores. *Analyst* **130,** 1551–1556 (2005).

53. Nishimura, G., Shiraishi, Y. & Hirai, T. A fluorescent chemosensor for wide-range pH detection. *Chem. Commun.* 5313–5315 (2005). doi:10.1039/B508136J
54. Vasylevska, A. S., Karasyov, A. A., Borisov, S. M. & Krause, C. Novel coumarin-based fluorescent pH indicators, probes and membranes covering a broad pH range. *Anal. Bioanal. Chem.* **387,** 2131–2141 (2007).
55. Qi, J. *et al.* Fluorescent pH Sensors for Broad-Range pH Measurement Based on a Single Fluorophore. *Anal. Chem.* **87,** 5897–5904 (2015).
56. Killoran, J., Allen, L., Gallagher, J. F., Gallagher, W. M. & O'Shea, D. F. Synthesis of BF2 chelates of tetraarylazadipyrromethenes and evidence for their photodynamic therapeutic behaviour. *Chem. Commun. Camb. Engl.* 1862–1863 (2002).
57. Killoran, J., McDonnell, S. O., Gallagher, J. F. & O'Shea, D. F. A substituted BF2-chelated tetraarylazadipyrromethene as an intrinsic dual chemosensor in the 650–850 nm spectral range. *New J. Chem.* **32,** 483–489 (2008).
58. Murtagh, J., Frimannsson, D. O. & O'Shea, D. F. Azide conjugatable and pH responsive near-infrared fluorescent imaging probes. *Org. Lett.* **11,** 5386–5389 (2009).
59. McDonnell, S. O. & O'Shea, D. F. Near-infrared sensing properties of dimethlyamino-substituted BF2-azadipyrromethenes. *Org. Lett.* **8,** 3493–3496 (2006).
60. Cooper, M. E., Gregory, S., Adie, E. & Kalinka, S. pH-Sensitive Cyanine Dyes for Biological Applications. *J. Fluoresc.* **12,** 425–429 (2002).
61. Schröder, C. R., Weidgans, B. M. & Klimant, I. pH fluorosensors for use in marine systems. *Analyst* **130,** 907–916 (2005).
62. Schutting, S. *et al.* NIR optical carbon dioxide sensors based on highly photostable dihydroxy-aza-BODIPY dyes. *J Mater Chem C* **3,** 5474–5483 (2015).
63. Jeevarajan, A. S., Vani, S., Taylor, T. D. & Anderson, M. M. Continuous pH monitoring in a perfused bioreactor system using an optical pH sensor. *Biotechnol. Bioeng.* **78,** 467–472 (2002).
64. John, G. T., Goelling, D., Klimant, I., Schneider, H. & Heinzle, E. pH-Sensing 96-well microtitre plates for the characterization of acid production by dairy starter cultures. *J. Dairy Res.* **70,** 327–333 (2003).
65. Zhang, W. *et al.* A highly sensitive acidic pH fluorescent probe and its application to HepG2 cells. *Analyst* **134,** 367–371 (2009).

66. Zhang, Z. & Achilefu, S. Design, synthesis and evaluation of near-infrared fluorescent pH indicators in a physiologically relevant range. *Chem. Commun.* 5887–5889 (2005). doi:10.1039/B512315A
67. Hilderbrand, S. A., Kelly, K. A., Niedre, M. & Weissleder, R. Near infrared fluorescence-based bacteriophage particles for ratiometric pH imaging. *Bioconjug. Chem.* **19,** 1635–1639 (2008).
68. Liebsch, G., Klimant, I., Krause, C. & Wolfbeis, O. S. Fluorescent Imaging of pH with Optical Sensors Using Time Domain Dual Lifetime Referencing. *Anal. Chem.* **73,** 4354–4363 (2001).
69. Bambot, S. B., Sipior, J., Lakowicz, J. R. & Rao, G. Lifetime-based optical sensing of pH using resonance energy transfer in sol—gel films. *Sens. Actuators B Chem.* **22,** 181–188 (1994).
70. Chan, Y.-H. *et al.* Development of Ultrabright Semiconducting Polymer Dots for Ratiometric pH Sensing. *Anal. Chem.* **83,** 1448–1455 (2011).
71. Peng, H., Stolwijk, J. A., Sun, L.-N., Wegener, J. & Wolfbeis, O. S. A Nanogel for Ratiometric Fluorescent Sensing of Intracellular pH Values. *Angew. Chem. Int. Ed.* **49,** 4246–4249 (2010).
72. Georgiev, N. I. *et al.* A novel pH sensitive water soluble fluorescent nanomicellar sensor for potential biomedical applications. *Bioorg. Med. Chem.* **21,** 6292–6302 (2013).
73. Borisov, S. M. & Klimant, I. A versatile approach for ratiometric time-resolved read-out of colorimetric chemosensors using broadband phosphors as secondary emitters. *Anal. Chim. Acta* **787,** 219–225 (2013).
74. Hiruta, Y., Yoshizawa, N., Citterio, D. & Suzuki, K. Highly Durable Double Sol–Gel Layer Ratiometric Fluorescent pH Optode Based on the Combination of Two Types of Quantum Dots and Absorbing pH Indicators. *Anal. Chem.* **84,** 10650–10656 (2012).
75. Li, Z. & Zhang, Y. Monodisperse Silica-Coated Polyvinylpyrrolidone/NaYF4 Nanocrystals with Multicolor Upconversion Fluorescence Emission. *Angew. Chem. Int. Ed.* **45,** 7732–7735 (2006).
76. Fischer, L. H., Harms, G. S. & Wolfbeis, O. S. Upconverting nanoparticles for nanoscale thermometry. *Angew. Chem. Int. Ed Engl.* **50,** 4546–4551 (2011).
77. Sun, L.-N., Peng, H., Stich, M. I. J., Achatz, D. & Wolfbeis, O. S. pH sensor based on upconverting luminescent lanthanide nanorods. *Chem. Commun.* 5000–5002 (2009). doi:10.1039/B907822C

78. Meier, R. J., Simbürger, J. M. B., Soukka, T. & Schäferling, M. Background-Free Referenced Luminescence Sensing and Imaging of pH Using Upconverting Phosphors and Color Camera Read-out. *Anal. Chem.* **86,** 5535–5540 (2014).
79. Xie, L., Qin, Y. & Chen, H.-Y. Polymeric optodes based on upconverting nanorods for fluorescent measurements of pH and metal ions in blood samples. *Anal. Chem.* **84,** 1969–1974 (2012).
80. Ma, T. *et al.* Dye-conjugated upconversion nanoparticles for ratiometric imaging of intracellular pH values. *J. Mater. Chem. C* **3,** 6616–6620 (2015).
81. Arppe, R. *et al.* Photon upconversion sensitized nanoprobes for sensing and imaging of pH. *Nanoscale* **6,** 6837–6843 (2014).
82. Yan, L. *et al.* Biocompatible and flexible graphene oxide/upconversion nanoparticle hybrid film for optical pH sensing. *Phys. Chem. Chem. Phys.* **16,** 1576–1582 (2013).
83. Killoran, J., Allen, L., Gallagher, J. F., Gallagher, W. M. & O'Shea, D. F. Synthesis of BF2 chelates of tetraarylazadipyrromethenes and evidence for their photodynamic therapeutic behaviour. *Chem. Commun. Camb. Engl.* 1862–1863 (2002).
84. Jokic, T. *et al.* Highly photostable near-infrared fluorescent pH indicators and sensors based on BF2-chelated tetraarylazadipyrromethene dyes. *Anal. Chem.* **84,** 6723–6730 (2012).
85. Borisov, S. M., Gatterer, K. & Klimant, I. Red light-excitable dual lifetime referenced optical pH sensors with intrinsic temperature compensation. *The Analyst* **135,** 1711–1717 (2010).
86. Lim, C. S. *et al.* Triple molybdate scheelite-type upconversion phosphor NaCaLa(MoO4)3:Er3+/Yb3+: structural and spectroscopic properties. *Dalton Trans.* **45,** 15541–15551 (2016).
87. Crosby, G. A. & Demas, J. N. Measurement of photoluminescence quantum yields. Review. *J. Phys. Chem.* **75,** 991–1024 (1971).
88. Schutting, S., Jokic, T., Strobl, M., Borisov, S. M. & Klimant, D. de B. and I. NIR Optical Carbon Dioxide Sensors Based on Highly Photostable Dihydroxy-aza-BODIPY Dyes. *J Mater Chem C* (2015). doi:10.1039/C5TC00346F
89. Rtishchev, N. I., Samoilov, D. V., Martynova, V. P. & El'tsov, A. V. Luminescence Properties of Nitro Derivatives of Fluorescein. *Russ. J. Gen. Chem.* **71,** 1467–1478

90. Shao, X. *et al.* Highly Selective and Sensitive 1-Amino BODIPY-Based Red Fluorescent Probe for Thiophenols with High Off-to-On Contrast Ratio. *Anal. Chem.* **87,** 399–405 (2015).
91. Netto, E. J., Peterson, J. I., McShane, M. & Hampshire, V. A fiber-optic broad-range pH sensor system for gastric measurements. *Sens. Actuators B Chem.* **29,** 157–163 (1995).
92. Haque, M. M., Lee, H.-I. & Kim, D.-K. Luminescent properties of Eu^{3+}-activated molybdate-based novel red-emitting phosphors for LEDs. *J. Alloys Compd.* **481,** 792–796 (2009).
93. Zhao, D., Miller, D., Xian, X., Tsow, F. & Forzani, E. S. A novel real-time carbon dioxide analyzer for health and environmental applications. *Sens. Actuators B Chem.* **195,** 171–176 (2014).
94. Mills, A., Lepre, A. & Wild, L. Breath-by-breath measurement of carbon dioxide using a plastic film optical sensor. *Sens. Actuators B-Chem.* **39,** 419–425 (1997).
95. Trivedi, S., Mehta, H. & Kashyap, R. Correlation of end tidal and arterial carbon dioxide levels in critically Ill neonates and children. *Indian J. Crit. Care Med.* **18,** 348 (2014).
96. Rost, B., Zondervan, I. & WolfGladrow, D. Contribution to the Theme Section 'Effects of ocean acidification on marine ecosystems' Sensitivity of phytoplankton to future changes in ocean carbonate chemistry: current knowledge, contradictions and research directions. *Mar. Ecol. Prog. Ser.* **373,** 227–237 (2008).
97. Doney, S. C., Fabry, V. J., Feely, R. A. & Kleypas, J. A. in *Annual Review of Marine Science* **1,** 169–192 (Annual Reviews, 2009).
98. Punt, A. E., Poljak, D., Dalton, M. G. & Foy, R. J. Evaluating the impact of ocean acidification on fishery yields and profits: The example of red king crab in Bristol Bay. *Ecol. Model.* **285,** 39–53 (2014).
99. Fabricius, K. E. *et al.* Losers and winners in coral reefs acclimatized to elevated carbon dioxide concentrations. *Nat. Clim. Change* **1,** 165–169 (2011).
100. Puligundla, P., Jung, J. & Ko, S. Carbon dioxide sensors for intelligent food packaging applications. *Food Control* **25,** 328–333 (2012).
101. Weigl, B. *et al.* Optical Triple Sensor for Measuring Ph, Oxygen and Carbon-Dioxide. *J. Biotechnol.* **32,** 127–138 (1994).
102. Beuermann, T. *et al.* On-line carbon balance of yeast fermentations using miniaturized optical sensors. *J. Biosci. Bioeng.* **113,** 399–405 (2012).

103. Carroll, A. G. *et al.* Environmental considerations for subseabed geological storage of CO2: A review. *Cont. Shelf Res.* **83,** 116–128 (2014).
104. Mills, A. & Hodgen, S. Fluorescent carbon dioxide indicators. *Adv. Concepts Fluoresc. Spectrosc. Pt Small Mol. Sens.* **9,** 119–161 (2005).
105. Zosel, J., Oelßner, W., Decker, M., Gerlach, G. & Guth, U. The measurement of dissolved and gaseous carbon dioxide concentration. *Meas. Sci. Technol.* **22,** 072001 (2011).
106. Clegg, M., Sullivan, C. & Eastin, J. Sensitive Technique for Rapid Measurement of Carbon-Dioxide Concentrations. *Plant Physiol.* **62,** 924–926 (1978).
107. Arieli, R., Ertracht, O. & Daskalovic, Y. Infrared CO2 analyzer error: an effect of background gas (N-2 and O-2). *J. Appl. Physiol.* **86,** 647–650 (1999).
108. Jokic, T. *et al.* Highly Photostable Near-Infrared Fluorescent pH Indicators and Sensors Based on BF2-Chelated Tetraarylazadipyrromethene Dyes. *Anal. Chem.* **84,** 6723–6730 (2012).